The distal border of the equine navicular bone: a radiographic and computed tomographic study

Sarah Claerhoudt

Thesis submitted in fulfillment of the requirements for the degree of Doctor of Philosophy (PhD) in Veterinary Sciences, Faculty of Veterinary Medicine, Ghent University

2014

Promotor:
Prof. Dr. J.H. Saunders

Department of Medical Imaging and Small Animal Orthopaedics
Faculty of Veterinary Medicine
Ghent University

This PhD thesis was supported by a scientific research grant of the Ghent University Special Research Fund (BOF10/DOC/345).

Printed by University Press, Zelzate, Belgium. www.universitypress.be

The distal border of the equine navicular bone: a radiographic and computed tomographic study

Sarah Claerhoudt

Vakgroep Medische Beeldvorming van de Huisdieren en Orthopedie van de Kleine Huisdieren

Faculteit Diergeneeskunde

Universiteit Gent

ISBN: 978-90-5864-370-4

No part of this work may be reproduced in any form without written permission of the author.

Geluk moeten we onderweg zoeken
en niet aan het einde van de weg,
want dan is de reis afgelopen.

Kris Brand

TABLE OF CONTENT

LIST OF ABBREVIATIONS

CE-CT	Contrast-enhanced Computed tomography
CI	Confidence interval
CSL	Collateral sesamoidean ligaments
CT	Computed tomography
DDAL	Distal digital annular ligament
DDFT	Deep digital flexor tendon
DIPJ	Distal interphalangeal joint
DSIL	Distal sesamoidean impar ligament
GRE	Gradient echo
HU	Hounsfield unit
IRU	Increased radiopharmaceutical uptake
IV	Intravenous
kHz	kiloHertz
kV	kilovoltage
mAs	milliAmpère x seconds
MHz	MegaHertz
MRI	Magnetic resonance imaging
OR	Odds ratio
PIPJ	Proximal interphalangeal joint
RI	Reference interval
ROI	Region of interest
SD	Standard deviation
STIR	Short Tau inversion recovery
T	Tesla
TE	Time of echo
TR	Time of repetition
US	Ultrasonography
w	weighted
WL	Window level
WW	Window width

Abbreviations of the radiographic projections

DPa(Pl)	Dorsopalmar(plantar)
DPr-Pa(Pl)DiO	Dorsoproximal – palmaro(plantaro)distal oblique
D45°-70°Pr-PaDiO	Dorso 45°-70° proximal - palmarodistal oblique
D55°Pr-PaDiO	Dorso 55° proximal - palmarodistal oblique
D65°Pr-PaDiO	Dorso 65° proximal - palmarodistal oblique
DL(M)-Pa(Pl)M(L)O	Dorsolateral(medial) – palmaro(plantaro)medial(lateral) oblique
D60°L(M)-Pa(Pl)M(L)O	Dorso 60° lateral(medial) – palmaro(plantaro)medial(lateral) oblique
LM	Lateromedial
Pa(Pl)Pr-Pa(Pl)DiO	Palmaro(plantaro)proximal – palmaro(plantaro)distal oblique

PREFACE

Foot pain causing lameness is frequently observed in the horse. A common cause of uni- or bilateral foot pain typically affecting middle-aged riding horses is podotrochleosis, better known as navicular disease. Abnormalities of the navicular bone (also called distal sesamoid bone) are frequently observed radiographically in horses with navicular disease (14.9% - 87.6% in Warmbloods). Until now, radiography is the first choice of imaging technique to show the bony changes in horses with clinical evidence of navicular disease. Particularly the distal border of the navicular bone is evaluated in depth during a radiographic examination and is graded during a veterinary purchase examination, according to a specific standardised protocol. The intended purpose to devise such radiographic scoring systems was to standardize the radiographic evaluation of different horses and serial radiographs of the same horse. Based on the total radiographic score of the screening joints, the risk for developing future lameness is predicted.

The presence of a bony fragment and/or abnormal (in number, depth and/or shape) synovial invaginations at the distal navicular border are considered important radiographic abnormalities and are potentially related to navicular disease. The association between the presence of distal border fragments and lameness is not universally accepted, but these fragments have recently gained increasing support as a cause of palmar foot pain. However, they may also occur in non-lame horses and different opinions exist among countries as well. Moreover, there still remains considerable debate between veterinarians as to the clinical significance of abnormal synovial invaginations and bone fragments at the distal border of the navicular bone. This substantiates the difficulty of evaluating the navicular bone and predicting soundness in a performance horse from its pre-purchase exam.

Research on the synovial invaginations of the navicular bone has been performed in the ‘90s, but nowadays, in depth studies on these invaginations are scarce. As a starting point for using the scoring systems, it is needed to know the relative ability of diagnostic techniques, such as radiography, to characterize the distal navicular border invaginations.

CHAPTER 1

General introduction

The equine navicular bone

PART 1.1

Anatomy and imaging techniques

ANATOMY

The navicular bone, also called distal sesamoid bone or *os sesamoideum phalangis distale*, is located palmar/plantar in the equine foot between the distal part of the deep digital flexor tendon (DDFT) and the distal interphalangeal joint (DIPJ) (Fig. 1). This sesamoid bone plays a role in shock absorption of the compressive forces from the DDFT and provides a constant angle for sliding of the tendon. At 100 days of gestation, the navicular bone is completely cartilaginous and at 330 days of gestation, a central ossification centre could be detected in the bones of all foeti (1). At birth, the navicular bone has an oval shape on radiographs, with a single proximal and distal border (2). At the age of 3-4 months, the bone is completely ossified and adopts its mature shape during the first year *postpartum* (1, 2). The mature bone has a typical 'navicular' (boat) shape with a proximal and distal articular border, proximal and distal flexor border and a lateral and medial wing. It has 2 articular surfaces, which are covered with a layer of articular (hyaline) cartilage, and a flexor surface (*facies flexoria*) covered with fibrocartilage. The navicular bone forms a part of the DIPJ at its dorsal surface, which is in contact with the articular facet of the distal phalanx and the middle phalanx. The palmar/plantar surface of the bone is the flexor surface, which provides a gliding surface for the DDFT and is evenly divided by the sagittal ridge. Between the tendon and the flexor surface of the navicular bone, a fluid-filled synovial cavity called the navicular (*podotrochlear*) bursa, is present. This bursa has a proximal and distal recess. Due to its position between the tendon and the distal phalanx, the navicular bone requires stabilizing ligaments. The distal flexor border of the navicular bone is broad and the distal sesamoidean impar ligament (DSIL) unites the bone with the distal phalanx. This ligament separates the DIPJ from the distal recess of the navicular bursa. The lateral and medial collateral sesamoidean ligaments (CSL) insert on the lateral and medial wing of the navicular bone respectively, and sagittally unite, to form a broad ligament, called the 'proximal sesamoidean ligament', which inserts on the proximal flexor border of the navicular bone. A connective tissue attachment of the DDFT to the palmar/plantar surface of the middle phalanx and to the proximal border of the navicular bone, called the 'lamina transversa' or 'T-ligament' in the literature, separates the dorsodistal recess of the digital flexor tendon sheath from the proximal recess of the navicular bursa and palmaro(plantaro)proximal recess of the DIPJ.

The navicular bone is made up of spongious and compact bone. The spongious bone ('medulla') consists of trabeculae, which have a regular

dorsoproximal/palmaro(plantaro)distal orientation, and fat (3). A subchondral bone plate is present beneath the cartilage layers. The thickness of the compact bone at the flexor surface differs from horse to horse and depends on the breed, type of horse, exercise level and pathology (3).

The term ‘navicular bone’ is preferably used in this thesis instead of ‘distal sesamoid bone’, since the first term is commonly used in recent literature as well.

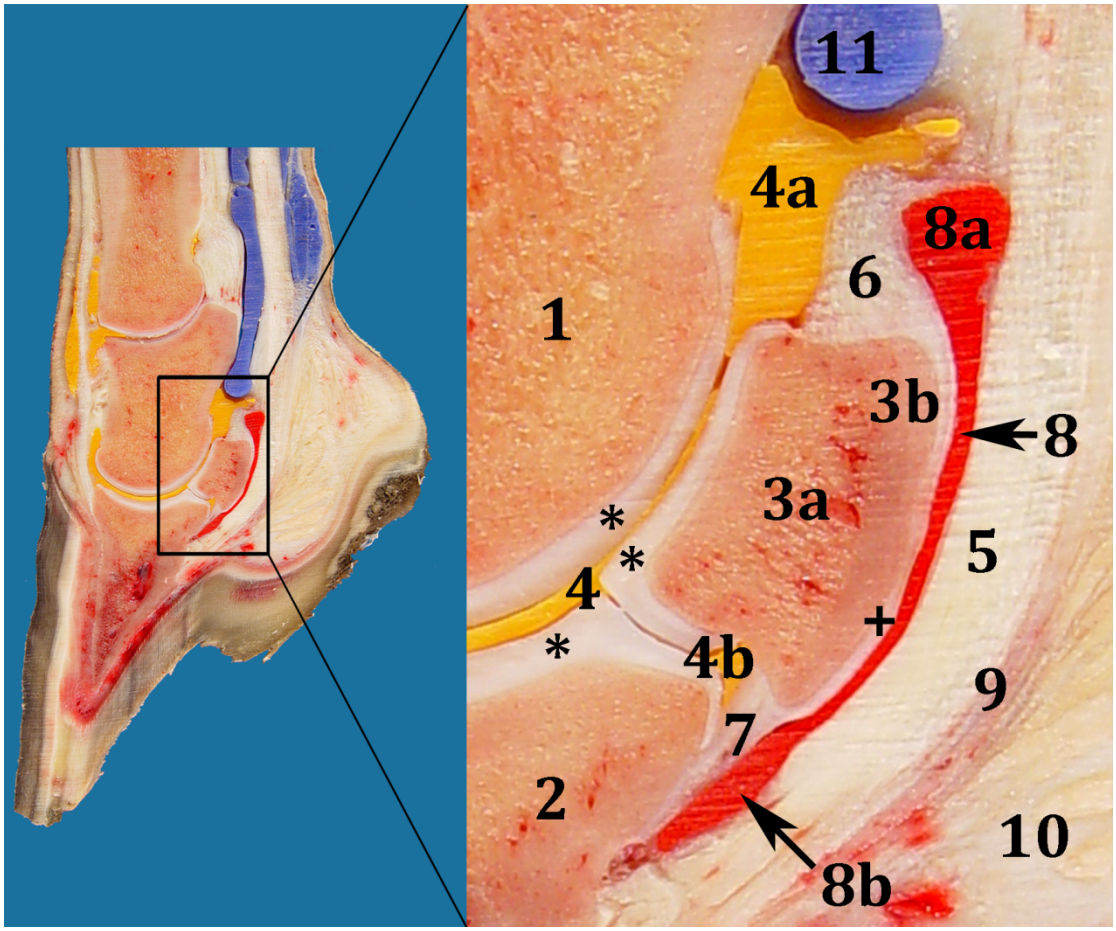

Fig. 1: Left image: sagittal anatomical slice of an equine foot; right image: magnified photograph of the palmar part the foot (*podotrochlear* region) (1: middle phalanx; 2: distal phalanx; 3: navicular bone: 3a = spongious bone; 3b = compact bone; 4: distal interphalangeal joint (filled with yellow dye): 4a = palmaroproximal recess; 4b = palmarodistal recess; *: hyaline cartilage; +: fibrocartilage; 5: deep digital flexor tendon; 6: proximal sesamoidean ligament; 7: distal sesamoidean impar ligament; 8: podotrochlear bursa (filled with red dye): 8a = proximal recess; 8b = distal recess; 9: distal digital annular ligament; 10: digital cushion; 11: dorsodistal recess of the digital flexor tendon sheath (filled with blue dye)). Courtesy of Katrien Vanderperren.

Until 200 days of gestation, the distal articular border is directly linked to the DSIL. Gradually, indentations of the distal articular surface or a narrow groove between the articular border and the ligament, with or without locally some dorsal indentations, are formed (1). Before birth, the dorsal indentations are covered with cartilage, fibrous, connective and synovial tissue (1). These dorsal indentations are localised around nutrient foraminae. After birth, these foraminae are visible as sharply delineated radiolucent areas and situated in the centre of the distal groove, with an average number of 3 to 4 short foraminae distally (Fig. 2). They are also seen proximally in the ossification centre, but their number and extent decrease gradually as the ossification process proceed. Ten weeks after birth, a synovial inversion is first noticed in the nutrient foramina, which is now surrounded by bone tissue (osteoblasts) instead of cartilage. Synovial tissue extends in the majority of the foraminae till halfway the foramina (4).

Fig. 2: Dorsal (A) anatomical slice and distal view (B) of a navicular bone, showing some distal border nutrient foraminae (arrowheads). The 'spongious' appearance of the spongious bone can well be depicted on figure A (arrow).

The vascular supply of the navicular bone in foeti, adult normal horses and horses with navicular disease, has been described thoroughly in arteriographic and histological studies (1, 4-6). Before 125 days of gestation, the vascular supply of the navicular bone differs from that seen in the mature horse, since no vessels entered the navicular bone. At 145 days of

gestation, networks of anastomosing vessels are formed and penetrate into the bone from 4 directions (proximal, distal, lateral and medial). These vessels are branches of the *ramus palmaris phalangis mediae*, *ramus navicularis distalis* and *rami naviculares laterales and mediales* respectively, itself originating from the *Arteria digitalis medialis and lateralis* of the foot.

In the literature, different definitions are given to the nutrient foraminae. Rijkenhuizen and co-workers describe the nutrient foraminae as the entrance and guidance of the nutrient vessels and its branches into the bone (4) (Figs. 3 and 4). According to Hertsch and Dammer, the distal arteries enter the navicular bone with or without a foramina (5). Others describe the nutrient foramina as a radiolucency formed by cones of anastomosing branches derived from the distal arteries (7).

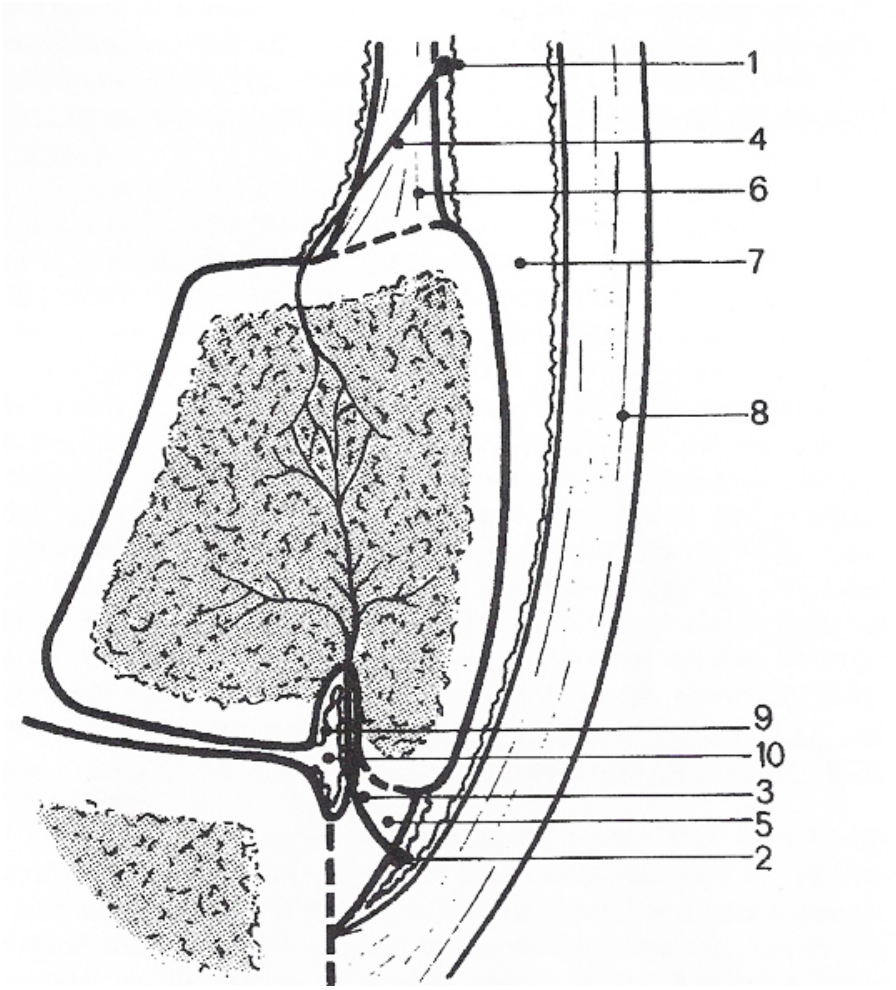

Fig. 3: Diagram of the arterial anatomy of the normal navicular bone in lateromedial projection. (1: ramus palmaris phalangis mediae; 2: ramus navicularis distalis; 3: distal artery; 4: proximal artery; 5: distal sesamoidean impar ligament; 6: proximal sesamoidean ligament; 7: navicular bursa; 8: deep digital flexor tendon; 9: synovial introversion; 10: nutrient foramina). From Rijkenhuizen et al., 1989.

Fig. 4: Arteriogram of the distal part of the normal navicular bone in proximodistal projection (A: flexor surface; B: articular surface of the navicular bone). Black arrow points towards the artery situated inside a nutrient foramina. From Rijkenhuizen et al., 1989.

Within the bone, an anastomosing network is formed between the arteries entering the bone from the different directions (1, 4, 5). The navicular bone can be divided into 11 parts based on the receiving blood supply arising from one or more directions (Fig. 5). The existence of areas in the bone being blood supplied by arteries coming from one, two or three directions, may be an important factor in the pathogenesis of navicular disease (4).

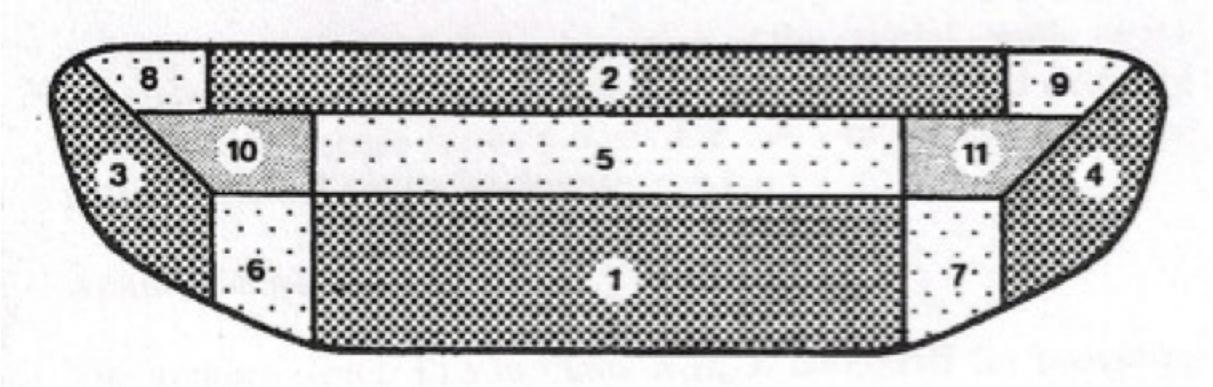

Fig. 5: Diagram of the suggested arterial anatomy of the navicular bone. Parts 1-4 receive arteries from one direction (distal (1), proximal (2), medial (3) and lateral (4)). Parts 5-9 receive arteries from two directions (distal and proximal (5), distal and medial (6), distal and lateral (7), proximal and medial (8), proximal and lateral (9)). Parts 10 and 11 receive arteries from three directions (proximal, distal and medial (10) or lateral (11). From Rijkenhuizen et al., 1989.

After birth, extensive anastomoses of vessels are formed and an increase in the diameter of the arteries is seen, most likely as a response to proceeding bone ossification and increasing function and workload (1, 7). The foraminae at the distal border of the navicular bone contain loose connective tissue, nutrient vessels (1 to 3 arteries, arterioles, veins and capillary plexi), synovial introversions and myelinated nerves. The presence of synovial tissue from the DIPJ into the nutrient foraminae has been proven radiographically by injecting contrast medium into the joint. A clear connection was seen (5).

Literature lacks information concerning the morphology of the foraminae at the proximal, medial and lateral borders of the navicular bone. They are usually not seen radiographically, most likely because of their small size in a normal horse. The radiographic visible lucencies at the distal border (on a dorsoproximal-palmaro(plantaro)distal oblique (DPr-Pa(Pl)DiO) projection) are normally smoothly outlined and conical in shape.

Before 270 days of gestation, the foetal blood supply had an extra route of blood supply to the navicular bone compared with that of young and adult horses (1, 7). Blood vessels were found in the superficial layer of the fibrocartilage, which gradually retracted after 270 days of gestation and disappeared at 6 months after birth. Consequently, thinning of the fibrocartilage was noticed, generally located at the centrodistal aspect of the sagittal ridge of the navicular bone, which is described as a frequent location of fibrocartilage lesions in the navicular bone of horses with navicular disease (6). Moreover, Rijkenhuizen and co-workers described a

positive correlation between enlarged nutrient foraminae and thinning of the fibrocartilage (1).

Circulatory disturbances of the blood supply (inside or close to) the distal border of the navicular bone resulting in ischemia have been described to be a cause of navicular disease. Partial or total occlusion of the main arteries due to (sub)intimal thickening, arterial obstruction, thrombosis, arterio(lo)sclerosis and venous congestion, have been reported as variable causes for the altered blood supply to the bone (6-10). Bones with abnormally shaped (rounded to lollipop-shaped) distal border nutrient foraminae showed a decreased distal blood supply with a shift towards the proximal, lateral and medial supply. Compensatory, proximal vessel enlargement and distal new vessel formation (arterioles) were noticed (6, 7, 9) (Fig. 6). Consequently, proximal nutrient foraminae may become visible radiographically. Arterial wall changes were also seen in foals and horses without radiographic abnormalities, however with a lower incidence compared to those with radiographic enlargement of the foraminae (1, 4).

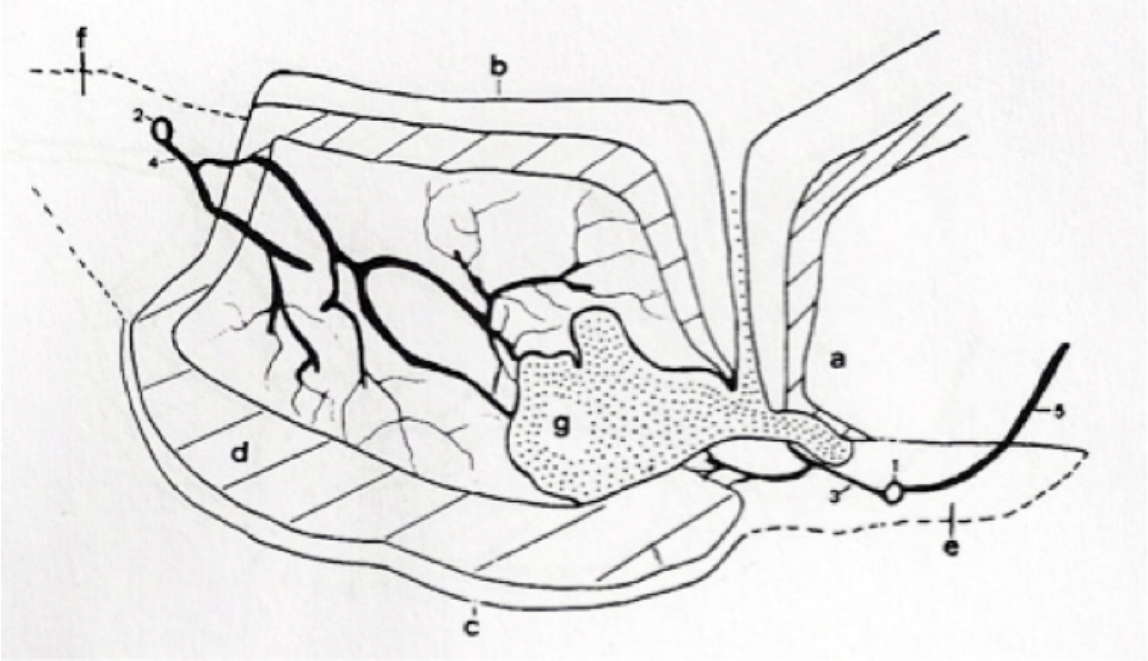

Fig. 6: Diagram of the arterial anatomy of the navicular bone of a horse with navicular disease in lateromedial projection. (a: distal phalanx; b: cartilage of the articular surface of the navicular bone; c: cartilage of the flexor surface of the navicular bone; d: compact bone; e: distal sesamoidean impar ligament; f: proximal sesamoidean ligament; g: enlarged nutrient foramina; 1: ramus navicularis distalis; 2: ramus palmaris phalangis mediae; 3: distal artery; 4: proximal artery (enlarged); 5: arteries entering the distal phalanx). Adapted from Hertsch and Dammer, 1988.

In the literature, different theories are described to explain the change in shape seen in the distal border nutrient foraminae. The compensatory (collateral) revascularisation around the distal nutrient foramina(e) seen in horses with navicular disease, is assumed by Colles and Hickman to cause osteoporosis at the tip of the foramina, resulting in an enlargement of the foramina (7). Rijkenhuizen and co-workers agreed this finding and described substantial bone remodelling around the nutrient foramina, in which bone resorption predominated (6). Moreover, the bone density surrounding the abnormal foramina increased later on because of new bone deposition. Histologically, an increased amount of fibrous connective and synovial tissue was noticed in lollipop-shaped distal border nutrient foraminae (6, 9).

Biomechanical changes, such as hypertension and/or increased pressure in the DIPJ, have also been described to be a cause of increased number and size of the distal border nutrient foraminae (5, 6). Pressure atrophy would cause an enlargement of the nutrient foramina, since the (hypertrophied) synovia is pushed deeper into the foramina, thereby defining its form.

MacGregor postulated that the presence of a nutrient foramina with a shape other than conical, is in itself not diagnostic for navicular disease, but the more nutrient foraminae with abnormal shapes present, the more likely it is evidence of navicular disease (11). However, the exact etiopathogenesis of navicular disease and the significance of enlarged distal border nutrient foraminae still remain unclear. Furthermore, the radiographic morphology of the nutrient foraminae shows anatomical variation and is related to many factors. It varies significantly with the limb (fore- or hindlimb), gender, age, breed, type, frequency and regularity of the training of the horse (3, 7, 12).

In the literature, different terms, such as synovial invaginations, synovial fossae, canales sesamoïdales or vascular channels, are used to describe the radiographically visible distal radiolucencies. The term ‘synovial invaginations’ is preferably used further in this thesis, since this term is widely used in the literature nowadays.

IMAGING TECHNIQUES

RADIOGRAPHY

Radiography is the first imaging modality for investigating disorders affecting the foot. It uses x-ray attenuation as principle for image formation, and is therefore effective in evaluating anatomical structures with a varied inherent high tissue density, such as bony structures. Proper cleaning and trimming of the hoof is crucial prior to radiography. The shoe must be removed and the frog clefts and sulci have to be filled with packing material, to avoid radiolucent artifacts. The radiographic projections for the equine foot are at least a lateromedial (LM) and DPr-Pa(Pl)DiO projection, using different degrees of proximodistal obliquity (preferable 50 – 65°) (Fig. 7A and B) (13). For the latter projections, the x-ray beam of the tube is kept horizontal and centered 2 cm proximal to the coronary band at the midline of the foot. The foot is placed on a wooden block with a slope of for example 55° with the horizontal. A second D65°Pr-Pa(Pl)DiO projection is advised and is achieved by placing a wedge with a slope of 10° on the wooden block. In addition, a palmaro(plantaro)proximal-palmaro(plantaro)distal oblique (Pa(Pl)Pr-Pa(Pl)DiO) radiographic projection may be required, to evaluate the flexor surface of the navicular bone and the spongious-compact bone interface (Fig. 7C), and a weight-bearing dorsopalmar/plantar (DPa(Pl)) projection to detect entheseophytes on the lateral and medial wings of the navicular bone (14). Also several dorsolateral(medial)-palmaro(plantaro)medial(lateral) oblique (DL(M)-Pa(Pl)M(L)O) projections, such as D60°L(M)-Pa(Pl)M(L)O projections on a flexed or weight-bearing limb, need to be performed for the evaluation of for example the joint margins in case of degenerative joint disease (13, 15). However, radiography provides only few information regarding soft tissues changes, which may explain the inconsistent correlation with clinical signs (16). Besides, radiography permits a limited assessment of acute bone changes, since at least 30% of change in bone density is required before the alteration can be identified (13). Another limitation of radiography is that a three-dimensional structure is projected onto a two-dimensional radiograph, leading to superimposition of bony structures. Mainly on the DPr-Pa(Pl)DiO projection, the navicular bone is superimposed over the distal part of the second phalanx (13).

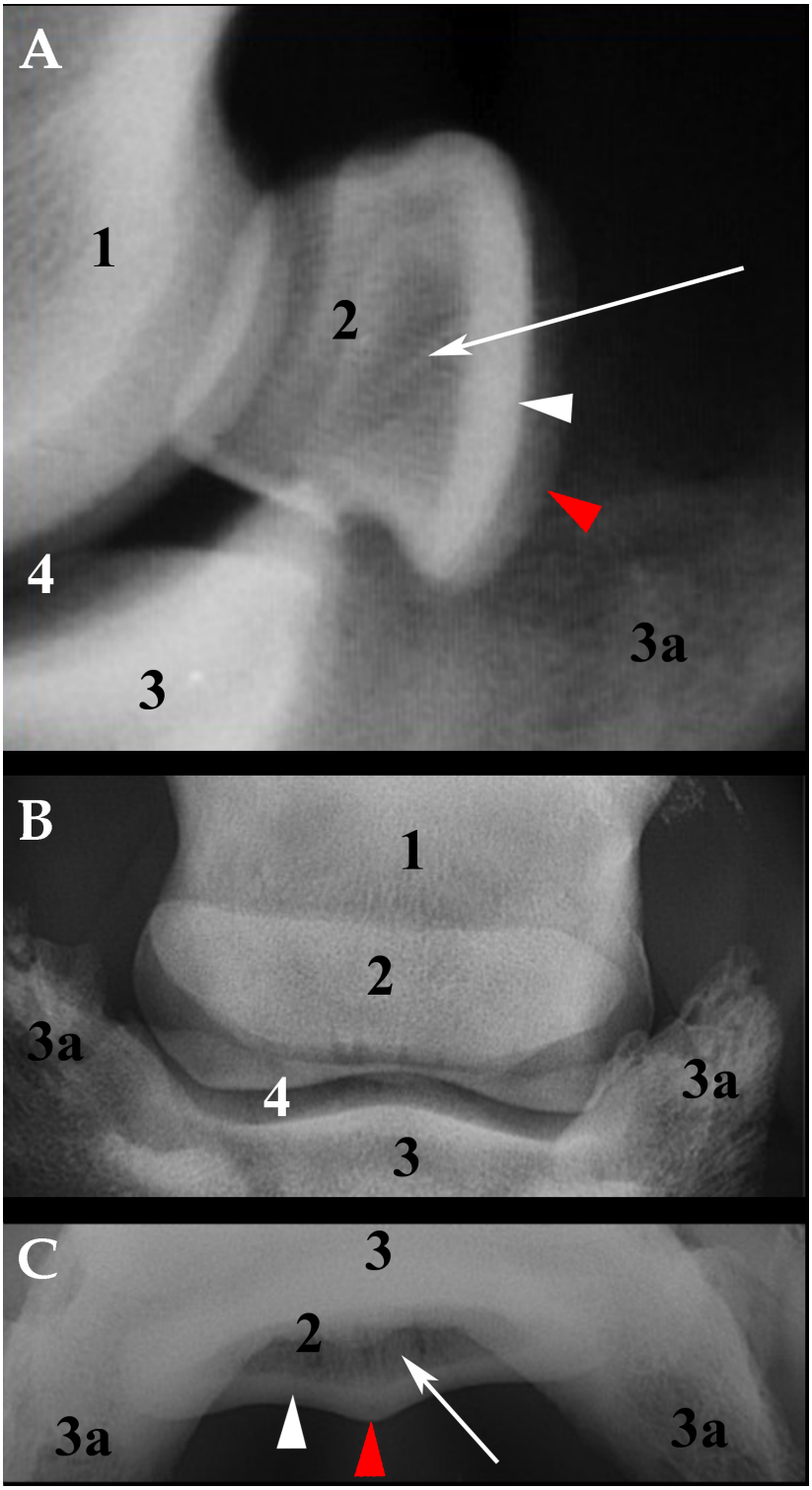

Fig. 7: Lateromedial (A), Dorsoproximal-palmarodistal oblique (B) and palmaroproximal-palmarodistal oblique (C) radiographs of the navicular bone of 3 front feet. A demarcation between the spongious (arrow) and compact bone (white arrowhead) of the navicular bone can be seen on radiographs A and C, which is more distinct on radiograph C. The sagittal ridge of the navicular bone is visible on radiographs A and C (red arrowhead). (1: middle phalanx; 2: navicular bone; 3: distal phalanx; 3a: palmar processes; 4: distal interphalangeal joint). Left = dorsal (A); lateral (B, C).

ULTRASONOGRAPHY

Ultrasonography (US) is widely available and for most body parts, it is complementary to radiography. This technique uses ultrasound (frequency >20 kHz) waves. Pulses of ultrasound are sent into the tissues and tissue interfaces with different acoustic impedance (product of the tissue density en propagation speed) reflect them back to the transducer, forming an image. Ultrasonographic images of the foot are produced with a 7.5 MHz microconvex transducer and no stand-off pad is required. Prior to examination, the palmar/plantar aspect of the distal pastern and heel area are clipped, washed with warm water and covered with coupling gel. When the body of the frog is used as the acoustic window (transcuneal approach), the frog is trimmed to moist, pliable horn tissue. The horn is further moistered by either placing the foot in a basin with warm water for 10-15 minutes, or by fixing a wet sponge under the frog. The central cuneal sulcus is then filled with gel to enhance coupling between the surface of the transducer and the frog. The limb of the horse is flexed and the toe is placed on the operator's knee to induce an extension of the interphalangeal joints.

The echogenicity of the structure is based on the amount of reflected sonowaves, with the bone surfaces being hyperechoic (white) and fluid anechoic (black). Ultrasonography is sensitive for the evaluation of soft tissues and bone contour regularity (17). Compared to the other diagnostic imaging modalities, US gives a dynamic view of the tissues. Via a transcutaneous approach between the bulbs of the heels, it is possible to evaluate the proximal third of the flexor surface of the navicular bone, the DDFT at that level, proximal part of the distal digital annular ligament (DDAL), proximal sesamoidean ligament, the proximal recess of the podotrochlear bursa and the proximopalmar/plantar recess of the DIPJ (18) (Fig. 8). Using a transcuneal approach, acceptable assessment of more distal structures of the podotrochlear apparatus (DSIL, distal part of the navicular flexor surface and insertion of the DDFT to the distal phalanx) is possible (19), however, the middle part of the flexor surface of the navicular bone and the DDFT at that level are difficult to evaluate ultrasonographically, and depend mainly on the hoof conformation and its quality. Comparison with symmetrical structures and the contralateral limb is essential.

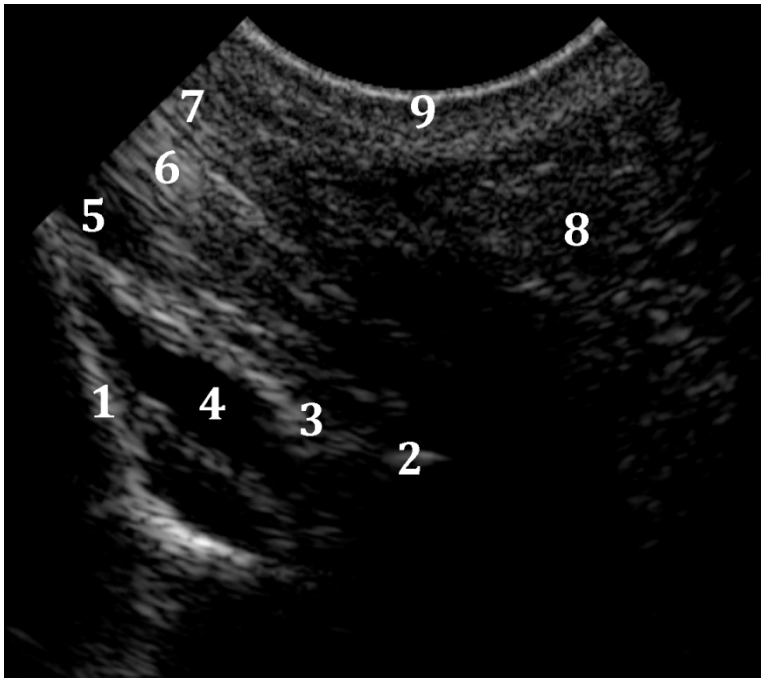

Fig. 8: Sagittal ultrasonographic scan through the bulbs of the heel of the forelimb of a horse in longitudinal section. (1: middle phalanx (distal part); 2: navicular bone (flexor surface); 3: proximal sesamoidean ligament; 4: palmaroproximal recess of the distal interphalangeal joint (filled with anechoic fluid); 5: digital flexor tendon sheath (dorsodistal recess); 6: deep digital flexor tendon; 7: distal digital annular ligament; 8: digital cushion (toric part); 9: skin). Left = proximal; top = palmar.

COMPUTED TOMOGRAPHY

Computed tomography (CT) of the equine foot can be of great value when results of radiography and US are inconclusive. As for radiography, CT scanning also uses x-ray attenuation and suited best for the evaluation of the osseous skeleton. Moreover, the CT images are a set of cross-sectional images, contiguous or overlapping, of a body part. When a horse is selected for a CT examination, an intravenous (IV) jugular catheter is placed in the horse, which is then anesthesized. A possible anesthetic protocol can be: premedication with an α2-adrenoceptor agonist (romifidine 80 μg/kg, IV, Sedivet®, Brussels, Belgium or detomidine 0.01-0.02 mg/kg, IV, Domosedan®, the Netherlands), anesthesia induction with midazolam (0.06 mg/kg, IV, Dormicum®, Brussels, Belgium) and ketamine (2.2 mg/kg, IV, Anesketin®, Heusden-Zolder, Belgium) and maintenance on inhalational anesthesia (isoflurane: Isoflo®, Kent, United Kingdom). The horse is positioned in a lateral recumbency with the leg to be examined dependent within the gantry of the CT scanner. Images are acquired in the transverse plane (the plane of the rotating x-ray beam with respect to the body

axis), and thanks to postprocessing, the transverse images can be reconstructed to dorsal and sagittal plane images, their gray scale settings can be altered and other ways of image manipulation is possible (20). Contrary to conventional radiography, CT produces, at a high scanning time, detailed, high spatial resolution images without superimposition and with a small slice thickness. This technique is very sensitive for subtle bone changes, since each pixel's density is measured based on its x-ray attenuation factor and is given a Hounsfield unit (HU) number (CT number range from -1000 to +3095; displayed as 256 different shades of gray). The final image contrast and brightness can be adjusted via a postprocessing tool called window width (WW) and window level (WL). Narrower windows result in greater contrast, but increased visible noise. Routinely, images are displayed using at least two different window width and level settings.

Computed tomography has been shown to be mandatory to depict specific bone pathology, such as complex comminuted fractures, and to allow a clear diagnosis of pathology in the navicular bone region (16, 21). Osseous fragments near the distal border, altered synovial invaginations, increased density of the spongious bone of the navicular bone, small cyst-like lesions and flexor surface defects, are better and earlier assessed with CT compared to radiography (16, 22, 23).

Although CT has an inherent low contrast for tissues with similar attenuation such as soft tissues and fluid, with the administration of intra-vascular positive contrast medium (contrast-enhanced computed tomography (CE-CT)), the characterization of soft tissues lesions in the foot has improved and the stage of tendon healing can be determined (20, 24). Prior to intra-arterial contrast injection, the medial aspect of the carpus is properly clipped and aseptically prepared, and a catheter is inserted into the medial palmar metacarpal artery at the level of the carpometacarpal joint using US guidance. Iodinated positive contrast material (diatrizoate meglumine and diatrizoate sodium, RenoCal-76®, 400 mgI/ml, Princeton, USA; diluted 1:1 with 0.9% NaCl) is injected using a pressure injector (25). The contrast material is continuously infused while scanning the distal limb.

Also, the vascular anatomy of the equine foot has been described by the use of CT-angiography (26).

The gantry size of a CT system allows scanning of certain body parts, such as the distal limbs, head and cranial cervical region. Newer, larger CT gantries can scan up to the carpus and even the stifle of the horse. The major disadvantage of CT is its necessity for a general anaesthesia with consequent higher costs. A feasible technique for CT of the foot in standing

horses has been described and was suitable for the evaluation of bony structures, but not for the soft tissue structures (27).

MAGNETIC RESONANCE IMAGING

A magnetic resonance system produces a magnetic field and uses the tissue protons of hydrogen nuclei in the body elements, who act like small magnets, to obtain the magnetic resonance imaging (MRI) signal when exposed to this external magnetic field. After these protons are excited by a radiofrequency pulse, they return back to their original parallel alignment to the external magnetic field. At that time, an MRI signal is produced. This time of relaxation, also called T1 relaxation time, is tissue-specific and faster for fat, but slower for fluids/water (28). Simultaneously, but independent to the T1 relaxation, the protons start to dephase from the transverse plane back to their original status, at a rate which is tissue-dependent. This relaxation time is called T2 relaxation time and is longer for fluids/water and very short for fat. The contrast 'weighting' of an MRI image is controlled and depends on 2 acquisition parameters: time of echo (TE) and time of repitition (TR). With a short TE and short TR, a T1-weighted (T1-w) image will be formed with hypointense (or black) fluid and hyperintense (or white) fat. A long TE and long TR, will create a T2-weighted (T2-w) image, where fluid will appear hyperintens and fat hypointens. The signal intensity (gray scale value) varies in different tissues, due to their inherent differences in proton density. Thanks to the many possible imaging pulse sequences, which can be set up during a MRI examination, the different tissues with possible lesion(s) can be visualised. A very useful sequence in clinical MRI is the short Tau inversion recovery (STIR) pulse sequence. It allows better visualization of pathological tissues with a longer T1 relaxation time than fat (for example fluids).
Magnetic resonance imaging is a cross-sectional diagnostic imaging technique, which shows superior soft tissue contrast in high detail (Fig. 9). It is the method of choice to depict bone edema, fibro- and hyaline cartilage pathology and soft tissue lesions of the foot (23, 29, 30). Intraosseous fluid accumulation is more easily identified on STIR, fat-saturated or T2-w images as a hyperintense signal in areas of bone inflammation, haemorrhage, osteonecrosis, fibrosis or edema. The high-resolution images, excellent in high-field MRI systems (1.5 to 3 Tesla (T)), can demonstrate early structural and physiological tissue abnormalities, which are not (yet) detectable with other imaging modalities (16, 23). A significant association between MRI features and *post mortem* histological findings in the equine foot has been described (29, 31). A limitation of MRI, particularly of the low-field MRI system, is its longer scanning time

compared to CT, and consequently higher sensitivity for motion artifacts. The use of general anaesthesia is avoided by standing low-field MRI, which reduces costs and morbidity/mortality prevalence, but the overall image quality is much lower compared with high-field MRI images (32).

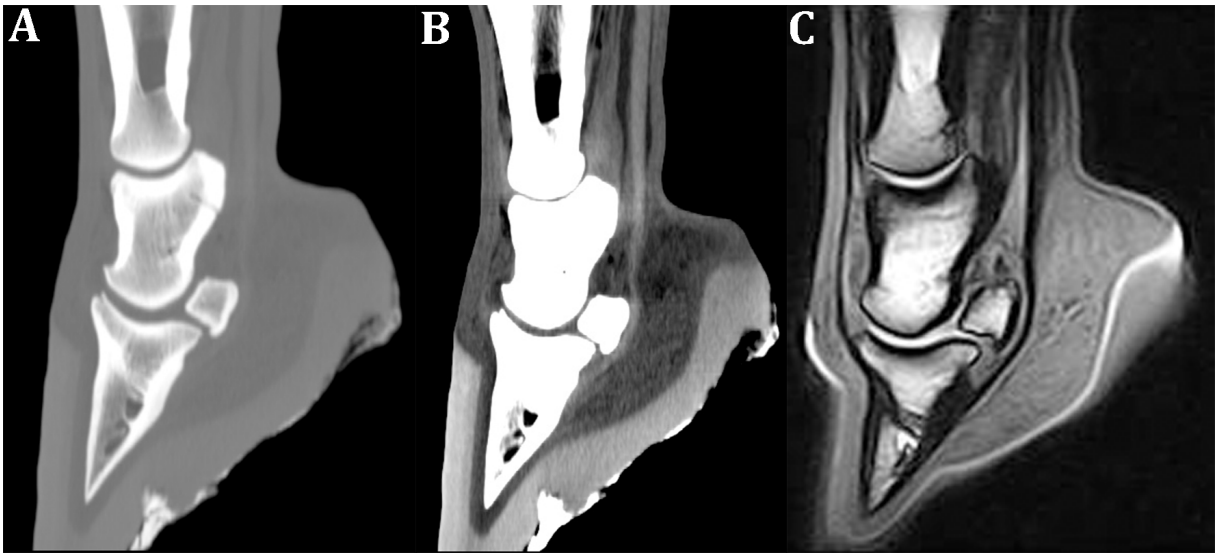

Fig. 9: Sagittal reconstructed CT image with bone window settings (A); soft tissue window settings (B) and sagittal T1 GRE-weighted (C) MRI image of normal equine feet, illustrating the different contrast resolution of both modalities. Courtesy of E.HJ. Bergman, Veterinary clinic 'The Lingehoeve', Lienden, the Netherlands and Davide Zani, University of Milan, Italy.

SCINTIGRAPHY

Nuclear scintigraphy is an emission technique which uses a radiopharmaceutical, consisting of a radionuclide attached to a tracer, injected intraveneously, to detect places in the body with (early) increased bone activity, displayed as 'hot spots' (areas of increased radiopharmaceutical uptake (IRU)). In equines, the most commonly used radionuclide is technetium 99m (^{99m}Tc), usually bounded with (hydroxy)methylene diphosphonate. The tracer binds with hydroxyapatite in bone, and the amount of accumulation depends on the osteoblast (metabolic) activity and amount of blood flow to the particular area. Scintigraphy has a high sensitivity to detect the region of increased bone activity (reflecting bone pathology or normal 'physiological' remodelling) and extent of active bone lesions (Fig. 10). A significant positive correlation was found between the intensity of IRU and severity of lesions at the flexor borders and medulla of the navicular bone on MRI images (33). However, false positive and negative results are seen (33, 34).

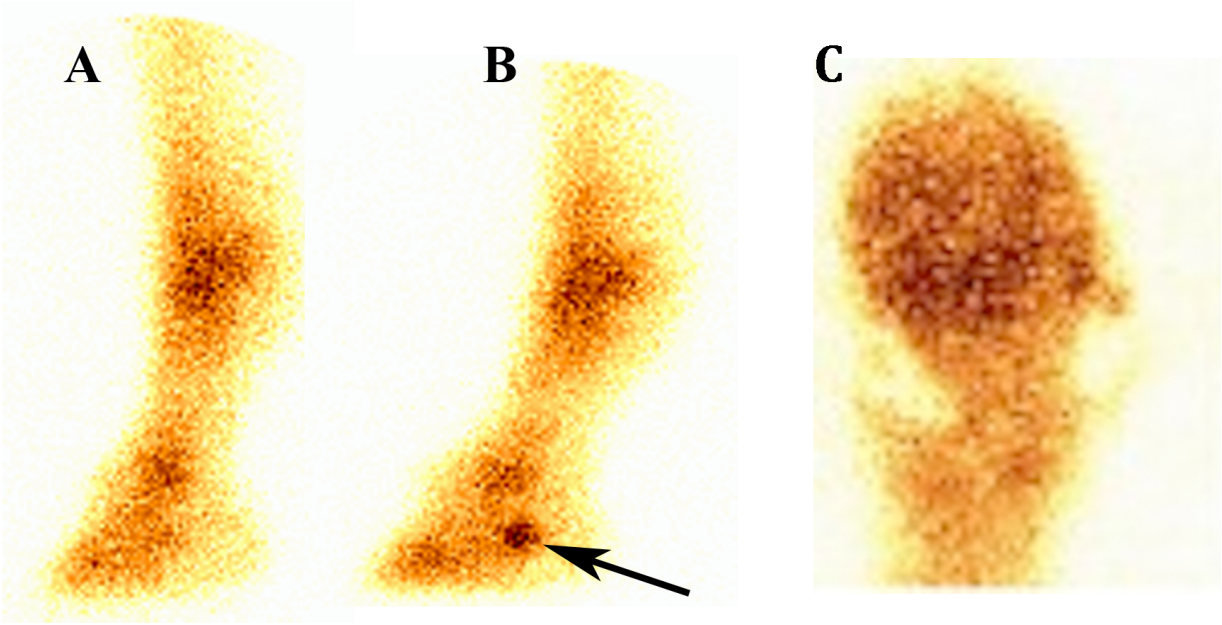

Fig. 10: A) Illustration of pattern of normal radiopharmaceutical uptake at the distal limb of the right front foot of a Dutch Warmblood horse. B) Pattern of focal increased radiopharmaceutical uptake (arrow) in the left navicular bone region (confirmed by the solar view (C). Differentials include fracture, infection or navicular disease. Courtesy of E.HJ. Bergman, Veterinary clinic 'The Lingehoeve', Lienden, the Netherlands.

CONCLUSIONS

A combination of a radiographic and US examination should be routinely performed in horses with foot pain. With the advent of a transcuneal approach, information on processes occuring within the hoof has become available. Complementary diagnostic imaging techniques such as CT, particularly in combination with contrast administration, and MRI has improved our knowledge concerning soft tissue pathology of the foot. Cross-sectional imaging techniques, such as CE-CT and MRI (at least a STIR pulse sequence) should be considered in all horses with foot pain localized by use of perineural analgesia for which a definitive diagnosis could not be made via radiography, US or other imaging techniques such as nuclear scintigraphy.

PART 1.2

Disorders of the navicular bone

1. Congenital disorders

Multipartite navicular bone

Bi- or tripartite navicular bones are seldomly seen. They arise from multiple non-fused centers of ossification and are frequently bilateral and symmetric. Based on the history, age of the horse and radiographic appearance, multipartite navicular bones may be differentiated from pathological fractures, although with difficulty. On radiography, the congenital abnormal bones have wide vertical radiolucent lines with smooth, rounded edges of both bone parts (35, 36). Horses with this congenital condition may be sound or mildly lame. However, lameness may occur due to degenerative changes of the DIPJ caused by instability at the level of the separate osseous centers.

Navicular bone agenesis

Phalangeal bone hypoplasia (agenesis) is a rare condition. In an old case report, a foal with unilateral phalangeal dysgenesis and navicular bone agenesis is described (37). Horses with this anomaly are lame, show asymmetry of the hoof size and abnormal limb conformation. Radiography is the modality of choice for the diagnosis of this disorder. Often multiple congenital anomalies occur and a radiographic examination of the contralateral limb is advised.

2. Acquired disorders

Fractures

Complete fractures

A fracture of the navicular bone usually occurs secondary to trauma or it can be pathologic, and was diagnosed more frequently in fore- than in hindlimbs of sporthorses (35, 38). The fracture is frequently simple and occurs parallel or slightly oblique (parasagittal) to the sagittal ridge of the bone. Occasionally, the fracture is comminuted along the long axis or runs parallel with the distal navicular border (14). Clinically, an acute onset of moderate to severe lameness is typical. Radiography (DPr-Pa(Pl)DiO and Pa(Pl)Pr-Pa(Pl)DiO projections) will confirm the diagnosis, but in the acute stage, the fracture lines may be missed due to insufficient demineralization (14). In fractured bones, the edges are more distinct and

radiolucent and/or sclerotic areas develop with time along the fracture lines (Fig. 11) (14, 36, 38). The overlying radiolucent artifactual lines produced by the sulci of the frog, should not be misdiagnosed as navicular bone fractures on a DPr-Pa(Pl)DiO radiographic projection.

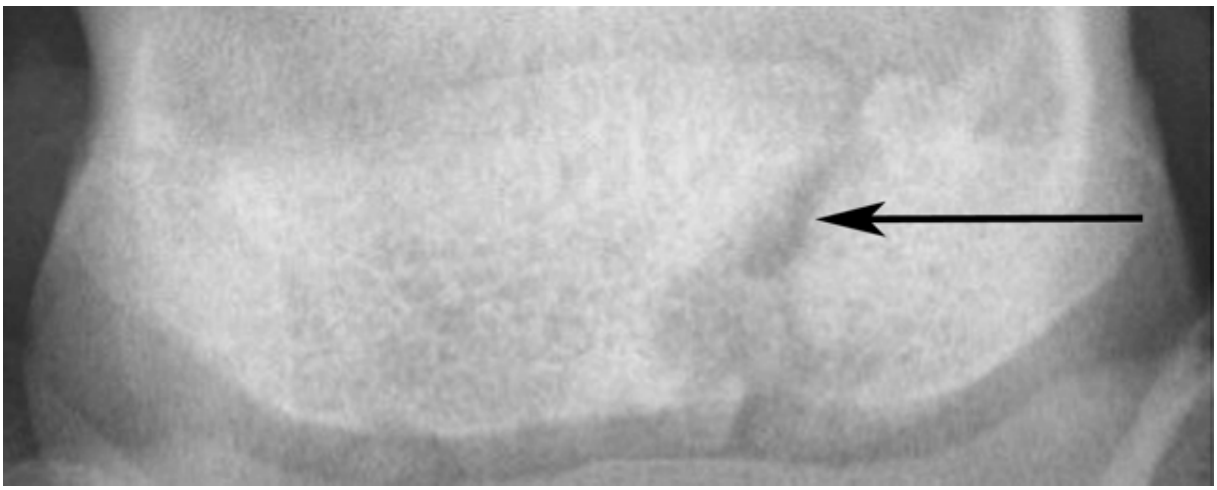

Fig. 11: Dorso 55° proximal-palmarodistal oblique radiographic projection of a 6-year old Warmblood horse with a right front lameness. An unilateral, parasagittal, poorly defined and irregular outlined fracture line is visible at the medial part of the navicular bone (arrow). Left = lateral.

Navicular border fragments

Osseous fragments at the junction between the distal horizontal and lateral and/or medial sloping borders of the navicular bone are relatively commonly observed. They are suggested to arise as avulsion fractures at the proximal insertion of the DSIL ('chip fractures'), fracture of an entheseophyte at the origin of the DSIL, dystrophic mineralization within the DSIL, osseous metaplasia, synovial osteoma or as separate ossification centers (13, 14, 36, 39). Fragments can be an incidental finding, especially if the opacity of the adjacent navicular bone is normal (14). Dorsoproximal-palmaro(plantaro)distal oblique radiographic projections with different angles to the horizontal appeared to be the best projections to visualize distal border fragments, as well as the presence of an associated radiolucent area ('fracture bed') in the adjacent distal margin of the navicular bone (Fig. 12). However, these fragments are frequently underdiagnosed with conventional radiography and are better visible with CT and MRI (Fig. 13) (16, 21, 22).

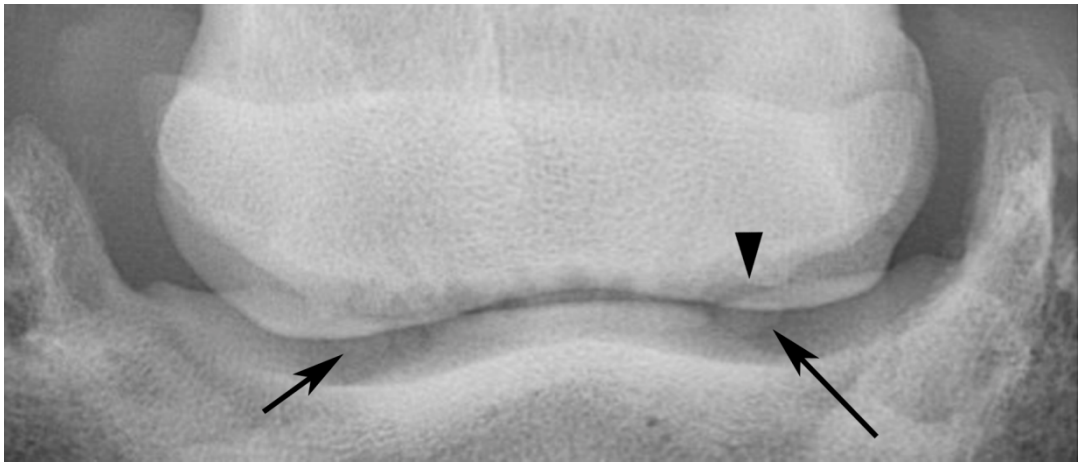

Fig. 12: Dorso 55° proximal-palmarodistal oblique radiographic projection of a navicular bone with a bony fragment at the lateral and medial distal sloping borders of the bone (arrows). A fracture bed is clearly visible medially (arrowhead). Left = lateral.

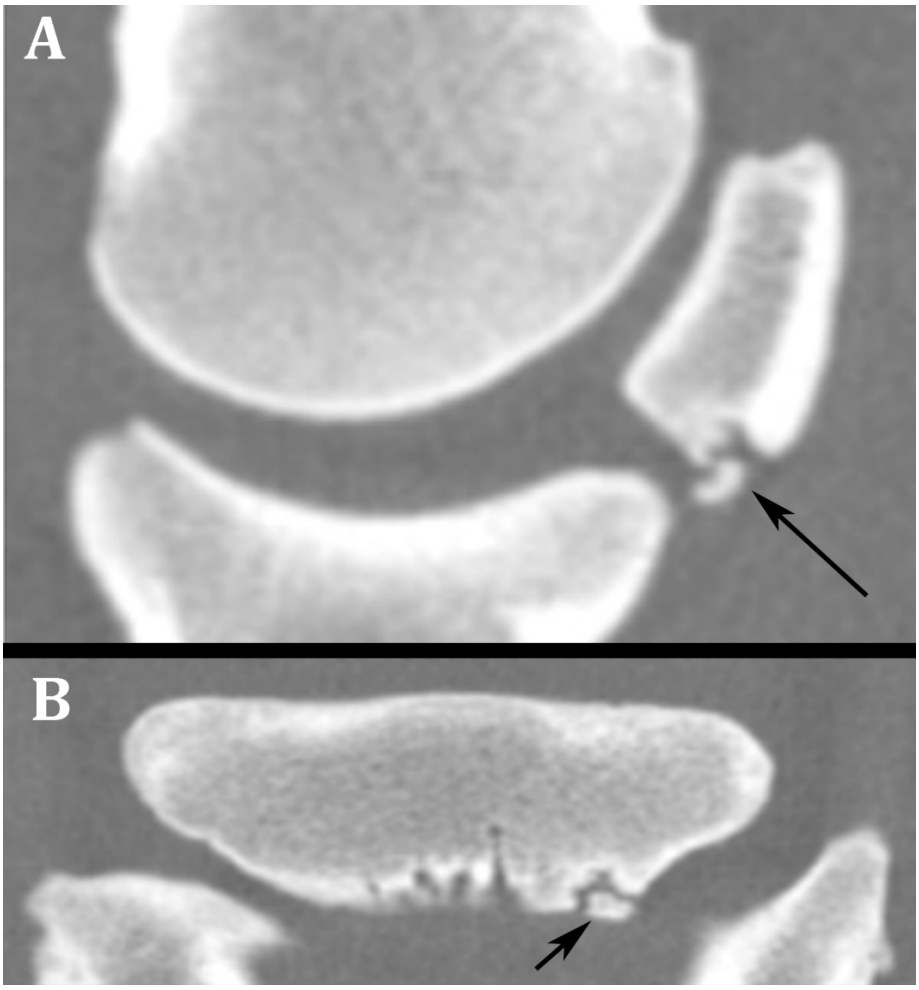

Fig. 13: Sagittal (A) and dorsal (B) reconstructed CT images with bone window settings of an equine navicular bone. A bony opacity with corresponding fracture bed is visible at the distomedial aspect of the bone (arrows). Left = dorsal (A); lateral (B). Courtesy of E.HJ. Bergman, Veterinary clinic 'The Lingehoeve', Lienden, the Netherlands.

Fragments at the proximal border of the navicular bone are rare and may reflect an avulsion fracture or fracture of an entheseophyte at the insertion of the CSL (13, 14).

Navicular sepsis

Puncture wounds of the hoof are frequently diagnosed in equines. Deep wounds in the central area of the frog and sulci can produce severe lameness. They are generally caused by nails or other foreign bodies, and can injure the DDFT, digital flexor tendon sheath, DSIL, navicular bursa, navicular bone, DIPJ and/or distal phalanx (40). Secondary bone changes, such as traumatic fractures, septic osteitis of the distal phalanx, osteomyelitis of the navicular bone and presence of a sequestrum, can be diagnosed. Radiography with the puncture object still in place should be performed, to evaluate the location and depth of the puncture tract. Radiographic signs of navicular bone infection are usually focal, ill-defined radiolucent areas in the flexor compact bone with disruption and irregularity of the flexor surface (36). It is important to take follow-up radiographs since these radiographic signs may be apparent 3 to 4 weeks post-injury. Positive contrast radiography (fistulography, bursography and/or arthrography) is a helpful diagnostic tool for identifying the tract and synovial structure involvement (41). Standing low-field MRI is useful in evaluating DDFT lesions and bone pathology associated with a penetrating wound (42).

Podotrochleosis - Navicular disease - Navicular syndrome

The term podotrochleosis, navicular disease or navicular syndrome denotes a progressive disorder typically affecting riding horses of middle age**,** and causes lameness of most frequently the forelimb(s) (43, 44). The aetiology and pathogenesis of the disease is still not completely understood and several theories have been proposed. Abnormalities observed in horses with navicular disease include injuries of the navicular bone, DDFT, ligaments and synovial structures such as the navicular bursa and DIPJ. Those abnormalities were also diagnosed in the hind foot of horses with hindlimb lameness, although less common (45). Radiography allows evaluation of navicular bone abnormalities associated with the disease, such as flexor surface defect, cystic lucency, proximal border remodelling, medullary sclerosis (thicker trabeculae), rounded- or inverted flask-shaped distal border synovial

invaginations and fragmentation of the distal border of the navicular bone (44, 46, 47) (Fig. 14). The recommended radiographic projections for evaluation of the foot are a LM, at least 2 DPr-PaDiO with different angles to the horizontal and a PaPr-PaDiO projection (14, 48). With respect to radiography, osseous changes of the navicular bone are more clearly defined with CT (16).

The presence of bony changes on radiographs is further based on the duration of the disease process. In a study of horses with recent onset of clinical navicular disease (< 6 months lameness duration), 86% of the horses had a hyperintense signal in the navicular bone on STIR sequences, but did not (yet) show radiographic abnormalities (49).

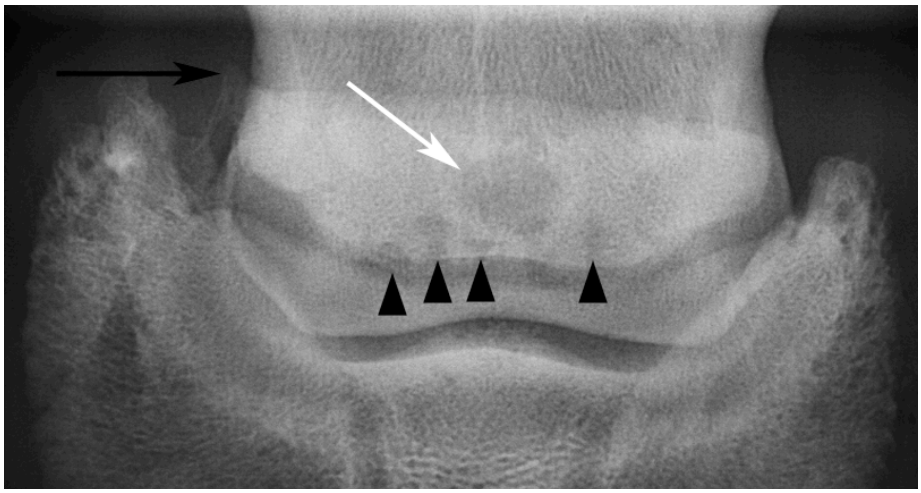

Fig. 14: Dorsoproximal-palmarodistal oblique projection of the left front foot of an 18-year-old Belgian Warmblood gelding with a history of bilateral chronic lameness. There is an osseous cyst-like lesion present in the navicular bone (white arrow), several abnormal (lollipop-) shaped distal border synovial invaginations (arrowheads) and an entheseophyte at the lateral margin of the proximal flexor border of the navicular bone (black arrow). These radiographic features are compatible with navicular disease. Left = lateral.

Ultrasonography is widely used and complementary to radiography. The normal tendon fibres of the DDFT proximal to the navicular bone are dark gray to black on an US exam through the bulbs of the heels, and echogenic areas in that region represent pathology such as fibrosis, mineralisations or malaligned fibres (50). The dorsal border of the DDFT has to be evaluated with care, since small irregularities may occur and represent fibrillation, granulation tissue herniation or degenerative changes (50). Also the DDAL, of which only the proximal part can be differentiated, has to be evaluated ultrasonographically for thickening and changes of echogenicity. A transcuneal approach is required for more distal lesions, however, lesions

located abaxially may be missed (19, 39, 51). Desmopathy of the CSL with concurrent navicular bursitis has been shown by the use of ultrasound (52).

As described above, MRI is used to identify soft tissue and cartilage/subchondral bone lesions associated with navicular disease. On MRI images, lesions of the DDFT, DSIL and CSL appear as a (focal) high to intermediate signal intensity on T2*-w gradient echo (GRE) images within the low signal tissues, with thickening of the tendon and ligaments (53, 54) (Figs. 15 and 16). In a study of horses with foot pain, abnormalities of the DDFT, DSIL, CSL, DIPJ and navicular bursa were seen in 82.6%, 38.2%, 10.5%, 42.3% and 49.4% of limbs, respectively (55). Although these percentages may differ among studies, the DDFT remains the most common affected structure and lesions in this tendon were more often located at the level of the CSL, proximal to the navicular bone, with core lesions, sagittal splits or dorsal abrasions as main findings (49, 53, 55). Recognition of the magic angle artifact is important to not misdiagnose pathology for example at the insertion site of the DDFT. This artifact occurs when collagen fibers are at angles of approximately 54.7° relative to the main magnetic field, and an increase in signal intensity in the tendon and/or ligament is seen (56-58). The main methods to avoid diagnostic confusion due to the magic angle effect, is to increase the echo time of the pulse sequence or use T2-w sequences. Navicular bone pathology has been shown to be associated with navicular bursitis and deep digital flexor tendonitis (50, 55). Fibrocartilage degeneration (thinning or loss of fibrocartilage) is a common pathological finding in horses with navicular disease and is best observed with MRI (23, 47, 59). They are frequently associated with soft tissue changes, such as adhesions with and pathology of the DDFT (13, 36, 59). The presence of intrabursal adhesions represents a poor prognosis. With the use of magnetic resonance bursography, the presence of small cartilage lesions as well as adhesions can be evaluated more clearly compared to non-contrast (plain) MRI images (60, 61). Injection of 6 ml of contrast medium has been described to be sufficient to separate the flexor surface of the navicular bone from the dorsal border of the DDFT (61). Injection of saline solution may also be interesting to highlight the navicular bursa and intrabursal adhesions, however, in standing horses only adhesions at the level of the proximal recess of the bursa can be detected due to loading of the DDFT (62). Changes in the bone contour of the palmar aspect of the navicular bone (flexor surface erosions) are better seen with CT and MRI than with conventional radiography (Fig. 17) (22, 23). These erosions can be seen radiographically when they are markedly deep and hence visible on the Pa(Pl)Pr-Pa(Pl)DiO at a certain angle of obliquity, and/or on the LM (22). Flexor surface defects has to be

differentiated from real osseous cyst-like lesions, which are defined on MRI images as well-defined fluid-filled lesions in the medulla of the navicular bone, separated from the synovial invaginations and not associated with any detectable abnormality of the compact bone and/or flexor surface fibrocartilage (63). The osseous cyst-like lesion is visualised as an area of increased signal intensity in the navicular bone on STIR images and intermediate signal intensity on T1-w GRE images, usually surrounded by a hypointense (mineralized) rim (63).

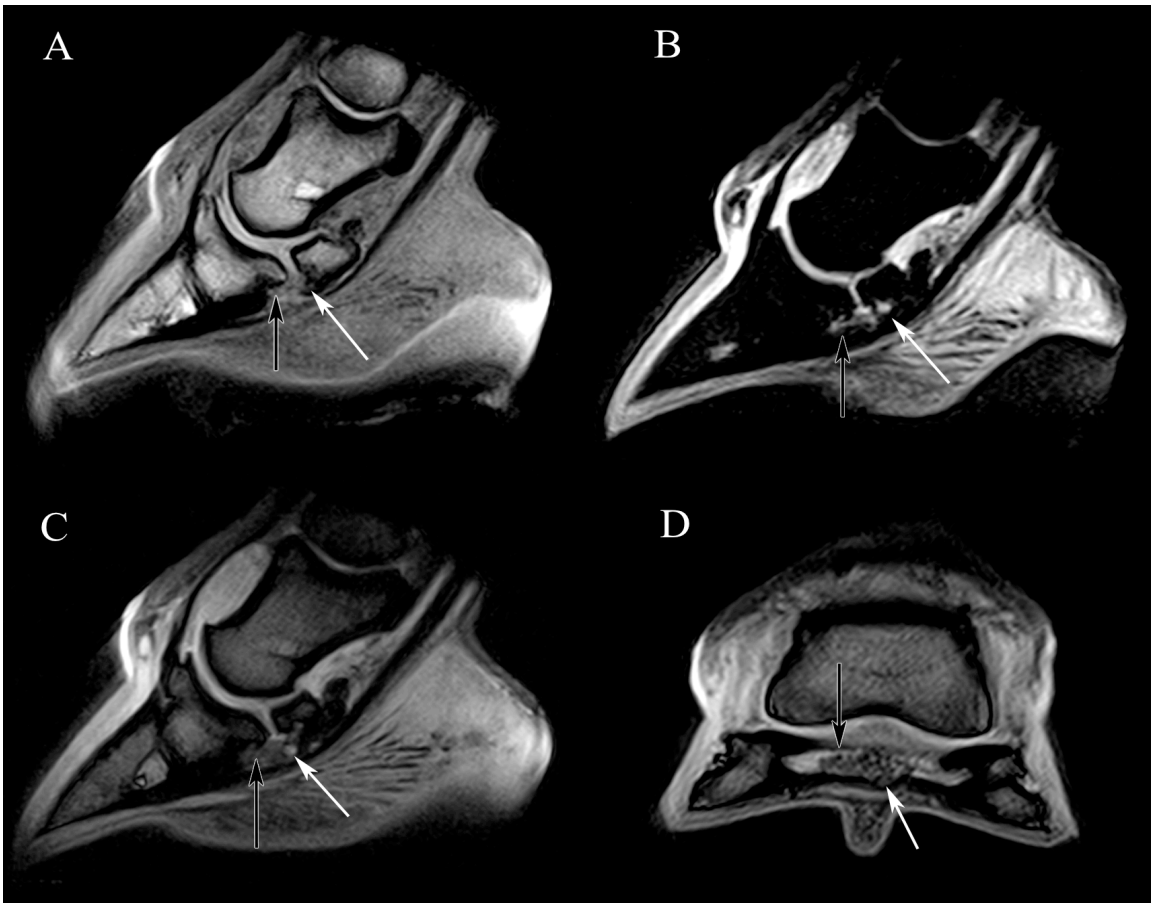

Fig. 15: Sagittal T1-weighted GRE (A), STIR (B), T2*-weighted GRE (C) and transverse T2*-weighted GRE (D) MRI images of the right front foot of an 11-year-old Belgian Warmblood gelding. A) – C): There is a focal hyperintense T2* and STIR signal, and hypointense T1 signal visible at the palmarodistal aspect of the navicular bone (white arrows) and palmaroproximal aspect of the third phalanx (black arrows), corresponding to the origin and insertion of the distal sesamoidean impar ligament. D) The distal sesamoidean impar ligament is thickened, irregularly delineated and shows a heterogenous signal intensity (black arrow). There is a hyperintense signal visible at the dorsal border of the medial lobe of the deep digital flexor tendon, opposing the distal sesamoidean impar ligament (white arrow). Chronic entheseopathy and desmitis of the ligament was diagnosed, in combination with deep digital flexor tendinopathy. Left = dorsal (A-C); lateral (D). Courtesy of F. Vandenberghe, Veterinary clinic 'The Bosdreef', Moerbeke-Waas, Belgium.

Fig. 16: Transverse 3D T1-weighted GRE MRI image at the supra-sesamoidean region of the right front foot of a 9-year-old Dutch Warmblood gelding. There is a focal hyperintense dorsal border lesion visible in the lateral lobe of the deep digital flexor tendon (arrow), with corresponding enlargement of the lobe. Left = lateral; top = dorsal. Courtesy of F. Vandenberghe, Veterinary clinic 'The Bosdreef', Moerbeke-Waas, Belgium.

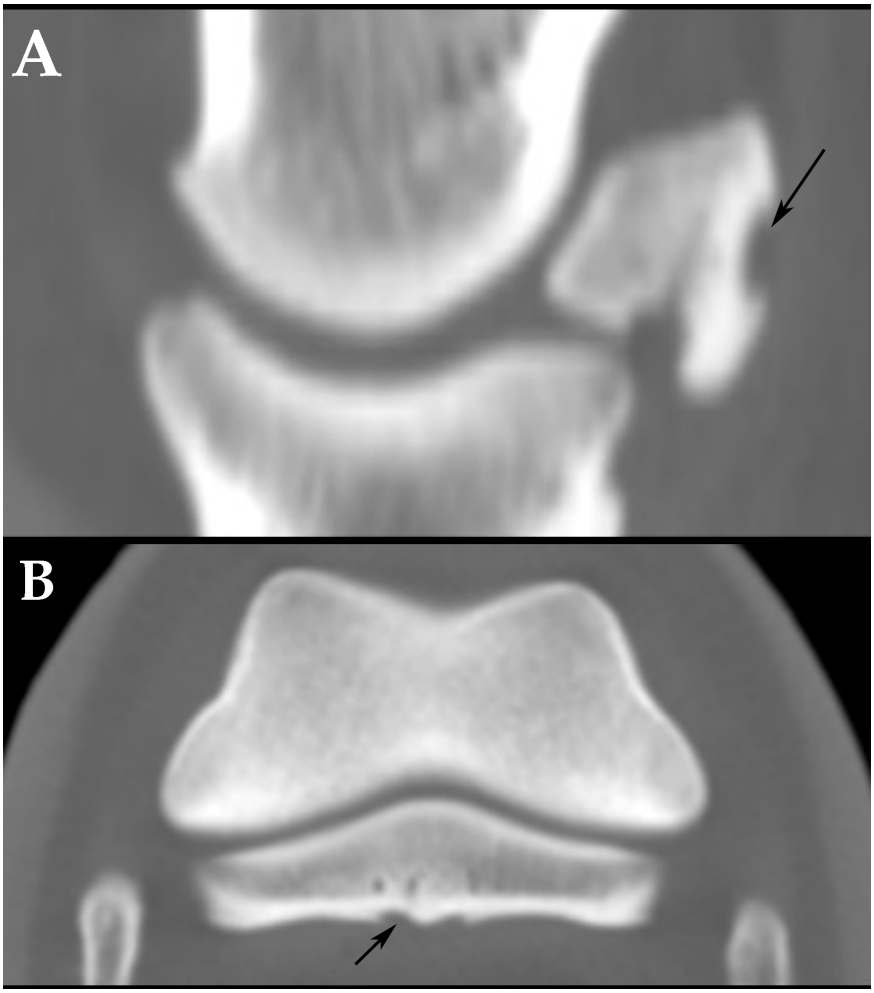

Fig. 17: Sagittal (A) and transverse (B) CT images with bone window settings of the left front foot of a 13-year-old Warmblood horse with foot lameness. A focal, well-demarcated defect of the flexor compact bone, involving the sagittal ridge of the navicular bone, is seen (arrows). The medullary cavity along the flexor surface is sclerotic. Left = dorsal (A); medial (B). Courtesy of E.HJ. Bergman, Veterinary clinic 'The Lingehoeve', Lienden, the Netherlands.

Computed tomography is the most appropriate imaging modality for detailed imaging of bony disorders and its diagnostic use for detecting soft tissue lesions has been improved by the administration of intra-arterial contrast (24, 64). Moreover, CE-CT has been suggested as an alternative to MRI for pathology of the DDFT (65) (Fig. 18). By the administration of intra-arterial contrast, the vascular patency of the lesions and information concerning the inflammation or healing of the tissue can be assessed. Contrast enhanced-CT more often identified a lesion at the level of the DDFT insertion and in the DSIL and CSL, than plain CT or low-field MRI (64).

The authors choose to use the term ‘navicular disease’ consistently throughout the text of this research project, since this term is frequently cited in the refered literature and used in daily practice.

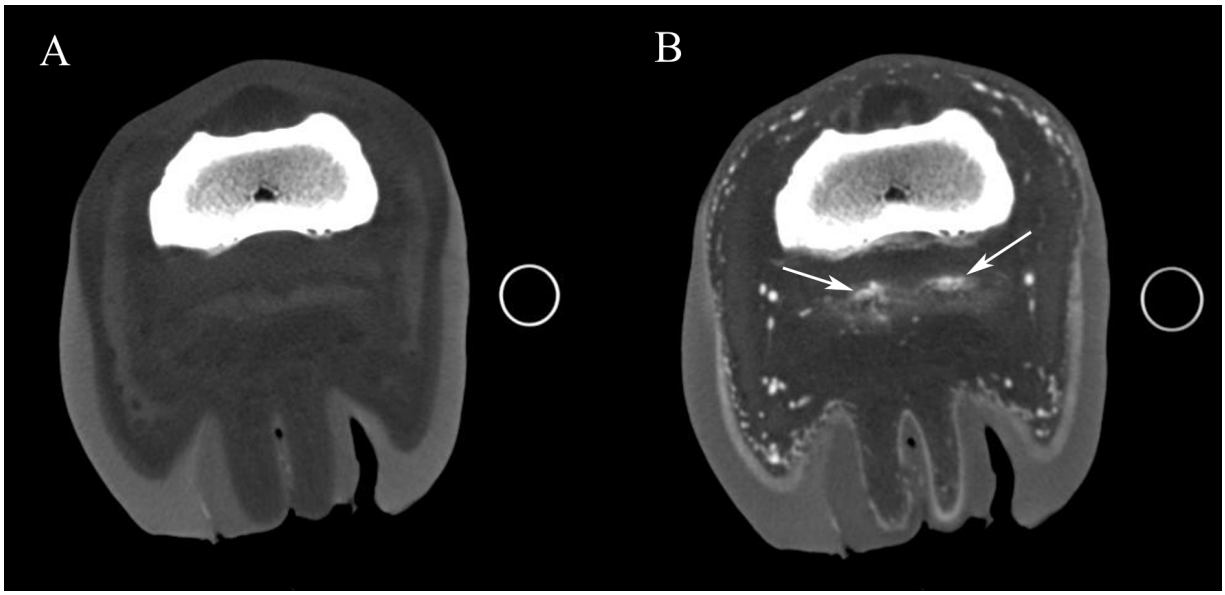

Fig. 18: Transverse pre- (A) and postcontrast (B) CT images with soft tissue window settings at the supra-sesamoidean region of the left front limb of a 13-year-old Dutch Warmblood gelding. A) Both lobes of the deep digital flexor tendon are enlarged and irregularly shaped. B) After contrast administration, the lesions are centrally, diffusely, moderately contrast enhancing (arrows). A deep digital flexor tendinopathy of the medial and lateral lobes was diagnosed. Left = lateral; top = dorsal. Courtesy of E.HJ. Bergman, Veterinary clinic ‘The Lingehoeve’, Lienden, the Netherlands.

REFERENCES

1. Rijkenhuizen A.B.M., Németh F., Dik K.J., et al. Development of the navicular bone in foetal and young horses, including the arterial supply. Equine Vet J 1989; 21: 405-412.
2. Dik K.J., van den Belt A.J.M., Enzerink E., et al. The radiographic development of the distal and proximal double contours of the equine navicular bone on dorsoproximal-palmarodistal oblique (upright pedal) radiographs, from age 1 to 11 months. Equine Vet J 2001; 33: 70-74.
3. Gabriel A., Jolly S., Detilleux J., et al. Morphometric study of the equine navicular bone: variations with breed and types of horses and influence of exercise. J. Anat. 1998; 193: 535-549.
4. Rijkenhuizen A.B.M., Németh F., Dik K.J., et al. The arterial supply of the navicular bone in the normal horse. Equine Vet J 1989; 21: 399-404.
5. Hertsch B., Dammer H. The blood supply of normal and diseased navicular bones. Vet Rad 1988; 29: 276-281.
6. Rijkenhuizen A.B.M., Németh F., Dik K.J., et al. The arterial supply of the navicular bone in adult horses with navicular disease. Equine Vet J 1989; 21: 418-424.
7. Colles C.M., Hickman J. The arterial supply of the navicular bone and its variations in navicular disease. Equine Vet J 1977; 9: 150-154.
8. Colles C.M. Ischaemic necrosis of the navicular bone and its treatment. Vet Record; 104: 133-137.
9. Rijkenhuizen A.B.M., Németh F., Dik K.J., et al. The effect of artificial occlusion of the Ramus navicularis and its branching arteries on the navicular bone in horses: An experimental study. Equine Vet J 1989; 21: 425-430.
10. Pleasant R.S., Baker G.J., Foreman J.H., et al. Intraosseous pressure and pathological changes in horses with navicular disease. Am J Vet Res 1993; 54: 7-12.
11. MacGregor C.M. Radiographic assessment of navicular bones, based on changes in the distal nutrient foramina. Equine Vet J 1986; 18: 203-206.
12. Gabriel A., Jolly S., Detilleux J. et al. Radiographic study of the sound navicular bone. Part 1: What about the canals on the distal border? Ann Méd Vét 1998; 142: 345-352.

13. Butler J.A., Colles C.M., Dyson S.J., et al. Foot, pastern and fetlock. In: Clinical Radiology of the Horse. Butler J.A., Colles C.M., Dyson S.J., Kold S.E., Poulos P.W.J. (eds), 2nd ed., Blackwell Science, Oxford, UK 2000: 21-130.
14. Dyson S. Radiological interpretation of the navicular bone. Equine Vet Educ 2008; 20: 268-280.
15. Sterc J., Crhakova T. Comparison of findings from oblique radiographs of the raised limb with those of the weight-bearing limb for selected diseases of the equine digit. Acta Vet Brno 2007; 76: 97-103.
16. Widmer W.R., Buckwalter K.A., Fessler J.F., et al. Use of radiography, computed tomography and magnetic resonance imaging for evaluation of navicular syndrome in the horse. Vet Radiol Ultrasound 2000; 41: 108-116.
17. Grewal J.S., McClure S.R., Booth L.C., et al. Assessment of the ultrasonographic characteristics of the podotrochlear apparatus in clinically normal horses and horses with navicular syndrome. J Am Vet Med Assoc 2004; 225: 1881-1888.
18. Bolen G., Busoni V., Jacqmot O. et al. Sonographic anatomy of the palmarodistal aspect of the equine digit. Vet Radiol Ultrasound 2007; 48: 270-275.
19. Busoni V., Denoix J.M. Ultrasonography of the podotrochlear apparatus in the horse using a transcuneal approach: technique and reference images. Vet Radiol Ultrasound 2001; 42: 534-540.
20. Puchalski, S.M. Advances in equine computed tomography and use of contrast media. Vet Clin North Am Equine 2012; 28: 563-581.
21. Tietje S. Computed tomography of the navicular bone region in the horse: a comparison with radiographic documentation. Pferdeheilkunde 1995; 11: 51-61.
22. Groth A.M., May S.A., Weaver M.P., et al. Intra- and interobserver agreement in the interpretation of navicular bones on radiographs and computed tomography scans. Equine Vet J 2009; 41: 124-129.
23. Whitton R.C., Buckley C., Donovan T., et al. The diagnosis of lameness associated with distal limb pathology in a horse: A comparison of radiography, computed tomography and magnetic resonance imaging. Vet J 1998; 155: 223-229.
24. Puchalski S.M., Galuppo L.D., Hornof W.J., et al. Intraarterial contrast-enhanced computed tomography of the equine distal extremity. Vet Radiol Ultrasound 2007; 48: 21-29.

25. Puchalski S.M., Snyder J.R., Hornof W.J., et al. Contrast-enhanced computed tomography of the equine distal extremity. In *Proceedings* 51th Annu Convention of Am Ass Equine Practnrs, Seattle, WA, USA 2005.
26. Collins J.N., Galuppo L.D., Thomas H.L., et al. Use of computed tomography angiography to evaluate the vascular anatomy of the distal portion of the forelimb of horses. Am J Vet Res 2004; 65: 1409–1420.
27. Desbrosse F.G., Vandeweerd J.-M.E.F., Perrin R.A.R., et al. A technique for computed tomography (CT) of the foot in the standing horse. Equine Vet Educ 2008; 20: 93-98.
28. Pooley R.A. Fundamental physics of MR imaging. Radiographics 2005; 25: 1087-1099.
29. Dyson S., Blunden. T., Murray R. Comparison between magnetic resonance imaging and histological findings in the navicular bone of horses with foot pain. Equine Vet J 2012; 44: 692-698.
30. Dyson S., Murray R., Schramme M. et al. Magnetic resonance imaging of the equine foot: 15 horses. Equine Vet J 2003; 35: 18-26.
31. Murray R.C., Blunden T.S,, Schramme M.C., et al. How does magnetic resonance imaging represent histologic findings in the equine digit? Vet Radiol Ultrasound 2006; 47: 17-31.
32. Bolen G., Audigié F., Spriet M. et al. Qualitative comparison of 0.27T, 1.5T and 3T magnetic resonance images of the normal equine foot. J Equine Vet Science 2010, 30: 9-20.
33. Dyson S., Murray R. Use of concurrent scintigraphic and magnetic resonance imaging evaluation to improve understanding of the pathogenesis of injury of the podotrochlear apparatus. Equine Vet J 2007; 39: 365-369.
34. Dyson S. Subjective and quantitative scintigraphic assessment of the equine foot and its relationship with foot pain. Equine Vet J 2002; 34: 164-170.
35. Lillich J.D., Ruggles A.J., Gabel A.A. et al. Fracture of the distal sesamoid bone in horses: 17 cases (1982-1992). J Am Vet Med Assoc 1995; 207: 924-927.
36. Toal R.L. The navicular bone. In: Textbook of Veterinary Diagnostic Radiology, 4th ed. Thrall D.E., ed. Saunders, Philadelphia, USA, 2002: 295-305.
37. Modransky P., Thatcher C.D., Welker F.H. et al. Unilateral phalangeal dysgenesis and navicular bone agenesis in a foal. Equine Vet J 1987; 19: 347-349.

38. Colles C.M. Navicular bone fractures in the horse. Equine Vet Educ 2011; 23: 255-261.
39. Heitzmann A.G., Denoix J.-M. Rupture of the distal sesamoidean impar ligament with proximal displacement of the distal sesamoid bone in a steeplechaser. Equine Vet Educ 2007; 19: 117-120.
40. Honnas C.M., Dabareiner R.M., McCauley B.H. Hoof wall surgery in the horse: approaches to and underlying disorders. Vet Clinic North Am Equine 2003; 19: 479-499.
41. Smith R.K.W., Schramme M.C.The use of contrast agents in the diagnosis of penetrating wounds of the foot in five cases. Equine Vet Educ 1992; 4: 177-182.
42. Kinns J., Mair T.S. Use of magnetic resonance imaging to assess soft tissue damage in the foot following penetrating injury in 3 horses. Equine Vet Education 2005; 17: 69-73.
43. Wright I.M. A study of 118 cases of navicular disease: clinical features. Equine Vet J 1993; 25: 488-492.
44. Dyson S., Murray R., Schramme M. et al. Current concepts of navicular disease. Equine Vet Educ 2011; 23: 27-39.
45. Biggi M., Dyson S. Hind foot lameness: Results of magnetic resonance imaging in 38 horses (2001-2011). Equine Vet J 2012; DOI: 10.1111/j.2042-3306.2012.00686.
46. Wright I.M. A study of 118 cases of navicular disease: radiological features. Equine Vet J 1993; 25: 493-500.
47. Wright I.M., Kidd L., Thorp B.H. Gross, histologic and histomorphometric features of the navicular bone and related structures in the horse. Equine Vet J 1998; 30: 220-234.
48. Seyrek-Intas D., Tellhelm B., Reckels F.-J. Interpretation and diagnostic value of some radiological findings in the navicular bone. Pferdeheilkunde 1999; 15: 406-418.
49. Sampson S.N., Schneider R.K., Gavin P.R., et al. Magnetic resonance imaging findings in horses with recent onset navicular syndrome but without radiographic abnormalities. Vet Radiol Ultrasound 2009; 50: 339-346.
50. Seignour M., Pasquet H., Coudry V. et al. Ultrasonographic diagnosis of injuries to the deep digital flexor tendon and associated structures in the equine foot (suprasesamoidean area). Equine Vet Educ 2011; 23: 369-376.
51. Sage A.M., Turner T.A. Ultrasonography of the soft tissue structures of the equine foot. Equine Vet Educ 2002; 14: 221-224.

52. Jacquet S., Coudry V., Denoix J.-M. Severe tear of the collateral sesamoidean ligament in a horse. Vet Record 2006; 159: 818-820.
53. Dyson S., Murray R., Schramme M., Branch M. Magnetic resonance imaging of the equine foot: 15 horses. Equine Vet J 2003; 35: 18-26.
54. Zubrod C.J., Farnsworth K.D., Tucker R.L. et al. Injury of the collateral ligaments of the distal interphalangeal joint diagnosed by magnetic resonance. Vet Radiol Ultrasound 2005; 46: 11-16.
55. Dyson S., Murray R. Magnetic resonance imaging evaluation of 264 horses with foot pain: The podotrochlear apparatus, deep digital flexor tendon and collateral ligaments of the distal interphalangeal joint. Equine Vet J 2007; 39: 340-343.
56. Spriet M., Zwingenberger A. Influence of the position of the foot on MRI signal in the deep digital flexor tendon and collateral ligaments of the distal interphalangeal joint in the standing horse. Equine Vet J 2009; 41: 498-503.
57. Spriet M., McKnight A. Characterization of the magic angle effect in the equine deep digital flexor tendon using a low-field magnetic resonance system. Vet Radiol Ultrasound 2009; 50: 32-36.
58. Busoni V., Snaps F. Effect of deep digital flexor tendon orientation on magnetic resonance imaging signal intensity in isolated equine limbs-the magic angle effect. Vet Radiol Ultrasound 2002; 43: 428-430.
59. Sherlock C., Mair T., Blunden T. Deep erosions of the palmar aspect of the navicular bone diagnosed by standing magnetic resonance imaging. Equine Vet J 2008; 40: 684-692.
60. Schramme M., Kerekes Z., Hunter S. et al. Improved identification of the palmar fibrocartilage of the navicular bone with saline magnetic resonance bursography. Vet Radiol Ultrasound 2009; 50: 606-614.
61. Maher M.C., Werpy N.M., Goodrich L.R. et al. Positive contrast magnetic resonance bursography for assessment of the navicular bursa and surrounding soft tissues. Vet Radiol Ultrasound 2011; 52: 385-393.
62. Gutierrez-Nibeyro S.D., Werpy N.M., White II N.A. Standing low-field magnetic resonance imaging in horses with chronic foot pain. Australian Vet J 2012; 90: 75 – 83.
63. Biggi M. and Dyson S. High-field magnetic resonance imaging investigation of distal border fragments of the navicular bone in horses with foot pain. Equine Vet J 2011, 43: 302-308.

64. Vallance S.A., Bell R.J.W., Spriet M. et al. Comparisons of computed tomography, contrast-enhanced computed tomography and standing low-field magnetic resonance imaging in horses with lameness localized to the foot: Part 2: Lesion identification. Equine Vet J 2012; 44: 149-156.
65. Puchalski S.M., Galuppo L.D., Drew C.P. et al. Use of contrast-enhanced computed tomography to assess angiogenesis in deep digital flexor tendonopathy in a horse. Vet Radiol Ultrasound 2009; 50: 292-297.

SCIENTIFIC AIMS

Foot pain is a major cause of lameness in the horse. Radiography is the first choice imaging modality for the diagnosis of bony changes in these horses. A common cause of uni- or bilateral foot pain is podotrochleosis, better known as navicular syndrome. Abnormalities of the navicular bone are frequently observed radiographically in horses with navicular syndrome, such as fragmentation and/or abnormal (in number, depth and/or shape) synovial invaginations at the distal navicular border. During a pre-purchase examination, radiographic evaluation of the navicular bone is performed routinely, since in sound horses, distal border abnormalities are considered prognostic indicators for future lameness.

The **general aim** of this research project was to describe the morphology of the distal border synovial invaginations of the navicular bone using radiography and CT, and to further unravel the etiopathogenesis of distal border fragments of the navicular bone.

Compared to radiography, CT is a more advanced imaging modality. To diagnose the source of foot pain on images, a good anatomical knowlegde is essential. To date, only one report describes the CT anatomy of the equine foot briefly, and a thorough comparison between the anatomy of the equine foot and CT is lacking. Therefore, the aim of the first two studies was to describe a detailed CT reference of the anatomically normal equine foot (**first** study, Chapter 3), and to describe in detail the morphology of the synovial invaginations of the equine navicular bone by the use of CT (**second** study, Chapter 4).

The second aim was to describe if radiography accurately assess the distal border synovial invaginations. The hypothesis was that the radiographic evaluation of the synovial invaginations is possibly not accurate and could maybe improve. Therefore, in the **thirth** study (Chapter 5), the variability and agreement between the morphology of distal border synovial invaginations of the navicular bone on radiography versus CT were calculated. In the **fourth** study (Chapter 6) the value of a hoof-angle dependent radiographic projection was studied.

The **fifth** and last study of this thesis (Chapter 7) aimed to be a contribution to the study of the etiopathogenesis of distal border fragmentation. It was hypothesized that distal navicular border fragments could be associated with other radiological abnormalities predicting navicular disease, including the shape of the proximal articular border of the navicular bone.

CHAPTER 3

Computed tomographic anatomy of the equine foot

Adapted from: Claerhoudt S, Bergman E.H.J, Saunders J.H. Computed tomographic anatomy of the equine foot. Anatomia, Histologia, Embryologia 2013; DOI: 10.1111/ahe.12091.

SUMMARY

This study describes a detailed CT reference of the anatomically normal equine foot. Ten forefeet of 5 adult cadavers, euthanized for reasons unrelated to the musculoskeletal system, were used. Computed tomography was performed on all feet. Two-mm thick transverse slices were obtained, and sagittal and dorsal planes were reformatted. The CT images were matched with the corresponding anatomical slices. The phalanges and the navicular bone showed excellent detail. The extensor and flexor tendons (including their attachments) could be clearly evaluated. The CSL could be readily located, but were difficult to delineate at their proximal attachment. The DDAL could only be distinguished from the DDFT proximal to the navicular bone, and its proximal attachment could be identified, but not its distal insertion. Small ligaments (impar ligament, chondrosesamoidean, -coronal, and –compedal ligaments, axial and abaxial palmar ligaments of the proximal interphalangeal joint (PIPJ), and 'T-ligament') were seen with difficulty and not at all slices. The joint capsules could not be delineated from the surrounding soft tissue structures. The lateral and medial proprius palmar digital artery and vein could be visualised occasionally on some slices. The ungular cartilages, corium and hoof wall layering were seen. The nerves, the articular and fibrocartilage of the navicular bone, and the chondroungular ligament could not be assessed. Computed tomography of the equine foot can be of great value when results of radiography and US are inconclusive. The compilation of images obtained in this study may serve as reference for CT in horses with foot injuries.

CHAPTER 3

INTRODUCTION

Foot pain is a major cause of lameness in the horse. Radiography is the first imaging modality for investigating disorders affecting the foot, however it provides few information regarding soft tissues changes (1). Ultrasonography is widely available and for most body parts, it is complementary to radiography. However, ultrasonography of the podotrochlear apparatus of the foot is complicated due to the hoof capsule. Therefore, cross-sectional imaging modalities such as CT and MRI may be required to arrive at a conclusive diagnosis.

Computed tomography is gaining interest to the equine clinician for the evaluation of bony and soft tissue injury in the horse. Computed tomography is superior to radiography in the diagnosis of subtle bone changes and specific bone pathology, such as complex comminuted fractures and their assessment prior to surgery, due to the acquisition of high-resolution images without superimposition (1, 2). Unfortunately, the use of CT in imaging the distal limb is still limited by the necessity for a general anaesthesia and consequent high costs. For the evaluation of the soft tissues of the foot, CT is considered inferior to MRI (1, 3), however, with the advent of CE-CT of the foot, the characterization of soft tissue changes within the hoof capsule with CT, has tremendously improved (4, 5). The vascular anatomy of the distal portion of the equine limb has been described by the use of CT-angiography (6). The purpose of the study was to describe a detailed CT reference of the anatomically normal equine foot.

MATERIALS AND METHODS

CT examination

Ten forefeet of 5 adult horses euthanized for reasons unrelated to the musculoskeletal system were used. The horses were euthanized with a combination[a] of embutramide, mebenzoniumiodide, and tetracaïne hydrochloride (4 to 6 mL/50 kg) injected intravenously via the vena jugularis. The feet were disarticulated at the metacarpophalangeal joint. To ensure the feet were anatomically normal, they were inspected, palpated and radiographed (LM and DPr-PaDiO projections). The CT examination was obtained within 24 hours after euthanasia. The CT scans were performed with a 4-detector row spiral CT scanner[b] in which the feet were placed in the gantry with the longitudinal axis of the foot oriented parallel to the CT table and perpendicular to the plane of the CT gantry. The medial side of the foot was placed upwards. The limbs were scanned in a proximo-to-distal direction. The output parameters were 120 kV and 280 mAs per slice. The slice thickness was 2 mm, pitch of 0.875 cm, 1 mm increment and 1-second rotation time. A bone window setting (WW: 2000 HU; WL: 300 HU) and 512 x 512 pixel matrix was used. The average total time required for scanning of each foot was 71.06 seconds. From the transverse images, sagittal and dorsal reconstructions with a slice thickness of 2 mm were reformatted by use of software[c]. The images were also analyzed with a soft tissue setting (WW: 280 HU; WL: 120 HU).

Image Analysis

Image analysis was performed by a PhD-student (SC) on a diagnostic imaging viewing station and flat screen monitor[d]. The CT images were used for the qualitative assessment of the phalanges, navicular bone, flexor and extensor tendons, collateral ligaments of the DIPJ and PIPJ, sesamoidean ligaments (CSL and DSIL), chondrosesamoidean, -coronal, –compedal and –ungular ligaments, axial and abaxial palmar ligaments of the PIPJ, DDAL, hoof wall, ungular cartilages, navicular bursa and digital flexor tendon sheath. The bones were evaluated qualitatively for assessment of the cortical and trabecular bone definition, and the synovial invaginations of the navicular bone.

Quantitative data were determined by use of manually drawn regions of interest (ROI). The macroscopic size and location of the ROIs within the same structure were similar. Quantitative data were collected by measuring the HU values of several soft tissue structures in 3 horses on images with the soft tissue window settings: the DDFT, collateral ligaments of

the DIPJ, CSL, ungular cartilages, hoof wall, frog and digital cushion. Mean values and standard deviation were calculated for each structure. The ROI was drawn, following the external surface of the tendon, ligaments and ungular cartilages, at 3 different locations of the DDFT: level PIPJ, level proximal portion of the navicular bone and level distal attachment of the DDFT to the distal phalanx; at the level of the proximal portion of the navicular bone for the collateral ligaments of the DIPJ, ungular cartilages, hoof wall, frog and digital cushion; and at the level of the mid portion of the middle phalanx for the CSL. The ROI were drawn centrally in the toric part of the digital cushion and frog, and followed the external margins of the hoof wall.

Anatomic sections

For this part of the study, the same feet were used as for the CT examinations. Four limbs were frozen in extension for at least 48 hours at -18°. Afterwards, they were cut with an electric bandsaw[e] into slices of approximately 10 mm thick, in a sagittal, parasagittal, dorsal or transverse plane. All anatomic sections were photographed.

Comparison of CT and anatomic images

For each slice, the corresponding CT image of the same foot was chosen on the basis of similar appearance. The bony and soft tissue structures were identified on the anatomic sections and corresponding CT images. For this purpose, a published atlas was consulted (7).

RESULTS

Computed tomographic images (in bone and soft tissue windows) from 10 sections in 3 planes were selected (Fig. 1) and compared with the corresponding anatomic slices: 6 in the transverse (Fig. 2), 2 in the dorsal (Fig. 3), and 2 in the sagittal plane (Fig. 4).

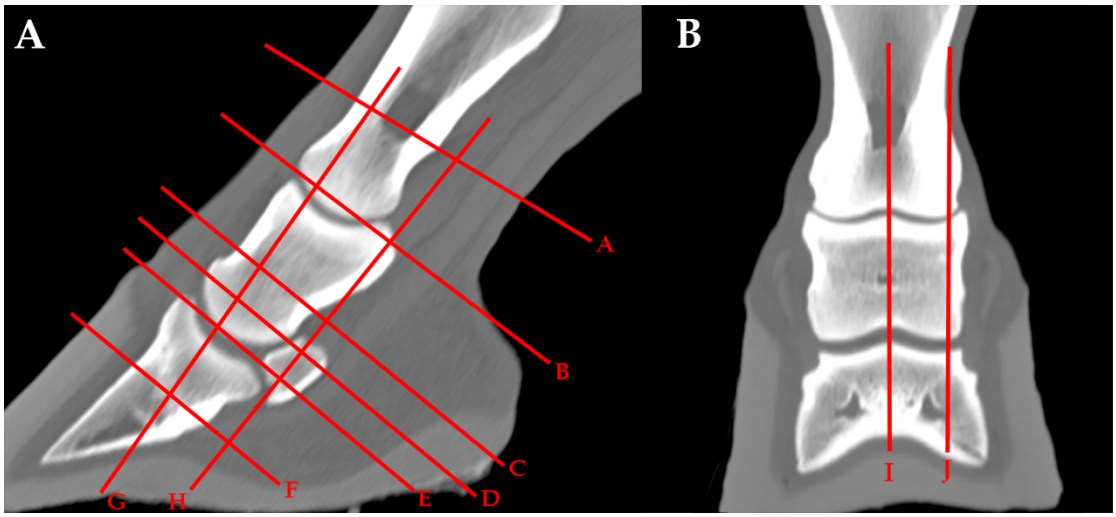

Fig. 1: A – Sagittal CT reconstructed view. Selected planes for the transverse CT images were the distal portion of the first phalanx (A), proximal interphalangeal joint space (B), mid portion of the middle phalanx (C), proximal portion of the navicular bone (D), distal interphalangeal joint space (E), and distal attachment of the deep digital flexor tendon (F). Selected planes for the dorsal CT images were attachments sites of the collateral ligaments (G), and attachments sites of the middle scutum and sesamoidean ligaments at the navicular bone (H). B – Dorsal CT reconstructed view. Selected planes for the sagittal CT images were the midsagittal plane (I), and parasagittal view (through the extremity of the navicular bone) (J).

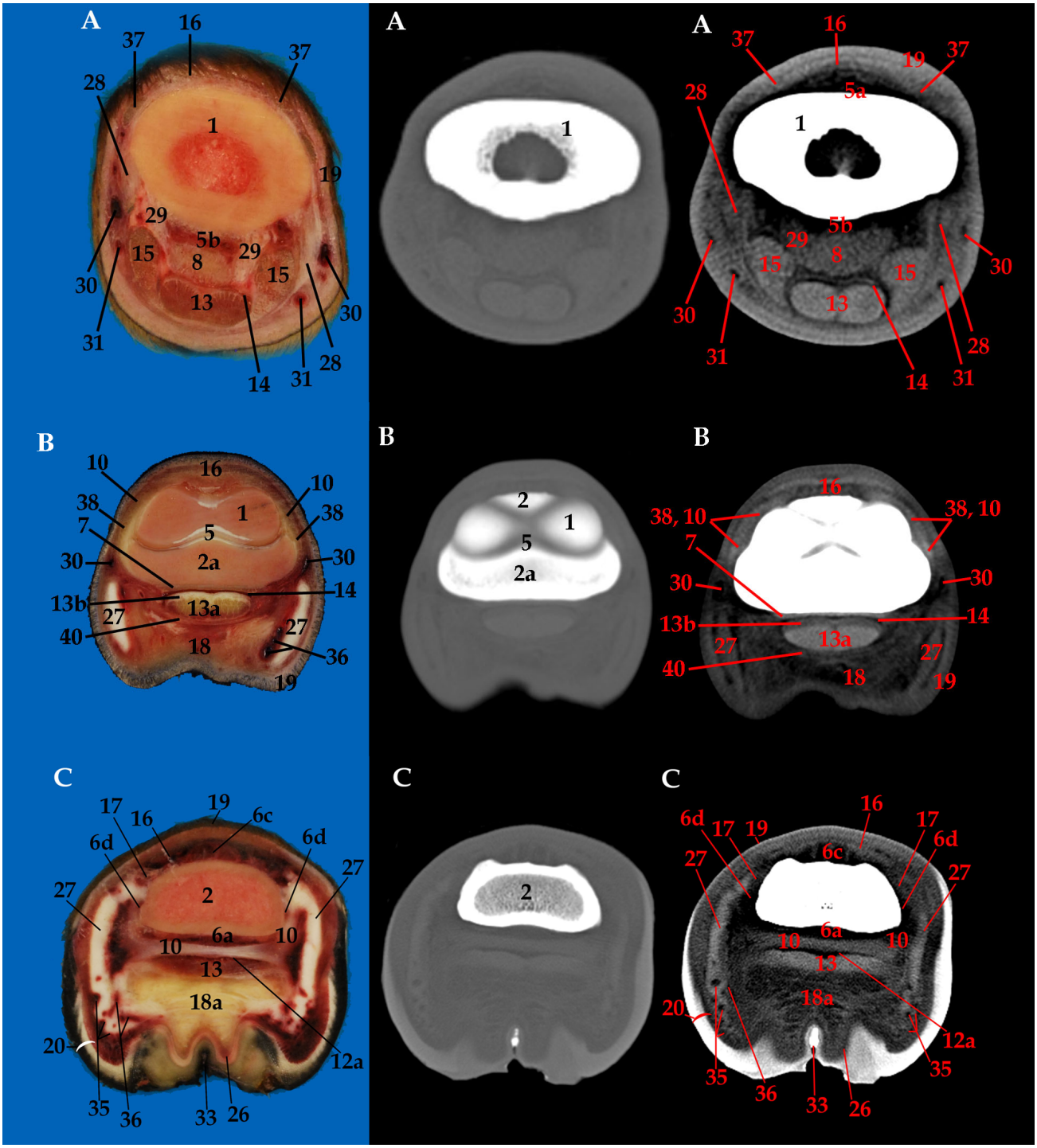
A
16
37
37
28
1
19
29
5b
15
8
29
15
30
13
30
31
14
31
28
B
10
16
10
38
1
38
7
5
30
2a
30
14
13b
27
13a
27
40
18
36
19
C
17
16
19
6c
6d
6d
27
27
2
10
6a
10
13
18a
20
12a
35
36
33
26
A
1
A
37
16
19
37
28
5a
1
5b
29
8
15
15
30
30
13
31
14
31
28
B
2
1
5
2a
B
16
38, 10
38, 10
7
30
30
13b
14
27
13a
27
40
18
19
C
2
C
6d
17
19
16
17
6d
27
6c
27
10
6a
10
13
18a
20
12a
35
36
33
26
35

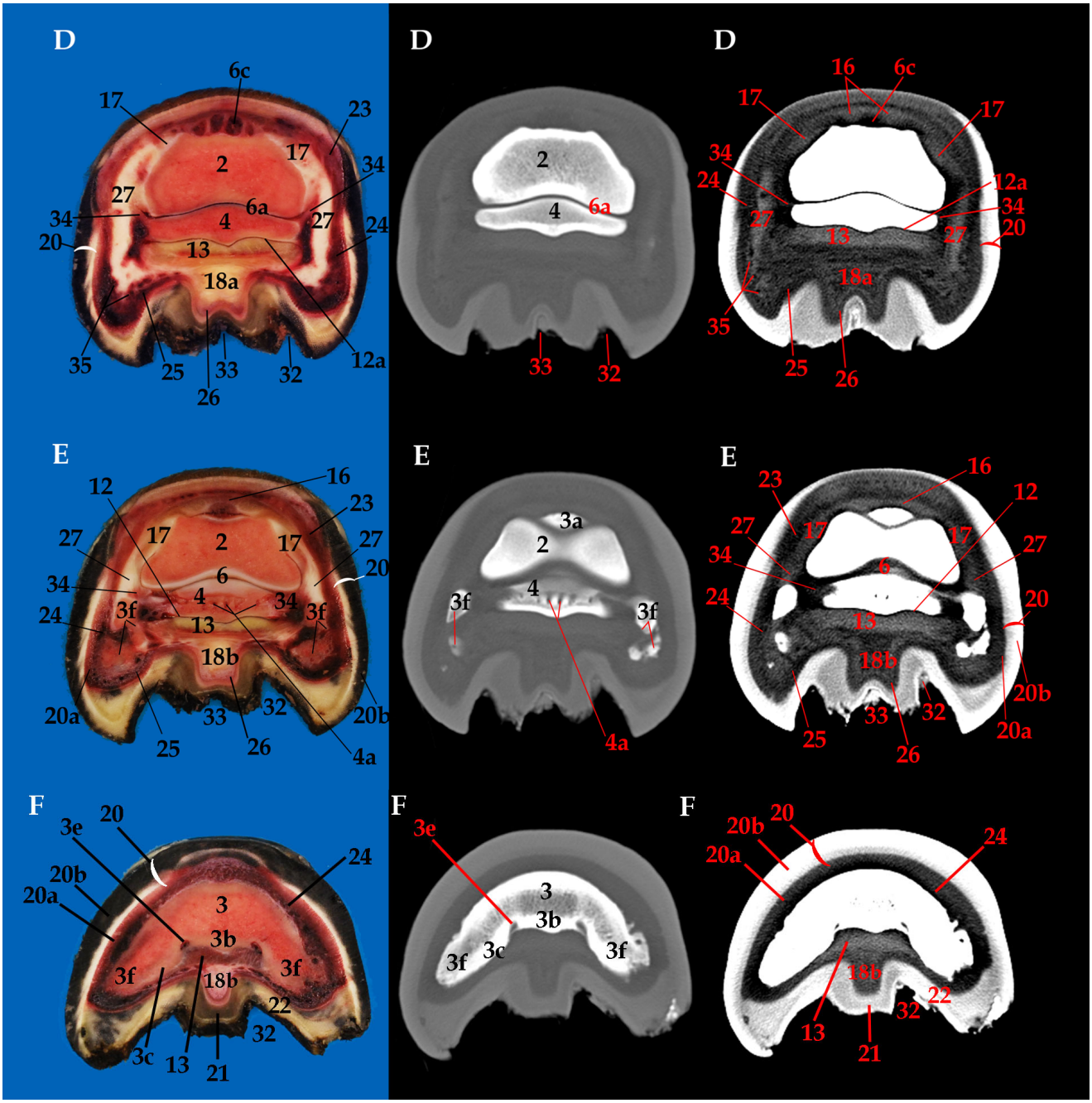
D
6c
17
23
2
17
34
27
6a
34
4
27
24
20
13
18a
35
25
33
32
12a
26
D
2
4
6a
33
32
D
16
6c
17
17
34
24
12a
34
27
13
27
20
18a
35
25
26
E
12
16
23
27
17
2
17
27
20
6
34
4
34
3f
3f
24
13
18b
20a
33
32
20b
25
26
4a
E
3a
2
4
3f
3f
4a
E
16
23
12
27
17
17
27
34
6
24
20
13
18b
20b
33
32
25
20a
26
F
20
3e
24
20b
20a
3
3b
3f
3f
18b
22
32
3c
13
21
F
3e
3
3b
3f
3c
3f
F
20b
20
20a
24
18b
22
32
13
21

Fig. 2: Photographs of transverse anatomic sections (left) and transverse CT images (middle: bone window, right: soft tissue window) sequentially displayed from proximal to distal (planes A-F as shown in Fig. 1A) as illustrated in Fig. 1. (1: proximal phalanx; 2: middle phalanx: 2a = flexor tuberosity; 3: distal phalanx: 3a = extensor process; 3b = flexor surface; 3c = planum cutaneum (compact bone); 3e = solar canal; 3f = palmar process; 4: navicular bone: 4a = synovial invaginations; 4b = flexor surface (compact bone); 5: proximal interphalangeal joint: 5a = dorsal recess; 5b = palmar recess; 6: distal interphalangeal joint: 6a = palmaroproximal recess; 6c = dorsal recess; 6d = collateral recess; 7: middle scutum; 8: straight sesamoidean ligament; 10: proximal (collateral) sesamoidean ligament; 11: distal sesamoidean impar ligament; 12: navicular bursa: 12a = proximal recess; 13: deep digital flexor tendon: 13a = fibrous part; 13b = fibrocartilaginous part; 14: digital flexor tendon sheath (cavity); 15: superficial digital flexor tendon; 16: dorsal digital extensor tendon; 17: collateral ligament of the distal interphalangeal joint; 18: digital cushion: 18a = toric part; 18b = cuneal part; 19: skin; 20: hoof wall: 20a = stratum internum; 20b = stratum medium + externum; 21: frog; 22: sole; 23: corium coronae; 24: corium parietis (with dermal lamellae); 25: corium soleae; 26: corium cunei; 27: ungular cartilage; 28: abaxial palmar ligament of the proximal interphalangeal joint; 29: axial palmar ligament of the proximal interphalangeal joint; 30: proper palmar digital vein; 31: proper palmar digital artery; 32: paracuneal sulcus; 33: central cuneal sulcus; 34: chondrosesamoidean ligament; 35: superficial ungular plexus; 36: deep ungular plexus; 37: extensor branch of the suspensory ligament; 38: collateral ligament of the proximal interphalangeal joint; 40: distal digital annular ligament). Left = lateral; top = dorsal.

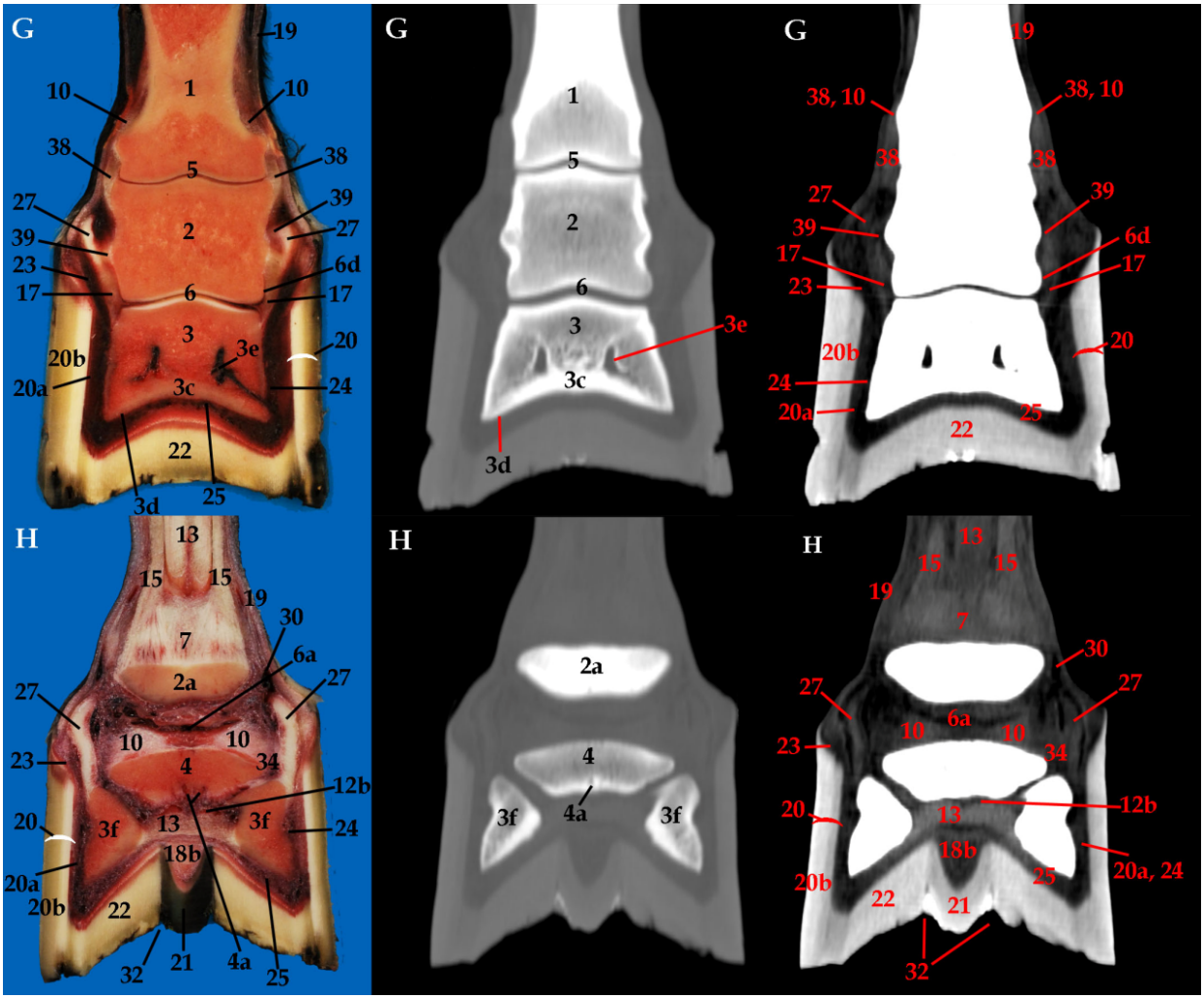

Fig. 3: Photographs of dorsal anatomic sections (left) and dorsal reconstructed CT images (middle: bone window, right: soft tissue window) (planes G and H as shown in Fig. 1A). (12b = distal recess of podotrochlear bursa; 39: chondrocoronal ligament). See Fig. 2 for remainder of key. Lateral = left; top = proximal.

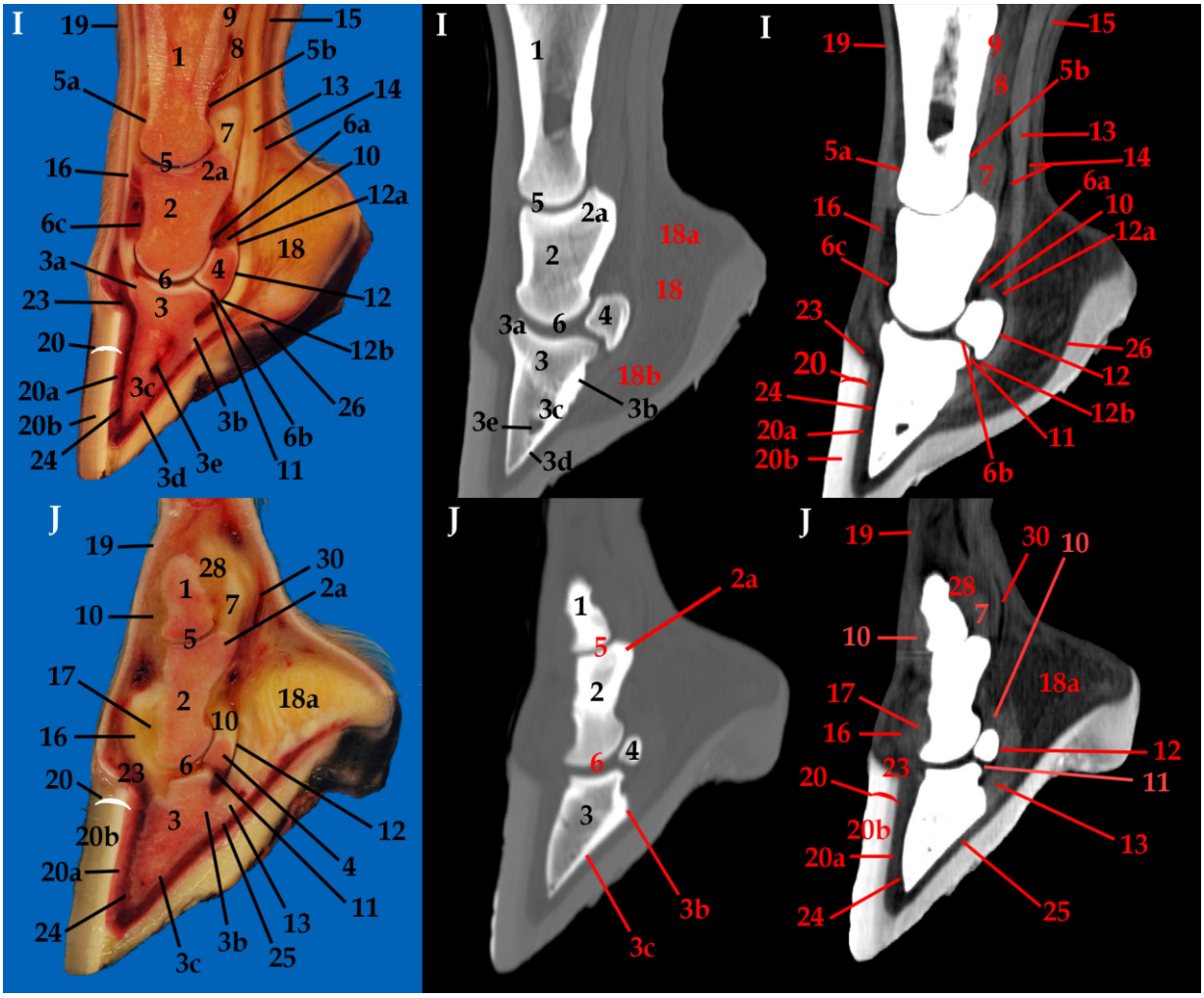

Fig. 4: Photographs of sagittal anatomic sections (left) and sagittal reconstructed CT images (middle: bone window, right: soft tissue window) (planes I and J as shown in Fig. 1B). (3d = solar border of the distal phalanx; 6b = palmarodistal recess of distal interphalangeal joint; 9: oblique sesamoidean ligament). See Figure 2 for remainder of key. Left = dorsal; top = proximal.

With image window and level settings adjusted for bone, the distal portion of the proximal phalanx, the middle and distal phalanges, and navicular bone were seen on the transverse-, dorsal- and sagittal-plane images. The compact, subchondral and spongious bone with its trabecular pattern, could be well differentiated on all images. The shape of the semilunar sinus, solar canal and perforating vascular channels of the distal phalanx could be well evaluated on the images with bone window settings. Sagittal and dorsal reconstructed views allowed clear delineation of the proximal and distal interphalangeal joint spaces, however the cartilage of the articular surfaces of the phalanges and navicular bone, and fibrocartilage of the flexor surface of the navicular bone, could not be identified on these plain CT images. The synovial invaginations at the distal border of the navicular bone could be depicted on all

three-plane images.

The HU values of the DDFT, collateral ligaments of the DIPJ, CSL, ungular cartilages, hoof wall, frog and digital cushion are summarized in Table 1.

Table 1: Mean HU ± SD values of the deep digital flexor tendon (DDFT), collateral ligaments (Col ligg) of the distal interphalangeal joint (DIPJ), collateral sesamoidean ligaments (CSL), ungular cartilages, hoof wall, frog and digital cushion, measured in 3 horses at variable sites on CT images with a soft tissue window.

Level	DDFT	Col ligg of DIPJ	CSL	Ungular cartilage	Hoof wall	Frog	Digital cushion
PIPJ	102 ± 8	-	-	-	-	-	-
Mid P2	-	-	61 ± 4	-	-	-	-
Prox navbone	91 ± 6	70 ± 7	-	115 ± 9	277 ± 6	179 ± 8	18 ± 3
Attach DDFT	86 ± 9	-	-	-	-	-	-

- = not applicable. Attach DDFT = level distal attachment of the deep digital flexor tendon to the distal phalanx. Mid P2 = level of mid portion of the middle phalanx. Prox navbone = level proximal portion of the navicular bone.

Images using a soft tissue window and level setting were useful to visualize the distal parts of dorsal digital extensor tendon, deep and superficial digital flexor tendons. The transverse images suited best to evaluate the tendons, which appeared as homogeneous, hyperattenuating, well-defined structures. The dorsal digital extensor tendon had a very wide and flat appearance. Its distal insertion on the extensor processes of the middle and distal phalanx was clearly seen on the sagittal reconstructed image (Fig. 4, section I). The fusion of the tendon with the extensor branches of the suspensory ligament was visible on the transverse images (Fig. 2, section A). At the level of the pastern region, the DDFT had a bilobed shape on the transverse images and its borders were well demarcated. More distally, the tendon became more flattened in a dorsal to palmar direction and inserted broadly on the palmar flexor surface of the distal phalanx (Fig. 2, section F). The margins of the distal DDFT could not be clearly delineated. With the soft tissue settings, the less attenuating fibrocartilaginous part at the dorsal aspect of the DDFT at the level of the proximal

interphalangeal joint (PIPJ) could be differentiated from its palmar fibrous part. Palmarly, the DDAL was only distinguishable from the palmar aspect of the DDFT proximal to the navicular bone. Its abaxial proximal attachment sites to the distal epicondyles of the proximal phalanx could be identified, but its distal insertion on the flexor surface of the distal phalanx not.

The distal attachment of the superficial digital flexor tendon and the straight sesamoidean ligament to the middle phalanx could be clearly evaluated. They both insert on the flexor tuberosity of the middle phalanx and form the middle scutum, which is a fibrocartilaginous structure (7).

The dorso- and palmarodistal recesses of the digital flexor tendon sheath (cavity) were best visualized on the sagittal and transverse images, as a thin hypoattenuating rim surrounding the DDFT. Other synovial structures, including the 5 synovial recesses of the DIPJ, 2 of the PIPJ and navicular bursa, could be located upon the CT images, particularly on the transverse images, due to the presence of hypoattenuating synovial fluid and intermediate attenuating synovium. The heterogeneous appearance of the dorsal recess of the DIPJ was evident on the transverse images (Fig. 2, section C). The joint capsule of the PIPJ and DIPJ could not be delineated from its surrounding soft tissue structures.

On the soft tissue window, the collateral ligaments of the distal and proximal interphalangeal joints could be readily identified, and appeared as homogeneous, symmetric, well-defined hyperattenuating structures. They were less hyperattenuating than the DDFT (Table 1). Anatomically, the collateral ligaments of the DIPJ originate proximally at the collateral fossae of the middle phalanx, run obliquely in a palmarodistal direction and insert on the collateral fossae of the distal phalanx (7). On the transverse images (Fig. 2, sections C and D), a close connection between the collateral ligament and ipsilateral, ungular cartilage was visualised. In fact, no clear separation between the entire ligament and ungular cartilage could be seen.

The ungular cartilages could be identified on all plane images with soft tissue window and level settings, as ill-defined structures, with a mild heterogeneous appearance and an intermediate attenuation between the frog and DDFT (see Table 1). The chondroungular ligament could not be differentiated on the CT images. The chondrosesamoidean, -coronal and -compedal ligaments were seen with difficulty and not at all images (Fig. 2). Anatomically, these ligaments connect the ungular cartilages with the navicular bone, middle and proximal phalanx, respectively (7). The chondrocoronal ligament is inserted close to the proximal insertion of the collateral ligament of the DIPJ.

At the superficial and deep aspects of the ungular cartilages, a hypoattenuating venous plexus

could be visualised on particularly the transverse images (Fig. 2, section C and D).

The ungular cartilages were strongly connected to the digital cushion. The cushion could be clearly assessed and had a heterogeneous, hypoattenuating appearance, compatible with its fatty and fibro-elastic architecture.

Other ligaments such as the DSIL, the axial and abaxial palmar ligaments of the PIPJ and the 'T-ligament' were identified with difficulty and not at all slices. The sagittal reconstructed images suited best for the visualisation of the short but wide DSIL. Anatomically, this ligament separates the DIPJ from the distal recess of the navicular bursa (7).

Parts of the 'T-ligament' could be seen (mainly the part attaching to the DDFT), but the ligament was overall difficult to delineate and to differentiate from the proximal (collateral) sesamoidean ligament.

On the dorsal slice at the level of the navicular bone (Fig. 3, section H), it can be clearly seen that the CSL are sagittally united to a broad ligament, nowadays called the 'proximal sesamoidean ligament', which is inserted on the entire proximal flexor border of the navicular bone. It had a triangular-shape and homogeneous appearance on the midsagittal section image (Fig. 4, section I). On all 3 planes, the ligament was well-defined and clearly outlined. The CSL could be seen on the transverse images, and appeared as symmetric, homogeneous, well-defined, oval-shaped structures, iso-attenuating to the collateral ligaments of the DIPJ. Proximally, the CSL were difficult to evaluate on the CT images (Fig. 3, section G) and a close palmar connection with the collateral ligaments of the PIPJ was seen.

The different layers of the hoof wall could be differentiated on the images. Also the corium could be occasionally seen, which appeared more hypoattenuating than the hoof wall. The stratum internum of the hoof wall is made of soft horn, and its epidermal lamellae are linked to the dermal lamellae of the corium parietis. Differentiation between both is possible on particularly the transverse images. The corium parietis is made of dermal lamellae and the corium coronae, soleae and cunei of papillae (7). The corium is intensely vascularised by the proprius digital artery. On CT, the soft horn of the frog is less attenuating than the hoof wall (Table 1).

The lateral and medial proprius palmar digital artery and vein could be visualised occasionally on some slices. Their dorsal and palmar anastomoses at the level of the phalanges and navicular bone could not be visualised on this plain CT images. The lateral and medial proprius digital nerve could not be seen.

CHAPTER 3

DISCUSSION

The present study was carried out to provide a detailed reference of CT anatomy of the equine foot. A sparse CT anatomic description of normal equine feet has been published in 1988, where they concluded that CT appeared excellent for the evaluation of osseous structures, but insufficient for soft tissue structures (8). Only single (transverse) plane images with a slice thickness of 5 mm were obtained by a second-generation scanner, and no comment was given over the used soft tissue settings. In the current study, 2 mm thick slices were made with a 4-slice spiral CT scanner, in 3 planes and with an appropriate bone and soft tissue algorithm.

As already concluded in the ’90s, CT is the most appropriate imaging modality for detailed imaging of bony disorders. Pathological changes of the navicular bone were better visualized and defined on CT images compared to radiographs (1-3). In the present study, the subchondral, compact and spongious bone with trabecular pattern were well depicted on all images with bony window.

Results of the current study showed that CT also displayed the soft tissue structures of the foot by use of soft tissue window and level settings. The soft tissue assessment with CT has been described in previous studies (9-11). A clear evaluation and border differentiation of several ligaments such as the DSIL, the collateral ligaments of the DIPJ, the chondrosesamoidean, -coronal, and –compedal ligaments, the axial and abaxial palmar ligaments of the PIPJ, ‘T-ligament’ and distal part of the DDAL, was difficult to impossible on the CT images. This can be explained by the close anatomical connection of some soft tissue structures, such as the collateral ligaments of the DIPJ with the ungular cartilage and chondrocoronal ligament, the collateral ligaments of the PIPJ with the CSL, and the DDAL adherence to the DDFT (7, 12) and by the inherent weaknesses of CT as diagnostic modality. The visualisation of structures is dependant on their anatomy and location, and the imaging technique specific factors, such as the slice thickness and pixel matrix (13). Computed tomography produces detailed, high spatial resolution images (ability to select a very small slice thickness) and requires less anaesthetic time, due to its higher scanning speed compared to MR imaging. It is a very sensitive technique for subtle bone changes and is described as superior to radiography and MRI for the evaluation of the distal border synovial invaginations and fragments of the navicular bone (1, 14). The disadvantages of CT are that it is limited by patient size, its necessity for a general anaesthesia and consequent higher costs, and its low contrast for tissues with similar attenuation such as soft tissues and fluid (15). A reasonable

alternative is the standing low-field MRI which avoids general anaesthesia. The strength of MRI is that it has excellent soft tissue contrast, allows detection of osseous hyperintenstity (in case of bone edema, necrosis, fibrosis, hemorrhage), cartilage damage and soft tissue lesions (16). Magnetic resonance imaging has been proven to represent accurately the histopathological findings of soft tissues in the foot (17). The disadvantages are its longer scanning time compared to CT, and its high sensitivity for metallic artifacts.

The characterization of soft tissue changes within the hoof capsule has tremendously improved with the advent of the multiplanar, cross-sectional diagnostic imaging techniques, CT and MRI. Computed tomography has been reported as inferior to MRI for the detection of soft tissue injury (1, 3), however, recent studies have demonstrated that its diagnostic use for soft tissue lesions has been improved by the use of contrast media (5, 11, 13, 15, 18-20). Moreover, intra-arterial contrast administration (CE-CT) has been suggested as an alternative to MRI for diagnosis of pathology of the DDFT (18). The vascular patency of the lesions and information concerning the inflammation or healing of the tissue can be assessed by its degree of contrast enhancement (12, 18). Intravascular contrast delivery to the foot was not performed in the current study since the contrast could obscure the anatomic visualization of structures (13).

A limitation of the present study is that no intrasynovial contrast was injected. If done so, the synovial structures, joint capsule and cartilage would be better visualised (13, 15).

In the present study, the fibrocartilage of the palmar surface of the navicular bone was not seen. Also, on MRI images, the fibrocartilage was not well visualized (1). With the use of magnetic resonance bursography, the presence of small fibrocartilage lesions as well as adhesions between the DDFT and navicular bone, can be evaluated more clearly compared to non-contrast MRI images (21, 22).

Histologically, the most distal part of the DDFT within the digital flexor tendon sheath is markedly infiltrated with fibrocartilage along its dorsal aspect (23). This hypoattenuating fibrocartilage layer can be seen on our CT images.

Based on the results of the present study, we may conclude that plain CT can be of value in the evaluation of particularly the bony and major soft structures of the equine foot. The images of this study could be used as a CT atlas in horses with foot pain, especially when radiography and US are inconclusive. As described above, recent literature has shown that the clinical utility of CT for the evaluation of soft tissues has gain more and more interest by the use of contrast media (including CE-CT, CT-arthrography and CT angiography).

FOOTNOTE

[a]T61©, Hoechst Roussel Vet GmbH, Unterschleissheim, Germany.

[b]Mx8000, Philips Medical Systems, AE Eindhoven, The Netherlands.

[c]Osirix Image processing Software, Geneva, Switzerland.

[d]Totoku monochrome LCD display, Lewisville, Texas, USA.

[e]Electric band saw, Eureka, Saviolo Lelio Snc, Coriano, Italy.

REFERENCES

1. Widmer W.R., Buckwalter K.A., Fessler J.F., et al. Use of radiography, computed tomography and magnetic resonance imaging for evaluation of navicular syndrome in the horse. Vet Radiol Ultrasound 2000; 41: 108-116.
2. Groth A.M., May S.A., Weaver M.P., et al. Intra- and interobserver agreement in the interpretation of navicular bones on radiographs and computed tomography scans. Equine Vet J 2000; 41: 124-129.
3. Whitton R.C., Buckley C., Donovan T., et al. The diagnosis of lameness associated with distal limb pathology in a horse: A comparison of radiography, computed tomography and magnetic resonance imaging. Vet J 1998; 155: 223-229.
4. Puchalski S.M., Galuppo L.D., Hornof W.J., et al. Intraarterial contrast-enhanced computed tomography of the equine distal extremity. Vet Radiol Ultrasound 2007; 48: 21-29.
5. Snyder J.R., Maher O., Puchalski S.M. Diagnosis of soft tissue injuries of the foot using contrast enhanced computed tomography. In *Proceedings* 10th Annu Meet Equine Med and Surgery 2007: 183-184.
6. Collins J.N., Galuppo L.D., Thomas H.L., et al. Use of computed tomography angiography to evaluate the vascular anatomy of the distal portion of the forelimb of horses. Am J Vet Res 2004; 65: 1409–1420.
7. Denoix J.M. The Equine Foot and The Equine Pastern. In: The Equine Distal Limb, London, UK: Manson Publishing Ltd 2000: 1-242.
8. Peterson P.R., Bowman K.F. Computed tomographic anatomy of the distal extremity of the horse. Vet Radiol 1988; 29: 147-156.
9. Vanderperren K., Ghaye B., Snaps F.R., et al. Evaluation of computed tomographic anatomy of the equine metacarpophalangeal joint. Am J Vet Res 2008; 69: 631-638.
10. Tietje S., Nowak M., Petzoldt S., et al. Computed tomographic evaluation of the distal aspect of the deep digital flexor tendon (DDFT) in horses. Pferdeheilkunde 2001; 17: 21-29.
11. Nowak M. The role of DDFT tendinitis in navicular syndrome – a CT perspective. In *Proceedings* 1th World Orthopaedic Veterinary Congress, Munich 2002: 155-156.

12. Puchalski S. Equine Foot. In: Veterinary Computed Tomography. Schwarz T., Saunders J., eds. UK: Wiley-Blackwell 2011: 463-471.
13. Vallance S.A., Bell R.J.W., Spriet M., et al. Comparisons of computed tomography, contrast-enhanced computed tomography and standing low-field magnetic resonance imaging in horses with lameness localized to the foot: Part 1: Anatomic visualization scores. Equine Vet J 2012; 44: 51-56.
14. Claerhoudt S., Bergman H.J., van der Veen H., et al. Differences in the morphology of distal border synovial invaginations of the distal sesamoid bone in the horse as evaluated with CT compared to radiography. Equine Vet J 2012; 44: 679-683.
15. Puchalski S.M. Advances in equine computed tomography and use of contrast media. Vet Clin North Am Equine 2012; 28: 563-581.
16. Kinns J., Mair T. Use of magnetic resonance imaging to assess soft tissue damage in the foot following penetrating injury in 3 horses. Equine Vet Educ 2005; 17: 69-73.
17. Murray R.C., Blunden T.S., Schramme M.C., et al. How does magnetic resonance imaging represent histologic findings in the equine digit? Vet Radiol Ultrasound 2006; 47: 17-31.
18. Puchalski S.M., Galuppo L.D., Hornof W.J., et al. Intraarterial contrast-enhanced computed tomography of the equine distal extremity. Vet Radiol Ultrasound 2007; 48: 21-29.
19. Puchalski S.M., Galuppo L.D., Drew C.P., et al. Use of contrast-enhanced computed tomography to assess angiogenesis in deep digital flexor tendonopathy in a horse. Vet Radiol Ultrasound 2009; 50: 292-297.
20. Vallance S.A., Bell R.J.W., Spriet M., et al. Comparisons of computed tomography, contrast-enhanced computed tomography and standing low-field magnetic resonance imaging in horses with lameness localized to the foot: Part 2: Lesion identification. Equine Vet J 2012; 44: 149-156.
21. Schramme M., Kerekes Z., Hunter S., et al. Improved identification of the palmar fibrocartilage of the navicular bone with saline magnetic resonance bursography. Vet Radiol Ultrasound 2009; 50: 606-614.
22. Maher M.C., Werpy N.M., Goodrich L.R., et al. Positive contrast magnetic resonance bursography for assessment of the navicular bursa and surrounding soft tissues. Vet Radiol Ultrasound 2011; 52: 385-393.

23. Kraus B.L., Kirker-Head C.A., Kraus K.H., et al. Vascular supply of the tendon of the equine deep digital flexor muscle within the digital sheath. Vet Surgery 1995; 24: 102-111.

CHAPTER 4

Computed tomographic morphology of the synovial invaginations of the navicular bone of the horse

Adapted from: Claerhoudt S, Bergman H.J, van der Veen H, Vanderperren K, Raes E.V, Saunders J.H. Computed tomographic morphology of the synovial invaginations of the distal sesamoid bone of the horse. Anatomia, Histologia, Embryologia 2011; 40: 55-60.

SUMMARY

The morphological features of the distal border synovial invaginations of the navicular bone in horses were described by use of CT. Transverse CT images were obtained on 50 cadaver forefeet from 25 Warmblood horses. Dorsal and sagittal planes were reformatted. The CT images allowed evaluation of the number, shape, depth of penetration and direction of the synovial invaginations into the bone. The total number of synovial invaginations was 295 (mean 5.9). The number of invaginations in a particular navicular bone ranged from 3 (n = 3), 4 (n = 6), 5 (n = 11), 6 (n = 12), 7 (n = 13), 8 (n = 3), 9 (n = 1) to 11 (n = 1). The shape of the synovial invaginations was ‘conical’ (n = 118), ‘linear’ (n = 109), ‘lollipop’ (n = 38) or ‘branched’ (n = 30). Penetration of the synovial invaginations into the navicular bone was ‘mild’ in 195 cases, ‘moderate’ in 67 cases and ‘deep’ in 33 cases. The synovial invaginations ran in a ‘straight’, ‘dorsoproximal’ and ‘palmaroproximal’ direction in 187, 28 and 80 cases, respectively. In only 6 navicular bones, all synovial invaginations ran in the same direction. The images obtained in this study may serve for future radiographic evaluation of these synovial invaginations.

CHAPTER 4

INTRODUCTION

The navicular bone is located between the distal part of the DDFT and the DIPJ. The navicular bone of the equine foot contains synovial invaginations, which are present along the distal, proximal and medial and lateral sloping borders of the bone. Radiographic evaluation of the distal border synovial invaginations, using a dorso45°-70°proximal-palmarodistal oblique (D45°-70°Pr-PaDiO) projection, is frequently included in the selection process of horses admitted as breeding stallion or in purchase examinations (1, 2). In the normal navicular bone, the synovial invaginations at the distal border of the navicular bone are radiographically visible as sharply delineated, conical-shaped radiolucent areas, while they are considered abnormal when they are increased in number and size, or when they show an inverted flask- or lollipop shape (3-5). These latter abnormalities are regarded, according to radiographic classification systems (1, 2), as moderate or severe radiographic findings, which are suggested to be responsible for future joint pain and lameness. However, literature lacks unanimity concerning the clinical relevance of radiographically abnormal synovial invaginations at the distal border of the navicular bone.

A recent study recorded that distal border synovial invaginations are recognized with a higher certainty with CT compared to radiography (6). In fact, CT is the most appropriate imaging modality for detailed imaging of normal bone and detection of bony disorders (7, 8). The possibility of reconstruction of multiplanar, high-resolution images without superimposition permits CT to provide detailed anatomical information of the synovial invaginations. Furthermore, radiography permits a limited assessment of bone changes since at least 30% of change in bone density is required before the change can be identified on radiographs (9).

To the authors' opinion, there is no study that describes the morphology in detail of the synovial invaginations of the navicular bone. Since CT provides unique anatomic information, the morphological features of the distal border invaginations of the navicular bone in the horse were described by the use of CT.

MATERIALS AND METHODS

Material

The material used in this study consisted of 50 forefeet of 25 Warmblood horses (age 3-9 years, mean weight 540 kg). All horses were subjected to euthanasia for reasons unrelated to this study. The medical history of the horses was unknown. All feet were severed at the level of the fetlock joint immediately after euthanasia. The shoe was removed and the sole was cleaned and trimmed. The feet were not selected by any particular criteria and both forefeet of each horse were included.

CT examination

The CT scans were performed with a 4-detector row spiral CT scanner[a] in which the feet were placed in the gantry with the longitudinal axis of the foot oriented parallel to the CT table and perpendicular to the plane of the CT gantry. A hollow polyvinylchloride pipe was attached at the medial side of the foot and used as an external marker. The limbs were scanned in a distal-to-proximal direction. The output parameters were 120 kV and 250 mAs per slice. The slice thickness was 0.6 mm, pitch of 0.875 cm, 0.3 increment and 1-second rotation time. Transverse CT scans were reconstructed from the level of the distal aspect to the level of the proximal aspect of the navicular bone using a bone window setting (WL: 200-600; WW: 1000-2000), 250 mm field of view and 512 x 512 pixel matrix. The average total time required for scanning of each foot was 46.25 seconds. From the transverse images, sagittal and dorsal reconstructions with a slice thickness of 0.6 mm were reformatted by use of software[b].

Image analysis

Image analysis was performed in consensus by one board-certified radiologist (JHS) and one PhD-student (SC). Four variables per navicular bone were evaluated: number, shape, depth of penetration into the bone and direction of the distal border synovial invaginations. The number of invaginations was determined using transverse slices and dorsal reconstructions. For this criterium, a numerical scale was recorded. The shape and depth of penetration of the invaginations were assessed using dorsal reconstructions. The shape was classified into ‘conical’, ‘linear’, ‘lollipop’ and ‘branched’ (Fig. 1). A synovial invagination was assigned as ‘branched-shaped’ when it had a single basis, but branched out towards proximally.

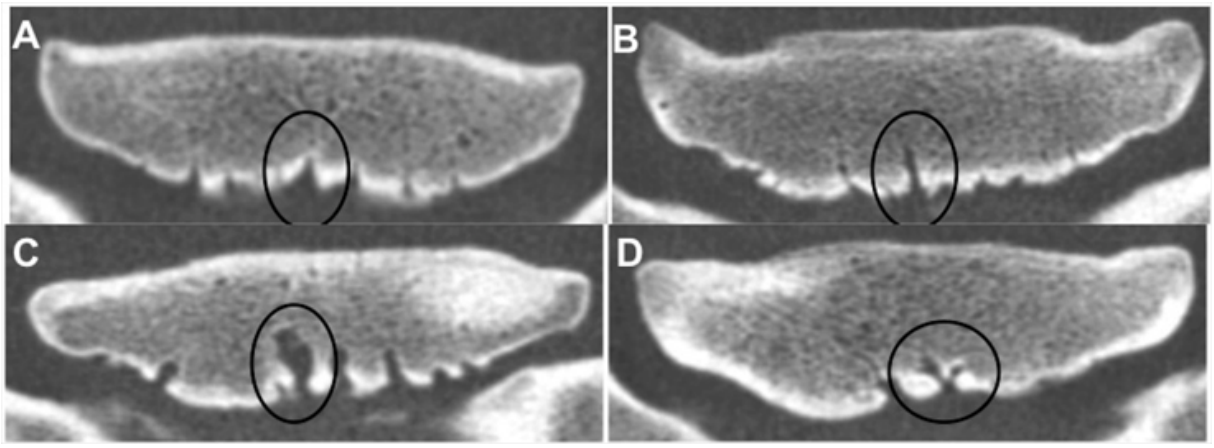

Fig. 1: Dorsally reconstructed CT images with bone window settings of 4 navicular bones, showing the 4 different shapes of synovial invaginations (circles): A) conical, B) linear, C) lollipop, D) branched shape. Left = lateral.

The depth of penetration of each synovial invagination was calculated on dorsal reconstructed CT images, using the following equation: $R = A/B$, where A = distance between the distal basis and the proximal top of the invagination, B = distance between the distal groove (level where the invaginations are located and assessed) and proximal border of the navicular bone. Based on this equation, the depth of penetration was classified into 'mildly penetrating' ($R \leq 0.33$), 'moderately penetrating' ($0.33 < R \leq 0.5$) and 'deeply penetrating' ($R > 0.5$) (Fig. 2).

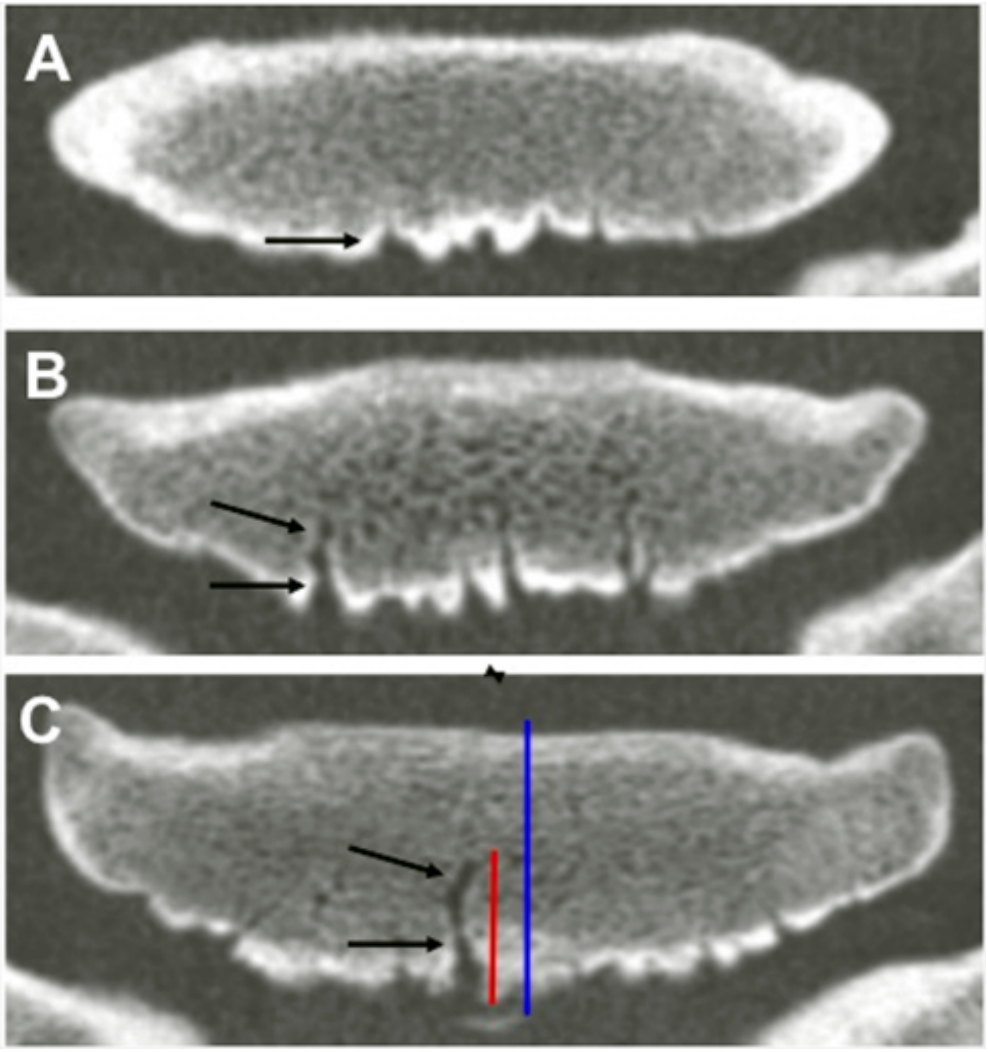

Fig. 2: Dorsally reconstructed CT images with bone window settings of 3 navicular bones, showing the 3 depths of penetration of the synovial invaginations into the bone (arrows), as well as the way of their measuring (equation of red to blue line length) A) mildly, B) moderately, C) deeply penetrating. Left = lateral.

The direction of each invagination was categorized into ‘straight’ (parallel to the flexor surface), ‘dorsoproximal’ and ‘palmaroproximal’ using sagittal reconstructions (Fig. 3).

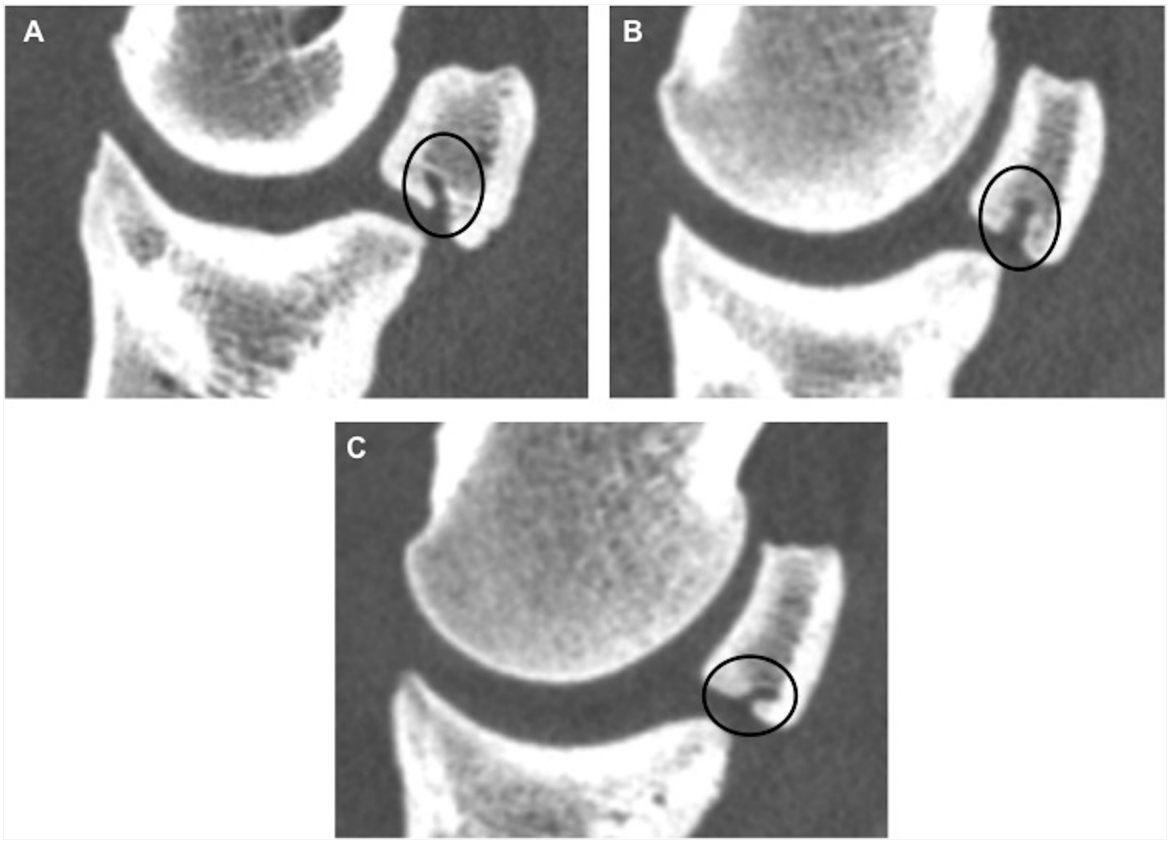

Fig. 3: Sagittally reconstructed CT images with bone window settings of a navicular bone, showing the 3 different directions of the synovial invaginations into the bone (circles) A) dorsoproximal, B) straight, C) palmaroproximal. Left = dorsal; top = proximal.

RESULTS

The total number of distal border synovial invaginations was 295, which corresponds with a mean number of 5.9 invaginations per navicular bone. There were 3 invaginations in 3/50 (6%), 4 in 6/50 (12%), 5 in 11/50 (22%), 6 in 12/50 (24%), 7 in 13/50 (26%), 8 in 3/50 (6%), 9 in 1/50 (2%) and 11 in 1/50 (2%) navicular bone (Fig. 4). Not a single navicular bone was recorded with 1, 2 or 10 synovial invaginations. Thirty-three (mean number of 0.7) invaginations were present in the medial and lateral distal sloping borders.

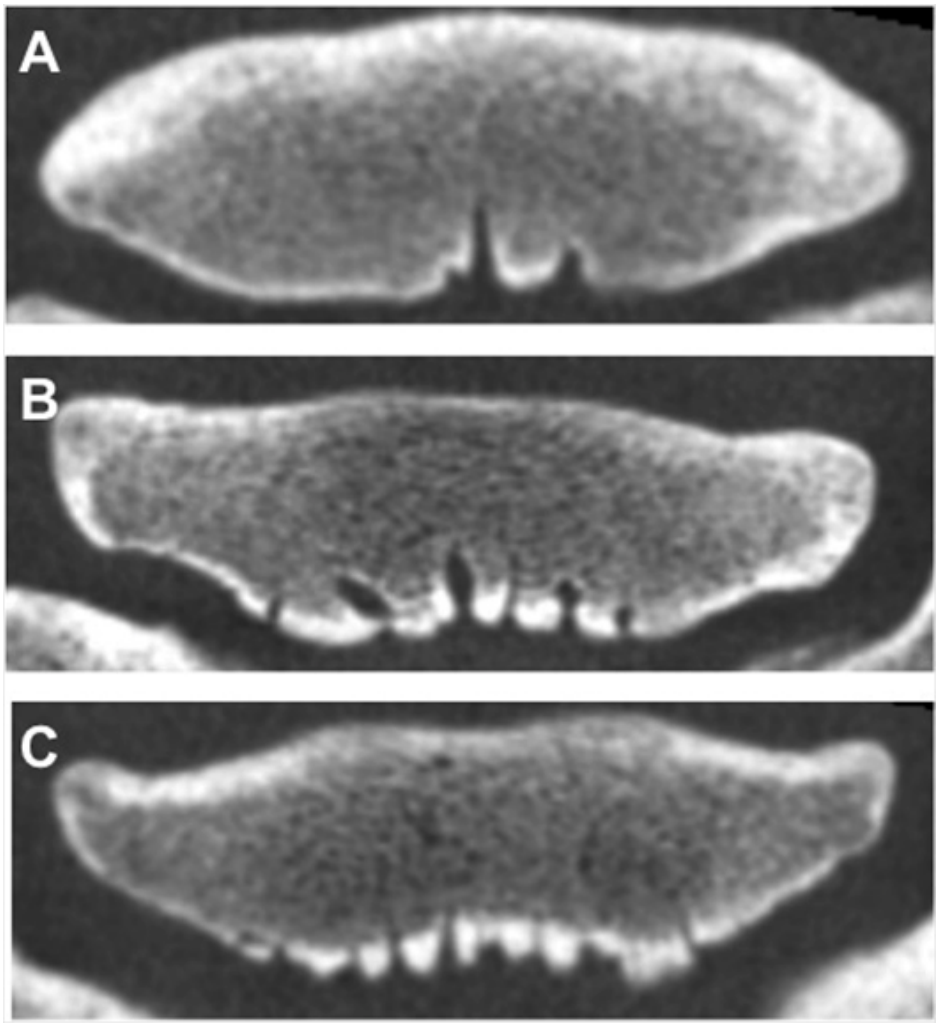

Fig. 4: Dorsally reconstructed CT images with bone window settings showing 3 (A), 6 (B) and 9 (C) distal border synovial invaginations of 3 navicular bones. Left = lateral.

The synovial invaginations were ‘conical-shaped’ in 118/295 (40%) cases, ‘linear-shaped’ in 109/295 (36.9%) cases, ‘lollipop-shaped’ in 38/295 (12.9%) cases and ‘branched’ in 30/295 (10.2%) navicular bones. ‘Lollipop’ and ‘branched’ distal invaginations were recognized in

42% (21/50) navicular bones representing 64% (16/25) of the horses. As for the depth of penetration, the synovial invaginations were ‘mildly penetrating’ in 195/295 (66.1%), ‘moderately penetrating’ in 67/295 (22.7%) and ‘deeply penetrating’ in 33/295 (11.2%) cases, which corresponds with a mean number of 3.9 ‘mildly penetrating’, 1.3 ‘moderately’ and 0.7 ‘deeply penetrating’ invaginations per navicular bone. The distal border invaginations ran in a ‘straight’, ‘dorsoproximal’ and ‘palmaroproximal’ direction in 187/295 (63.4%), 28/295 (9.5%) and 80/295 (27.1%) cases, respectively. In only 6/50 (12%) navicular bones, all invaginations ran in the same direction. In 12/50 (24%) bones, all invaginations ran in the same direction except one, whereas in 32/50 (64%) navicular bones, more than 1 synovial invagination ran in a different direction.

DISCUSSION

The present investigation was carried out to describe the morphological features of the distal border synovial invaginations of the navicular bone in the horse by use of CT. In fact, CT is the most appropriate imaging modality for detailed imaging of normal bone and detection of bony disorders (8). The possibility of reconstruction of multiplanar, high-resolution images without superimposition allows CT to provide detailed anatomical information of the synovial invaginations.

To the authors' knowledge, no literature has yet described the morphology by CT of the distal border invaginations. Results of this study indicated that synovial invaginations along the distal border of the navicular bone show a lot of variation.

In the present study, an average of 5.9 distal border synovial invaginations per navicular bone was found. Twenty-six percent of the navicular bones showed 7 invaginations, and only 2% to 6% showed more than 7 invaginations. According to the literature, a navicular bone with a total number of 1 to 7 distal border synovial invaginations on radiographs is considered normal (3, 10, 11), although an overlap between sound and lame horses is described (3). In our study, 33 invaginations were recognized at the medial and lateral sloping borders of the navicular bone. It has been reported that the presence of synovial invaginations in the proximal or lateral/medial distal sloping borders is abnormal on radiographs (12). However, due to lack of superimposition of surrounding bone and the high sensitivity of CT for detecting bone in detail, the presence of small synovial invaginations at the sloping borders may be observed in normal navicular bones (6).

On radiography, seven basic shapes of distal synovial invaginations are described (5). Based upon the radiographic appearance of distal border synovial invaginations, scoring systems were developed for use in a purchase examination, to predict the development of clinically navicular disease (5, 13). The presence of 'enlarged' invaginations on radiographs is considered potentially to be associated with navicular disease (3-5, 14, 15). In our study, the number of navicular bones showing ‘lollipop’ and ‘branched’ distal synovial invaginations was lower compared to a study of horses with clinical signs of navicular disease (42% versus 85%) (15). However, the number of affected horses in our study was much higher compared to a study of clinically healthy horses (64% versus 11%) (16).

In the current study, synovial invaginations were classified as ‘mildly penetrating’ (mean number of 3.9 per navicular bone) when they ran through maximum one third of the distance

between the distal groove and proximal border of the navicular bone, whereas ‘moderately penetrating’ invaginations (mean 1.3 per navicular bone) extended more proximally until maximum halfway the distance between the groove and proximal border. ‘Deeply penetrating’ invaginations (mean 0.7 per navicular bone) ran much more proximally (exceed halfway) into the bone. In contrast to our classification, the synovial invaginations in the reported radiographic classification of Dik (2) are divided in ‘moderately penetrating’ when they ran through maximum one third, and ‘deeply penetrating’ the moment they pass one third of the proximodistal width of the navicular bone. An increase in the depth of penetration of distal border synovial invaginations is considered a significant radiographic finding (2). It is reported that the depth of penetration of an invagination normally is at least one and a half times taller than their base width (17). According to Diks classification (2), a horse with a navicular bone having many (3 or more) ‘moderately’ or some (1 or 2) to many ‘deeply penetrating’ invaginations is assigned a poor to bad prognosis for future soundness. However, the clinical relevance of abnormal distal border invaginations on radiographs is until now unsure.

Results of the present study indicated that CT morphology of the synovial invaginations varied regarding their orientation into the navicular bone. This may be explained by the inherent function of the invaginations in the bone. They serve as the entrance of the nutrient vessels, and guide them and their branches towards different parts of the navicular bone (11). In the present study, this guidance function can be clearly depicted with the different running directions detectable: ‘straight’, ‘dorsoproximal’ or ‘palmaroproximal’ direction on the sagittal reconstructed images, and medial or lateral bending on the dorsally reconstructed images.

The history of lameness of the horses used in our study was unknown, however, to the authors' opinion this is not considered a limitation. The current study is a descriptive study, which only describes the morphology of the distal border synovial invaginations of the navicular bone by use of CT.

In conclusion, results of the current study indicate that synovial invaginations along the distal border of the navicular bone shows a lot of morphological variation. The CT images and the knowlegde gained in this study may aid in the radiographic evaluation of the distal navicular border synovial invaginations. Furthermore, it would be interesting to examine how far the appearance of these invaginations on corresponding radiographs fits in with the described CT-morphology.

FOOTNOTE

[a]Mx8000, Philips Medical Systems, AE Eindhoven, The Netherlands.

[b]Osirix Image processing Software, Geneva, Switzerland.

REFERENCES

1. Robert C., Valette J.P., Denoix J.M. Correlation between routine radiographic findings and early racing career in French Trotters. Equine Vet J Suppl 2006; 36: 473-478.
2. Dik K.J. Diagnostische beeldvorming. In: De Veterinaire Keuring van het Paard. Sloet van Oldruitenborgh-Oosterbaan M.M., Barneveld A., Van Den Belt A.J. (eds), Libre BV, Leeuwarden 2007: 85-112.
3. Rose R.J., Taylor B.J., Steel J.D. Navicular disease in the horse: an analysis of seventy cases and assessment of a special radiographic view. J Equine Med Surg 1978; 2: 492-497.
4. Colles C.M. Ischaemic necrosis of the navicular bone and its treatment. Vet Rec 1979; 17: 133-137.
5. MacGregor C.M. Radiographic assessment of navicular bones, based on changes in the distal nutrient foramina. Equine Vet J 1986; 18: 203-206.
6. Groth A.M., May S.A., Weaver M.P., et al. Intra- and interobserver agreement in the interpretation of navicular bones on radiographs and computed tomography scans. Equine Vet J 2009; 41: 124-129.
7. Tietje S. Computed tomography of the navicular bone region in the horse: a comparison with radiographic documentation. Pferdeheilkunde 1995; 11: 51-61.
8. Widmer W.R., Buckwalter K.A., Fessler J.F., et al. Use of radiography, computed tomography and magnetic resonance imaging for evaluation of navicular syndrome in the horse. Vet Radiol Ultrasound 2000; 41: 108-116.
9. Rijkenhuizen A.B.M. Navicular disease: a review of what's new. Equine Vet J 2006; 38: 82-88.
10. Colles C.M. Interpreting radiographs 1: The foot. Equine Vet J 1983; 15: 297-303.
11. Rijkenhuizen A.B.M., Németh F., Dik K.J., et al. Development of the navicular bone in foetal and young horses, including the arterial supply. Equine Vet J 1989; 21: 405-412.
12. Dyson S.J. Navicular disease and other soft tissue causes of palmar foot pain. In: Diagnosis and Management of Lameness in the horse. Ross M.W., Dyson S.J. (eds), W.B. Saunders, St Louis 2003: 286-299.
13. Huskamp V.B., Becker M. Diagnosis and prognosis of changes in the sesamoid bone of the forelimb of horses as seen by radiography during examination before sale. An

attempt to classify the findings. Der Praktische Tierarzt 1980; 10: 858-863.

14. Hertsch B., Dammer H. The blood supply of normal and diseased navicular bones. Vet Rad 1988; 29: 276-281.
15. Wright I.M. A study of 118 cases of navicular disease: radiological features. Equine Vet J 1993; 25: 493-500.
16. Kaser-Hotz B., Ueltschi G. Radiographic appearance of the navicular bone in sound horses. Vet Radiol Ultrasound 1992; 33: 9-17.
17. Colles C.M. Interpreting radiographs 1: The foot. Equine Vet J 1983; 15: 297-303.

CHAPTER 5

Differences in the morphology of distal border synovial invaginations of the navicular bone in the horse as evaluated by computed tomography compared with radiography

Adapted from: Claerhoudt S, Bergman H.J, van der Veen H, Duchateau L, Raes E.V, Saunders J.H. Differences in the morphology of distal border synovial invaginations of the distal sesamoid bone in the horse as evaluated by computed tomography compared with radiography. Equine Veterinary Journal 2012; 44: 679-683.

SUMMARY

The objective of our study was to measure the variability and agreement of the morphology of distal border synovial invaginations on radiography vs. CT.

Computed tomography scans and 3 DPr-PaDiO radiographs were obtained on 50 cadaver forefeet from 25 Warmblood horses. Computed tomography was assumed to be the standard test. The number, shape and depth of penetration of distal border synovial invaginations into the navicular bone were evaluated with both methods, and the comparison of their measurements was statistically described.

A statistically significant mean difference for number of distal synovial invaginations between CT and all 3 DPr-PaDiO projections was found, and approximately equal to 2, meaning that CT permits visualization of an average of 2 more invaginations compared to radiography. In no case of our sample of horses, radiography showed a higher number of invaginations than CT. A large variation in the difference of measurements for depth of penetration against their mean difference between CT and the 3 radiographic projections was seen. Radiography under- or overestimated the depth of the invaginations compared with CT, but underestimated more the deeper running invaginations. There was no statistically significant difference found for the mean difference of both techniques for depth. A moderate to good agreement between measurements on CT and the 3 DPr-PaDiO projections for shape was seen, in which the D55°Pr-PaDiO projection showed the best agreement. A high specificity (90-99%) and lower sensitivity (65%) for shape were found for all the 3 projections.

For the evaluation of the number and depth of distal synovial invaginations in the navicular bone, radiography shows only partially the morphology seen on CT.

CHAPTER 5

INTRODUCTION

Navicular disease is a chronic, progressive uni- or bilateral forelimb lameness typically affecting riding horses of middle age (1, 2). Radiographic evaluation plays an essential role in the diagnosis of navicular disease. However, radiography is limited to changes of the bony component of the navicular bone.

During the selection process of horses admitted as breeding stallions or in purchase examinations, the synovial invaginations of the distal border of the navicular bone are often graded according to radiographic classification systems, using a D45°-70°Pr-PaDiO radiographic projection. Although opinion is divided, some clinicians consider many moderately or some deeply penetrating rounded or inverted flask-shaped synovial invaginations as moderate or severe radiographic findings. These changes have been suggested by some authors to be predictors for future joint pain and lameness, and would impair a horse's future sport career (3, 4). Consequently, abnormal synovial invaginations are responsible for a negative advice in purchase examinations and therefore may have major financial consequences for horse owners. Although many authors describe these findings related to navicular disease, there is still discussion about their significance (1, 5-8).

Computed tomography is the most appropriate imaging modality for detailed imaging of normal bone and detection of bony disorders (9-11). Therefore, this imaging modality was assumed by the authors to be the standard test for the evaluation of the navicular bone in the present study.

The purpose of the study was to demonstrate if radiography is an accurate test for the evaluation of distal border synovial invaginations, by measuring the variability and agreement of the morphology of synovial invaginations of the navicular bone on radiography vs. CT.

MATERIALS AND METHODS

Material

The material used in this study consisted of 50 forefeet of 25 Warmblood horses (mean age: 7 years). All horses were subjected to euthanasia for reasons unrelated to this study. All feet were severed at the level of the fetlock joint immediately after euthanasia. The shoe and loose horn in the sole, if present, were removed and the frog was cleaned. The feet were not selected by any particular criteria and both forefeet of each horse were included.

CT examination

The CT scans were performed with a 4-detector row spiral CT scanner[a] in which the feet were placed in the gantry with the longitudinal axis of the foot oriented parallel to the CT table and perpendicular to the plane of the CT gantry. The medial side of the foot was marked. The limbs were scanned in a distal-to-proximal direction. The output parameters were 120 kV and 250 mAs per slice. The slice thickness was 0.6 mm, pitch of 0.875 cm, 0.3 increment and 1-second rotation time. Transverse CT scans were reconstructed from the level of the distal aspect to the level of the proximal aspect of the navicular bone using a bone window setting (WL: 200-600; WW: 1000-2000), 250 mm field of view and 512 x 512 pixel matrix. The average total time required for scanning of each foot was 46.25 seconds. From the transverse images, sagittal and dorsal reconstructions with a slice thickness of 0.6 mm were reformatted by use of software[b].

Radiographic examination

Radiographic examination was performed after the CT examination. A computed radiographic system[d] was used. The sulci of the frog were packed with modelling compound[c]. Three DPr-PaDiO radiographic projections with different hoof angles (D45°Pr-PaDiO, D55°Pr-PaDiO and D65°Pr-PaDiO) were performed on all feet. The x-ray beam of the tube was kept horizontal and centered 2 cm proximal to the coronary band at the midline of the foot. The foot was placed on a wooden block with a slope of 45° with the horizontal. By the use of wedges (slope 5°), D55°Pr-PaDiO and D65°Pr-PaDiO projections were made of all feet. The feet were radiographed using 60 kV and 12.5 mAs, a grid (6:1 ratio, 103 lines/cm) and a 100 cm focus-film distance.

Image analysis

Two observers, one board-certified radiologist (JHS) and one PhD-student (SC), interpreted all images together and a diagnosis was made in consensus. The radiographic images of a particular foot and hoof angle were reviewed in a randomized order at the same workstation, on the same diagnostic imaging screens[e] and using a similar evaluation[f], to determine the number of distal border synovial invaginations. Furthermore, for each synovial invagination, the depth and shape were determined. Next, the CT images of a particular foot were reviewed in a random order as well to determine the number of distal border synovial invaginations using transverse slices and dorsal reconstructions, and for each synovial invagination, the depth and shape were determined.

In a second step, the corresponding radiographic and CT images were considered together. To compare depth and shape assessments on the two imaging modalities, only synovial invaginations for which an assessment was available on both radiography and CT were used (some invaginations seen with CT were not seen with radiography).

The depth of penetration of the synovial invaginations was assessed on the dorsal reconstructed CT and radiographic images. Each synovial invagination was calculated by an imaging software programme[b], using the following equation: Depth $(R) = A/B$, where A = distance (in centimetre) between the most distal basis and the proximal top of the synovial invagination, B = distance (in centimetre) between the distal groove (level where the invaginations are located and assessed) and proximal border of the navicular bone on the CT images, and distance (in centimetre) between the most distal basis of the invagination and proximal flexor border on the radiographs. Data of depth were classified in three categories: $1 = R \leq 0.33$, $2 = 0.33 < R \leq 0.5$ and $3 = R > 0.5$.

The shape of the synovial invaginations was assessed on dorsal CT and radiographic images. The shape could be categorized as either ‘conical’, ‘linear’, ‘lollipop’ or ‘branched’ (4 categories, further described as ‘shape4’), with 1 = normal (conical- or linear-shaped), and 2 = abnormal (lollipop- or branched-shaped) (further described as ‘shape2’).

Data analysis

To compare the observed number of invaginations and the depth of the invagination between CT and the DPr-PaDiO projections, Student's paired t-test was used with foot as block variable for the number and invagination as block factor for the depth. The results were summarized by the average difference and corresponding 95% confidence interval (CI) and 95% reference interval (RI). The 95% reference interval is given by the mean difference +/- 2 times the standard deviation (SD), which contains 95% of the actual mean differences if the normal distribution assumption holds. Bland Altman plots are provided for CT vs. the different DPr-PaDiO projections, to investigate a possible relationship between the difference and the magnitude of the measurement. A global significance level of 0.05 was used, but each of the 3 pairwise comparisons was tested at a comparisonwise significance level equal to 0.0125 (Bonferroni adjustment).

Degree of agreement between CT and the DPr-PaDiO radiographic projections for number, depth (taken as categorical variables) and shape was quantified using the κ statistic. For only 2 categories as in 'shape2', the measured weighted and unweighted κ-values are the same. The guidelines for strength of agreement based on the values of κ were: < 0.20 poor, 0.21 - 0.40 fair, 0.41 - 0.60 moderate, 0.61 - 0.80 good and 0.81 - 1.00 very good (12).

RESULTS

The differences and variability between measurements on CT and the different radiographic projections for number and depth of distal border synovial invaginations are summarized in Table 1.

Table 1: Difference between CT and 3 radiographic projections for number and depth.

Comparison for number	**Mean difference**	**95% RI**	**95% CI**
CT vs. D45°Pr-PaDiO	1.88	-1.18 – 4.94	1.45 – 2.31
CT vs. D55°Pr-PaDiO	2.04	-0.95 – 5.03	1.62 – 2.46
CT vs. D65°Pr-PaDiO	2.20	-0.66 – 5.06	1.80 – 2.60
Comparison for depth			
CT vs. D45°Pr-PaDiO	0.003	-0.28 – 0.29	-0.02 – 0.02
CT vs. D55°Pr-PaDiO	0.016	-0.29 – 0.32	-0.01 – 0.04
CT vs. D65°Pr-PaDiO	0.012	-0.28 – 0.30	-0.01 – 0.03

Key: CI = confidence interval; RI = reference interval

Number

The average total number of synovial invaginations was 5.9 ± 1.56 on CT (total of 295), 4 ± 1.85 on the D45°Pr-PaDiO (total of 200), 3.9 ± 1.71 on the D55°Pr-PaDiO (total of 195) and 3.7 ± 1.81 on the D65°Pr-PaDiO projection (total of 185). In no case of our sample of horses, radiography showed a higher number of invaginations than CT (Figs. 1 and 2). In only 11/50 (22%), 7/50 (14%) and 6/50 (12%) feet, the number of synovial invaginations counted on CT scans and on the D45°Pr-PaDiO, D55°Pr-PaDiO and D65°Pr-PaDiO projections respectively, were equal (Fig. 2). Even in 2/50 (4%) feet, no synovial invaginations were detected on the 3 radiographic projections, however 3 and 4 invaginations respectively, were counted on CT.

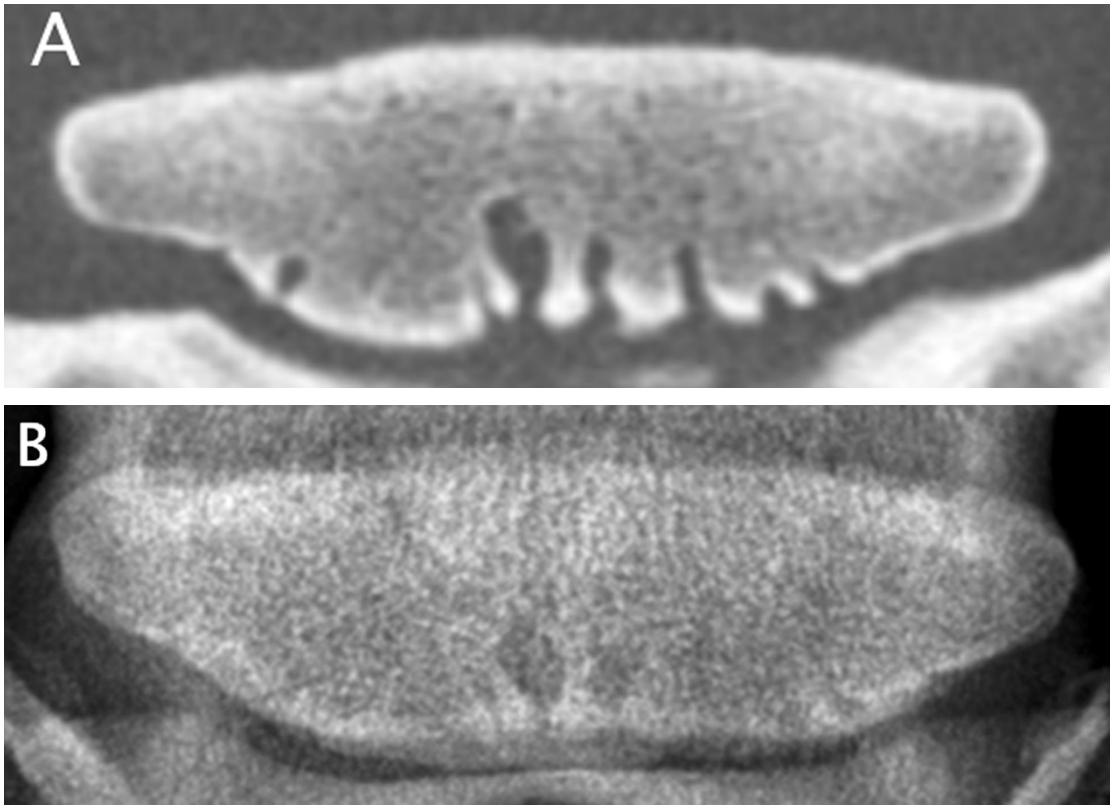

Fig. 1: Dorsally reconstructed CT image with bone window settings (A) and corresponding dorso 55° proximal-palmarodistal oblique radiographic image (B) of a navicular bone, showing 7 and 4 distal border synovial invaginations respectively. Left = lateral.

A statistically significant mean difference between CT and all 3 DPr-PaDiO projections was found ($P < 0.001$) and approximately equal to 2, meaning that CT permits visualization of an average of 2 more invaginations compared to radiography. The D45°Pr-PaDiO projection showed the smallest mean difference. The corresponding 95% RIs were wide for all 3 comparisons, reflecting a high variability of the differences between both techniques (Table 1). The Bland Altman plots of the differences for number between the methods against their mean are shown in Fig. 2.

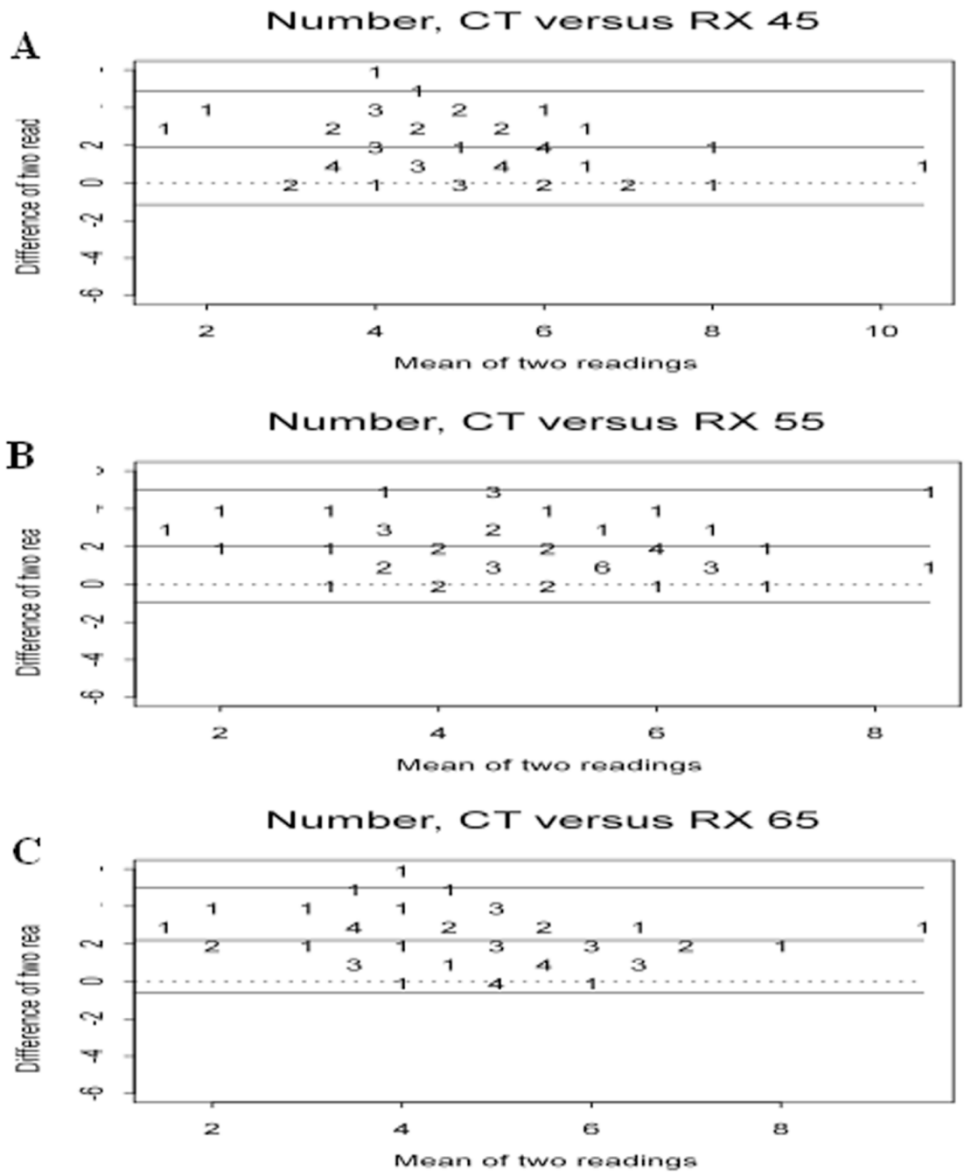

Fig. 2: Bland Altman plots: Differences of counted numbers (readings) on CT and radiographic images (A: D45°Pr-PaDiO; B: D55°Pr-PaDiO and C: D65°Pr-PaDiO) against their mean. The numerical code represents the number of navicular bones (total sum of 50) with the same difference in number against mean. Dashed line represents zero-level (no difference), upper line = mean + 2SD, middle line = mean, lower line = mean – 2SD.

The weighted κ-values for all 3 projections were very low, specifically for the D55°Pr-PaDiO and D65°Pr-PaDiO projections, meaning that a greater disagreement with CT for number was calculated for these 2 projections (Table 2).

Table 2: Agreement between CT and 3 radiographic projections for number, depth and shape (*: weighted and (unweighted) κ- values are the same for shape2).

Radiographic projection	Categorical variable	κ	Weighted κ
D45°Pr-PaDiO	number	0.12	0.24
D55°Pr-PaDiO	number	0.02	0.17
D65°Pr-PaDiO	number	0.01	0.15
D45°Pr-PaDiO	depth	0.23	0.30
D55°Pr-PaDiO	depth	0.19	0.26
D65°Pr-PaDiO	depth	0.23	0.29
D45°Pr-PaDiO	shape4	0.49	0.57
D55°Pr-PaDiO	shape4	0.50	0.60
D65°Pr-PaDiO	shape4	0.42	0.49
D45°Pr-PaDiO	shape2	0.68*	-
D55°Pr-PaDiO	shape2	0.7*	-
D65°Pr-PaDiO	shape2	0.55*	-

Depth

The linear measurements of depth of synovial invaginations (measurements *A* of equation) and distance between the distal groove and proximal border (measurement *B*) increased with radiographic angle in 25/50 (50%) navicular bones. There were no significant mean differences for depth between CT and the 3 radiographic projections, and the CIs were also narrow, meaning that there seems to be little or no bias. The mean differences of measurements for depth between CT and the 3 radiographic projections were all positive and small, with the D45°Pr-PaDiO projection showing the smallest mean difference. By evaluating the RIs, it is possible to see how precise the individual estimates are. Consequently, the RIs for all 3 DPr-PaDiO projections showed quite wide, comparable ranges (Table 1). Ninety-five percent of the differences between CT and the different DPr-PaDiO projections for depth lie between the limits -0.28 – 0.32 of the interval (0.28 below or 0.32 above zero-level). Also, the Bland Altman plots showed a large variation in the differences against their mean (Fig. 3). These plots show that radiography occasionally under- or overestimated the depth of the invaginations compared with CT, with a trend to more overestimate the mildly penetrating invaginations, and underestimate the deeper ones (Figs. 3 and 4).

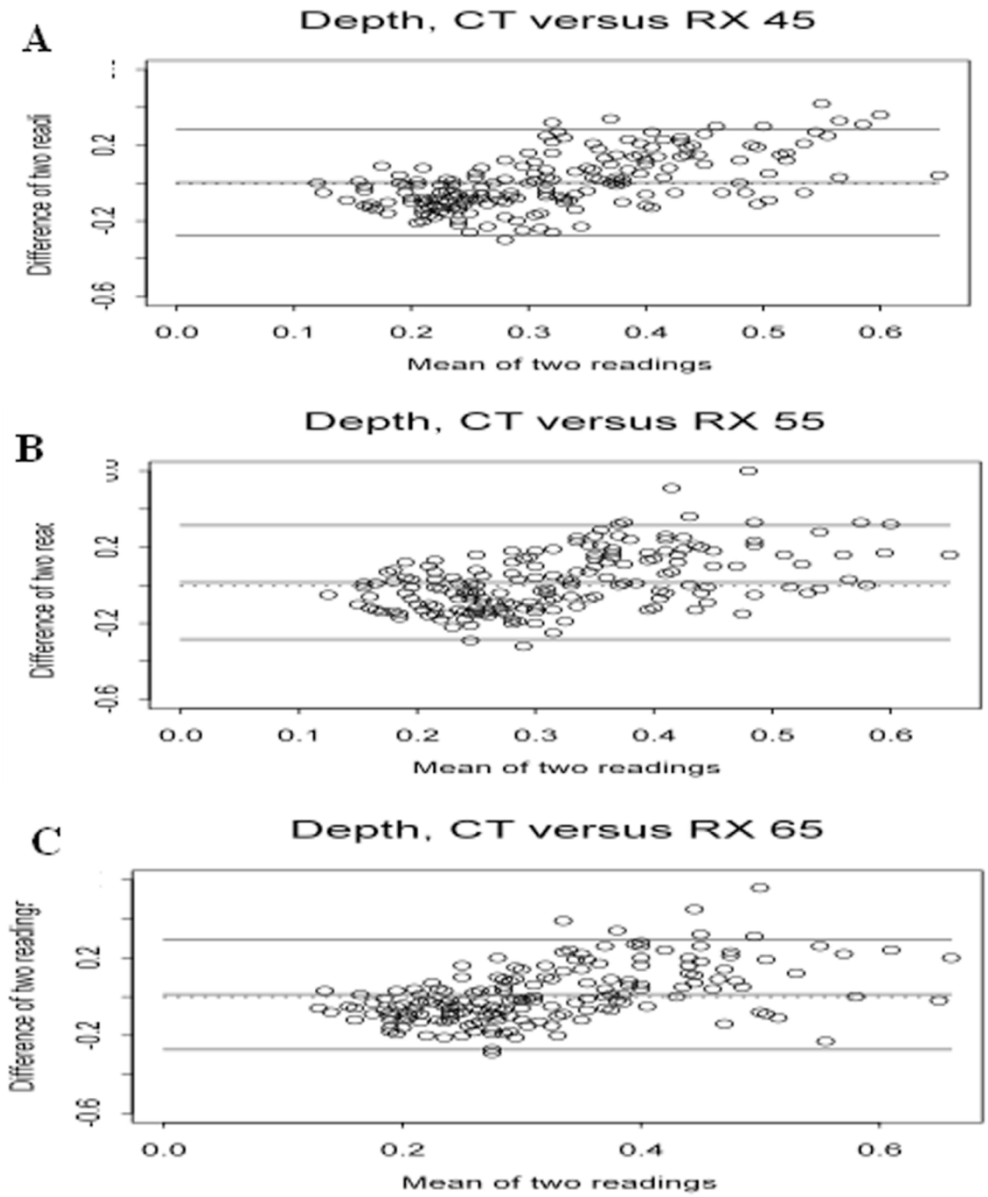

Fig. 3: Bland Altman plots: Differences of the equations of depth (readings) on CT and radiographic images (A: D45°Pr-PaDiO; B: D55°Pr-PaDiO and C: D65°Pr-PaDiO) against their mean. Each individual plot (O) represents a synovial invagination (total of 200 plots (A), 195 plots (B) and 185 plots (C)). Dashed line represents zero-level (no difference), upper line = mean + 2SD, middle line = mean, lower line = mean – 2SD.

The κ-statistics also revealed a quite poor agreement between both techniques (average κ-value of 0.21 and low weights to disagreements, as summarized in Table 2).

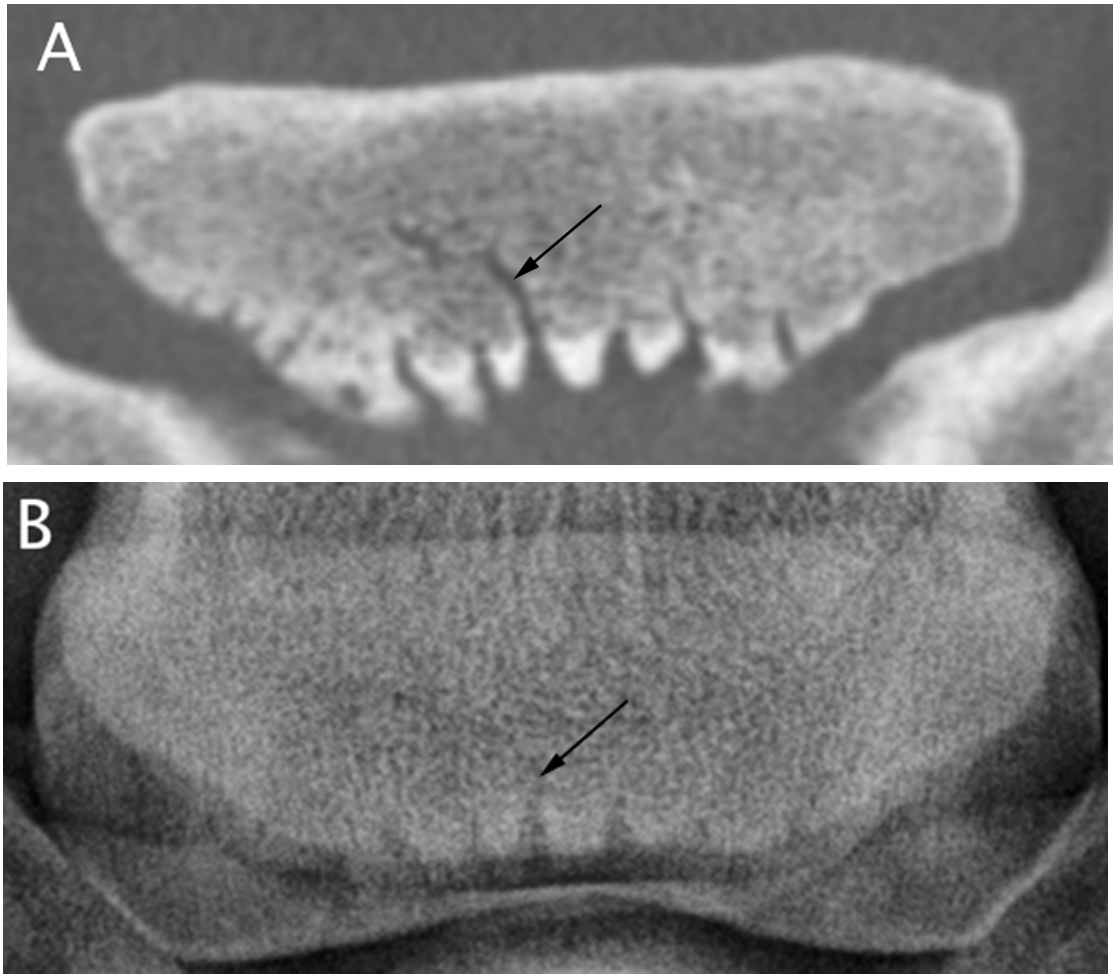

Fig. 4: Dorsally reconstructed CT image with bone window settings (A) and corresponding dorso 65° proximal-palmarodistal oblique radiographic image (B) of a navicular bone, showing a deeply penetrating invagination on the CT image (arrow), which is mildly penetrating on the radiographic image (arrow). Left = lateral.

Shape

In only 3/11 (27%), 4/7 (57%) and 3/6 (50%) feet with an equal number of synovial invaginations on both the CT scans and D45°Pr-PaDiO, D55°Pr-PaDiO and D65°Pr-PaDiO projections respectively, was the shape comparable by both methods (Fig. 5).

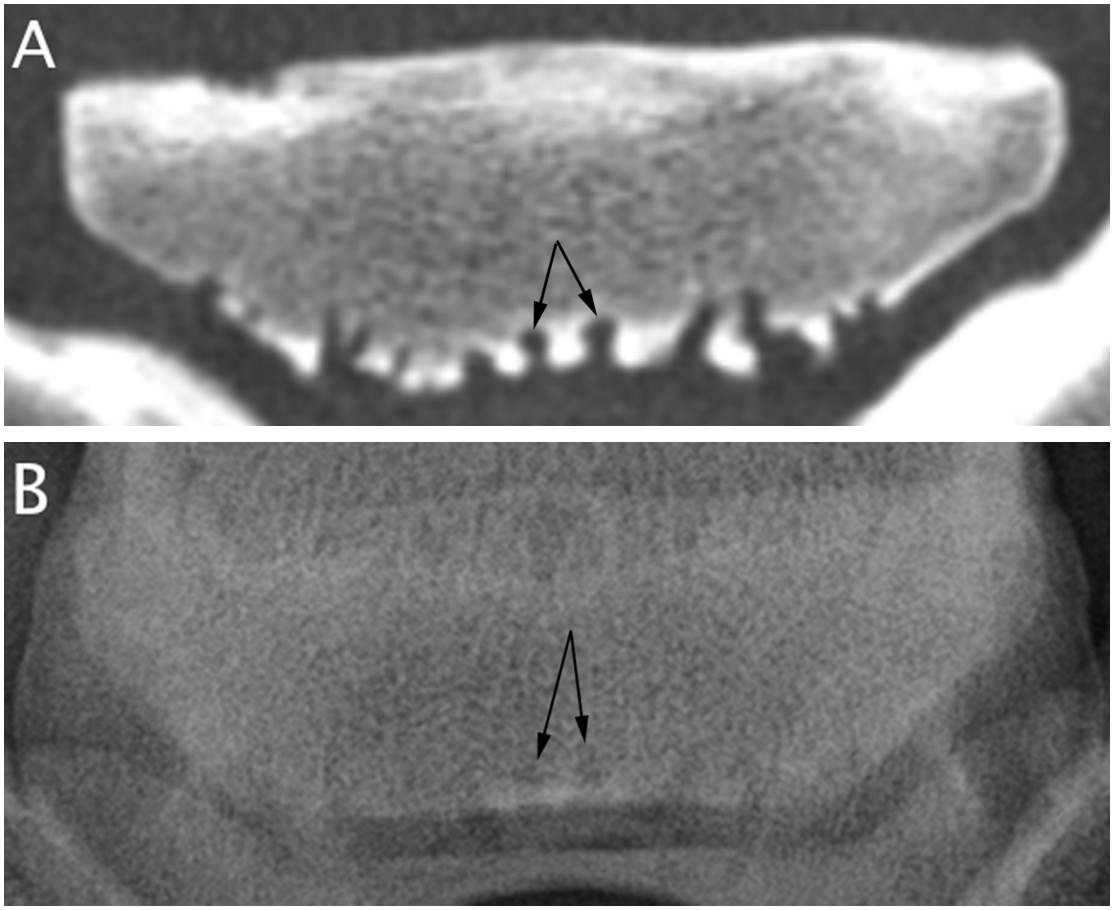

Fig. 5: Dorsally reconstructed CT image with bone window settings (A) and corresponding dorso 55° proximal-palmarodistal oblique radiographic image (B) of a navicular bone, showing 2 abnormally shaped invaginations on the CT image (arrows), which were normally shaped on the radiographic image (arrows). Left = lateral.

The agreement for shape4 ranged between $0.42 \leq \kappa \leq 0.50$, representing a moderate agreement, whereas the kappa value for shape2 was higher (range: $0.55 \leq \kappa \leq 0.71$), representing a moderate to good agreement. Weighted kappa for shape was higher for the D55°Pr-PaDiO projection, meaning that, relative to the other projections, a better agreement with the gold standard for shape was calculated for this projection.

The κ and weighted κ values for agreement of number, depth and shape are presented in Table 2. The sensitivity, specificity (both calculated for shape2) and corresponding 95% CIs for all 3 DPr-PaDiO projections for shape, with CT as the standard test, are summarized in Table 3.

Table 3: Sensitivity and specificity for all 3 radiographic projections for shape with CT as standard test.

Radiographic projection	**Sensitivity (95% CI)**	**Specificity (95% CI)**
D45°Pr-PaDiO	0.65 (0.51 – 0.78)	0.97 (0.92 – 0.99)
D55°Pr-PaDiO	0.65 (0.51 – 0.78)	0.99 (0.95 – 1)
D65°Pr-PaDiO	0.63 (0.48 – 0.76)	0.90 (0.84 – 0.95)

CHAPTER 5

DISCUSSION

The morphological features of the distal navicular border synovial invaginations of the present population were described in a previous study using CT (13). The present investigation was carried out to assess the variability and agreement between the appearance of distal border synovial invaginations of the navicular bone on radiographs vs. CT. Histology is regarded as the gold standard for the diagnosis of tissue abnormalities (14). In the present study, no histological examination was performed, however, due to the possibility of reconstruction of multiplanar, high-resolution images without superimposition, CT provides detailed anatomical information of the synovial invaginations (11). Therefore, CT was assumed by the authors to be the standard test in this study.

The total number of synovial invaginations counted on CT was comparable, but mostly higher compared to radiography. The mean differences between CT and the 3 DPr-PaDiO projections for number of synovial invaginations were all statistically significant and positive, with the D45°Pr-PaDiO projection showing the smallest mean difference. In fact, CT permitted visualization of an average of 2 more invaginations per navicular bone compared to radiography, indicating a better visibility of invaginations on CT compared to radiography. Similar conclusions were reported earlier (10, 11). The synovial invaginations that were ill-defined or undetectable on radiography were mostly small and located at the distal sloping borders of the navicular bone on the CT images. It has been described that the presence of small synovial invaginations at the sloping borders on CT may be observed in normal navicular bones, due to lack of superimposition of surrounding bone and the high sensitivity of CT for detecting bone in detail (11). However, the clinical significance of these subtle CT findings remains questionable.

In approximately 80% of the cases in our study, a navicular bone with 7 invaginations on radiography had more than 7 distal border invaginations on CT. According to the literature, up to 7 radiographically detectable distal border synovial invaginations are considered as normal, and more than 7 significant (15, 16), although an overlap between sound and lame horses is described (5).

The present results show that when the mean differences for depth on CT and radiography increase, the differences (measurements CT minus radiography) also seem to increase, resulting in a larger underestimation by radiography in case of deeper invaginations. As described above, CT appeared better in evaluating synovial invaginations compared to

radiography, due to the better visibility of subtle changes on CT (9-11). On CT, most deep invaginations were ending proximally as very tiny, deeply penetrating lines, which were undetectable on radiography. Therefore, care should be taken in judging the depth of distal border invaginations on radiographs during purchase examination, since deeply penetrating invaginations may be missed on DPr-PaDiO projections. It is reported that deeply penetrating distal border invaginations are significant radiographic findings that are considered predictors for future joint pain and lameness (3, 4). However, the clinical significance of subtle CT findings remains unclear. Further investigation with clinical association is necessary to determine the importance of these deeply penetrating, tiny synovial invaginations.

In the current study, the sensitivity and specificity for shape of the distal navicular border synovial invaginations were calculated on the 3 DPr-PaDiO projections using CT as the standard test. For radiography as diagnostic modality, both a high sensitivity (i.e. high number of correctly identified abnormal shaped invaginations) and a high specificity (i.e. correctly identified absence of abnormal shaped invaginations) are desired. False positive diagnosis (poor specificity) of abnormal shaped invaginations can have major consequences, because the literature describes these findings to be related with navicular disease (1, 5-8). However, our results show an almost 100% specificity for all projections for shape, meaning that nearly no false positive results were seen. On the other hand, more false negative results were present, resulting in a much lower sensitivity of 65% for shape. In other words, an abnormal invagination on radiography is effectively abnormal, but a normal one can in fact be abnormal.

The present results show a variable degree of agreement (κ-values) between measurements on CT and the DPr-PaDiO projections for the 3 variables. All data for shape were grouped into 2 (2 x 2 table) for shape2 and 4 (4 x 4 table) categories for shape4, resulting in variable values of κ. For the resulting 2 x 2 table, a better average κ-value of 0.65 was found, compared to κ=0.47 for the 4 x 4 table. In contrast, data on numbers were classified in 12 categories (0 being the lowest number of invaginations found and 11 the highest), logically resulting in very low κ-values. In theory, any value of κ much below 0.5 will indicate poor agreement. However, despite these published guidelines (12), no κ-value can be regarded universally as indicating some degree of agreement (17). Actually, the value of κ depends on the number of categories and upon circumstances, as demonstrated in our results. For multiple categories on an ordinal scale, weighted κ has the advantage that it 'weights' the degree of disagreements. Greater disagreement is penalised more, resulting in lower weighted κ values.

The results of the current study showed that the variability of the actual differences between CT and radiography is high for number and depth of penetration of distal navicular border synovial invaginations. This can be explained by 3 factors. A first factor is the variable orientation of the synovial invaginations in the navicular bone. Indeed, a recent study has demonstrated that the orientation of the distal border synovial invaginations into the navicular bone can vary from a straight, dorsoproximal to palmaroproximal direction (13). A second factor is the variable height of the heels. Pearce et al. (18) demonstrated that the degree of DIPJ angulation increases (increased joint flexion) with heel elevation, and van Dixhoorn et al. (19) reported that the navicular bone follows the coffin bone *in vitro* during DIPJ flexion. Thus, elevation of the heels results in at least an increased upright motion of the navicular bone in the sagittal plane. Finally, a third factor is the superimposition of the navicular bone over other structures on a DPr-PaDiO projection, preventing visualization of the exact point of origin of the synovial invaginations (10). The distal contour of the navicular bone on DPr-PaDiO projections is visualized as 2 lines, one representing the articular border and the other the flexor border, with the distal border synovial invaginations being situated in the groove between these two borders (16, 20).

A consequence of the variable orientation of the invaginations into the bone and of the large individual variation of heel height, is that the position of the distal navicular border synovial invaginations regarding to the horizontal x-ray beam varied individually when the front of the hoof wall is angled forward at approximately 45°, 55° and 65°. In fact, when elevating the heels, the depth of dorso- and palmaroproximal oriented synovial invaginations on DPr-PaDiO radiographic projections, shortens and enlarges respectively, relative to the degree of heel elevation. The opposite effects are obtained by lowering the heels.

A potential limitation of this study could be the absence of a PaPr-PaDiO projection, which permits evaluation of the navicular bone without superimposition. However, this projection only allows evaluation of the number and width of the distal border invaginations (5). Therefore, it was not included in our study.

In conclusion, the results of the present study indicated that radiography shows only partially the morphology of the distal navicular border synovial invaginations as seen on CT. CT is a much more sensitive method for the detection of these invaginations; therefore, regardless of the exact clinical meaning of the synovial invaginations, the criteria as used for radiography cannot be transposed to CT. Prospective epidemiological studies are necessary to assess the clinical significance of CT-detected abnormalities in this area.

FOOTNOTE

[a]Mx8000, Philips Medical Systems, AE Eindhoven, The Netherlands.

[b]Osirix Image processing Software, Geneva, Switzerland.

[c]Playdoh®: Rainbow Crafts, Cincinnati, Ohio, USA.

[d]Mobilux, X-ray Equipment Verachtert, Antwerpen, Belgium.

[e]Totoku monochrome LCD display, Lewisville, Texas, USA.

[f]Microsoft Excel, Microsoft Corp., Redmond, Washington, USA.

REFERENCES

1. Wright I.M. A study of 118 cases of navicular disease: radiological features. Equine Vet J 1993; 25: 493-500.
2. Dyson S., Murray R., Blunden T., et al. Current concepts of navicular disease. Equine Vet Educ 2006; 18: 45-56.
3. Robert C., Valette J.P., Denoix J.M. Correlation between routine radiographic findings and early racing career in French Trotters. Equine Vet J Suppl 2006; 36: 473-478.
4. Dik K.J. Diagnostische beeldvorming. In: De Veterinaire Keuring van het Paard, 3nd edn., Eds: Sloet van Oldruitenborgh-Oosterbaan M.M., Barneveld A., Van Den Belt A.J., Libre BV, Leeuwarden 2007: 85-112.
5. Rose R.J., Taylor B.J., Steel J.D. Navicular disease in the horse: an analysis of seventy cases and assessment of a special radiographic view. J Eq Med Surg 1978; 2: 492-497.
6. MacGregor C.M. Radiographic assessment of navicular bones, based on changes in the distal nutrient foramina. Equine Vet J 1986; 18: 203-206.
7. Hertsch B.**,** Dammer H. The blood supply of normal and diseased navicular bones. Vet Rad 1988; 29: 276-281.
8. Kaser-Hotz B., Ueltschi G. Radiographic appearance of the navicular bone in sound horses. Vet Radiol Ultrasound 1992; 33: 9-17.
9. Tietje S. Computed tomography of the navicular bone region in the horse: a comparison with radiographic documentation. Pferdeheilkunde 1995; 11: 51-61.
10. Widmer W.R., Buckwalter K.A., Fessler J.F., et al. Use of radiography, computed tomography and magnetic resonance imaging for evaluation of navicular syndrome in the horse. Vet Radiol Ultrasound 2000; 41: 108-116.
11. Groth A.M., May S.A., Weaver M.P., et al. Intra- and interobserver agreement in the interpretation of navicular bones on radiographs and computed tomography scans. Equine Vet J 2009; 41: 124-129.
12. Landis J.R., Koch G.G. The measurement of observer agreement for categorical data. Biometrics 1977; 33**:** 159-174.
13. Claerhoudt S., Bergman E.H.J., van der Veen H., et al. Computed tomographic morphology of the synovial invaginations of the distal sesamoid bone of the horse. Anat Histol Embryol 2011; 40: 55-60.
14. Murray R.C., Blunden T.S., Schramme M.C., et al. How does magnetic resonance

imaging represent histologic findings in the equine digit? Vet Radiol Ultrasound 2006; 47: 17-31.

15. Colles C.M. Interpreting radiographs 1: The foot. Equine Vet J 1983; 15: 297-303.
16. Rijkenhuizen A.B.M., Németh F., Dik K.J., et al. Development of the navicular bone in foetal and young horses, including the arterial supply. Equine Vet J 1989; 21: 405-412.
17. Altman D.G. Some common problems in medical research. In: Practical statistics for medical research, 1st edn, Ed: Altman D.G., Chapman & Hall, London 1991: 396-439.
18. Pearce S.G., Boure L.P., Bolger A., et al. Effect of heel elevation on forelimb conformation in horses. Aus Vet J 2004; 82: 558-562.
19. van Dixhoorn I.D.E., Meershoek L.S., Huiskes R., et al. A discription of the motion of the navicular bone during *in vitro* vertical loading of the equine forelimb. Equine Vet J 2002; 34: 594-597.
20. Dik K.J., van den Belt A.J.M., Enzerink E., et al. The radiographic development of the distal and proximal double contours of the equine navicular bone on dorsoproximal-palmarodistal oblique (upright pedal) radiographs, from age 1 to 11 months. Equine Vet J 2001; 33: 70-74.

CHAPTER 6

Morphology of distal border synovial invaginations of the equine navicular bone: Comparison between computed tomography and a hoof-specific radiographic projection

Adapted from: Claerhoudt S, Bergman H.J, van der Veen H, Duchateau L, Raes E.V, Saunders J.H. Morphology of distal border synovial invaginations of the equine distal sesamoid bone: Comparison between computed tomography and a hoof-specific radiographic projection. Veterinary and Comparative Orthopaedics and Traumatology 2012; 25: 453-459.

SUMMARY

Our objectives were to compare the variability and agreement of the morphology of distal border synovial invaginations on a DPr-PaDiO projection with hoof-specific angle vs. CT.
Computed tomography images and a DPr-PaDiO radiographic projection with hoof-specific angle were obtained on 50 cadaver forefeet from 25 Warmblood horses. Computed tomography was assumed to be the standard test. The number, shape and depth of penetration of distal border synovial invaginations into the navicular bone were evaluated with both methods, and the comparison of their measurements was statistically described.
Significantly more invaginations were seen on CT compared to radiography, with an observed average difference of 1.2. In no case of our sample of horses, radiography showed a higher number of invaginations than CT. No statistically significant difference for depth between CT and the DPr-PaDiO projection was seen, however, there was quite a large variation of the actual difference of measurements against their mean. Radiography mainly underestimated the depth of the deeper invaginations. The agreement between both modalities for shape was moderate to good. A high sensitivity and very high specificity of the specific DPr-PaDiO projection for shape was found (97%).
The radiographic projection with hoof-specific angle showed only partially the number and depth of the distal border synovial invaginations as evaluated with CT. Moreover, this projection did not assess the morphology of the straight running invaginations more accurately, as we had hypothesized, but more accurately evaluated the dorso-/palmaroproximal oriented invaginations.

CHAPTER 6

INTRODUCTION

Although abnormal distal border synovial invaginations of the navicular bone are described being related with navicular disease, their clinical relevance still remains unclear. The presence of more than 7 synovial invaginations, inverted flask-shaped, moderate to deeply penetrating invaginations along the horizontal or sloping distal navicular borders, are considered a poor condition and more likely of clinical significance (1-10).

During purchase examinations, the distal border synovial invaginations are often graded, according to radiographic classification systems, using a D45°-70°Pr-PaDiO radiographic projection. A recent study has reported a high variability concerning the number and depth, and a high specificity for shape of the distal border synovial invaginations between 3 radiographic projections (D45°Pr-PaDiO, D55°Pr-PaDiO and D65°Pr-PaDiO) and CT, which was used as the standard test (11). Three factors were suggested to explain the poor agreement: the variable height of the heels, the different orientations of the invaginations into the navicular bone (12), and the superimposition of the navicular bone over other structures on a DPr-PaDiO projection.

In the present study, the authors hypothesized that it should be possible to select a DPr-PaDiO projection that allowed better evaluation of the majority of synovial invaginations in the individual horse compared to the (standard) D55°/65°Pr-PaDiO radiographic projections. For this, the degree of angulation of the DPr-PaDiO projection is selected based on the height of the heels and the most common ‘straight’ direction of the invaginations in the navicular bone (12). The aim of the study was to compare the morphology of distal border synovial invaginations on this hoof-specific DPr-PaDiO projection with CT.

MATERIALS AND METHODS

Material

The material used in this study consisted of 50 forefeet of 25 Warmblood horses (mean age: 7 years). All horses were subjected to euthanasia for reasons unrelated to this study. All feet were severed at the level of the metacarpophalangeal joint immediately after euthanasia. The shoe and loose horn in the sole, if present, were removed and the frog was cleaned. The feet were not selected by any particular criteria and both forefeet of each horse were included.

CT examination

The CT scans were performed with a 4-detector row spiral CT scanner[a] in which the feet were placed in the gantry with the longitudinal axis of the foot oriented parallel to the CT table and perpendicular to the plane of the CT gantry. The medial side of the foot was marked. The limbs were scanned in a distal-to-proximal direction. The output parameters were 120 kV and 250 mAs per slice. The slice thickness was 0.6 mm, pitch of 0.875 cm, 0.3 increment and 1-second rotation time. Transverse CT scans were reconstructed from the level of the distal to the proximal aspect of the navicular bone using a bone window setting (WL: 200-600; WW: 1000-2000), 250 mm field of view and 512 x 512 pixel matrix. The average total time required for scanning of each foot was 46.25 seconds. From the transverse images, dorsal reconstructions with a slice thickness of 0.6 mm were reformatted by use of software[b].

Radiographic examination

Radiographic examination was performed after the CT examination. The sulci of the frog were packed with modelling compound[c]. A LM and DPr-PaDiO radiographic projection was performed on all feet. The LM projection was made without a grid with the foot placed on a flat wooden block, to calculate the specific slope used for the DPr-PaDiO projection. On the LM projection, first a line was drawn parallel to the flexor cortex of the navicular bone. A second line was drawn through the most proximal point of the extensor process of the distal phalanx bone perpendicular to the first line. The angle between this latter line and a horizontal line, representing the flat wooden block, was measured (Fig. 1). Further, the foot was placed on a wooden block with a slope of 45° with the horizontal, and by the use of wedges (slope of 2°, 3°, 4° and 7° with the horizontal), a DPr-PaDiO projection with specific slope for a particular foot was made, using a grid. If the measured angle was lower than 45°, a construction was made and the feet were angled until the specific angle was reached. The x-

ray beam of the tube[d] was kept horizontal and centered 2 cm proximal to the coronary band at the midline of the foot. By using this hoof-specific angle, the beam was directed perpendicular to the flexor cortex of the navicular bone, thus perpendicular to the straight running invaginations. The feet were radiographed using 60 kV and 12.5 mAs, a grid (6:1 ratio, 103 lines/cm) and a 100 cm focus-film distance.

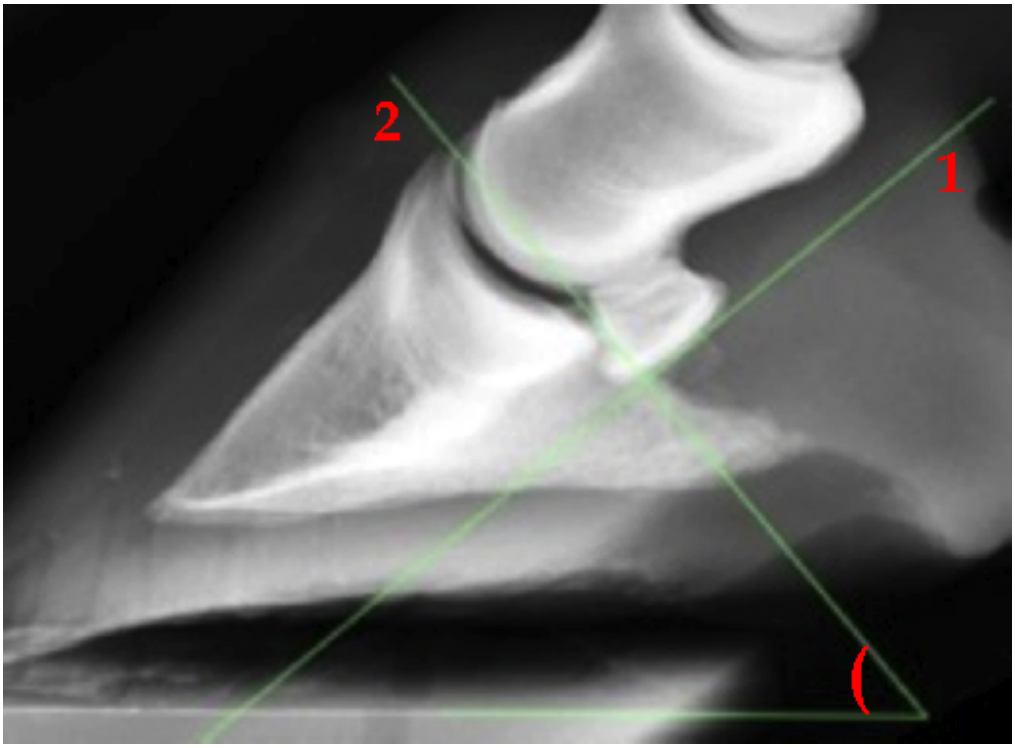

Fig. 1: Illustration of the specific slope measurement using the lateromedial radiographic projection. (1= first line parallel with the flexor cortex of the navicular bone; 2 = second line perpendicular to the first line and tangent line with the extensor process of the distal phalanx; bracket ' (' = hoof-specific angle). Left = dorsal; right = palmar.

Image analysis

Two observers, one board-certified radiologist (JHS) and one PhD-student (SC) interpreted all CT and radiographic images together and a diagnosis was made in consensus. The radiographic image of a particular foot and hoof angle were reviewed in a randomized order at the same workstation, on the same diagnostic imaging screens[e] and using a similar evaluation, to determine the number of distal border synovial invaginations. Furthermore, for each invagination, the depth and shape were determined. Next, the CT images of a particular foot were reviewed in a random order as well to determine the number of synovial invaginations

using transverse slices and dorsal reconstructions, and for each invagination, the depth and shape were determined.

In a second step, the corresponding radiographic and CT images were considered together. To compare depth and shape assessments on the 2 imaging modalities, only distal border synovial invaginations for which an assessment was available on both radiography and CT were used (some invaginations seen with CT were not seen with radiography).

The depth of penetration of the synovial invaginations was assessed on the dorsal reconstructed CT and radiographic images. Each invagination was calculated by an imaging software[b] using the following equation: Depth $(R) = A/B$, where A = distance (in centimetre) between the most distal basis and the proximal top of the invagination, B = distance (in centimetre) between the distal groove (level where the invaginations are located and assessed) and proximal border of the navicular bone on the CT images, and distance (in centimetre) between the most distal basis of the invagination and proximal flexor border on the radiographs. Data of depth were classified in 3 categories: $1 = R \leq 0.33$, $2 = 0.33 < R \leq 0.5$ and $3 = R > 0.5$.

The shape of the distal border synovial invaginations was assessed on dorsal CT and radiographic images. The shape could be categorized into 4 categories: 'conical', 'linear', 'lollipop' or 'branched'**.** For statistical aims, this group of 4 shapes will be further described as 'shape4'. Additionally, the group was divided into 2 groups (further described as 'shape2'), with group 1 representing the normal ('conical'- or 'linear'-shaped), and group 2 the abnormal shapes ('lollipop'- or 'branched'-shaped).

Since it is described that the synovial invaginations at the distal navicular border run in different directions in the navicular bone, they were classified as 'straight' or 'dorsoproximal/palmaroproximal' running invaginations (12).

Statistical analysis

To compare the observed number and depth of the distal border synovial invaginations between CT and the DPr-PaDiO projection, Student's t-test was used with foot as block variable for the number and invagination as block factor for the depth. The results were summarized by the average/mean difference and corresponding 95% CI and 95% RI. The 95% RI is given by the mean difference +/- 2 times the SD, which contains 95% of the actual differences if the normal distribution assumption holds. Bland Altman plots are provided for CT versus the DPr-PaDiO projection, to investigate a possible relationship between the difference and the magnitude of the measurement.

The effect of type of orientation of the synovial invaginations on the difference between CT and radiography for number and depth was evaluated by a mixed model, with horse and horse nested in foot as random effects. All tests were based on a significance level of 5% and performed using statistical software[f].

The degree of agreement between CT and the DPr-PaDiO projection for number, depth (taken as categorical variables) and shape was quantified using the κ-statistic. The guidelines for strength of agreement based on the values of κ were: < 0.20 poor, 0.21-0.40 fair, 0.41-0.60 moderate, 0.61-0.80 good and 0.81-1.00 very good (17).

RESULTS

The foot-specific angle ranged from 40° to 62°, with an average angle of 51.3° ± 5.2. Three feet (6%) had a measured angle lower than 45°.

Number

The average number of distal border synovial invaginations was 5.9 ± 1.56 on CT and 4.08 ± 1.61 on the DPr-PaDiO projection (total of 204), with 116/204 (56.9%) running straight and 88/204 (43.1%) running in a dorso-/palmaroproximal direction in the navicular bone, according to the CT images. In only 8/50 (16%) feet, the number of synovial invaginations counted on CT scans and on the DPr-PaDiO projection were equal. Even in 3/50 (6%) feet, no invaginations were detected on the radiographic projection, however 3, 4 and 6 invaginations respectively, were counted on CT. In no case of our sample of horses, radiography showed a higher number of invaginations than CT (Figs. 2 and 4).

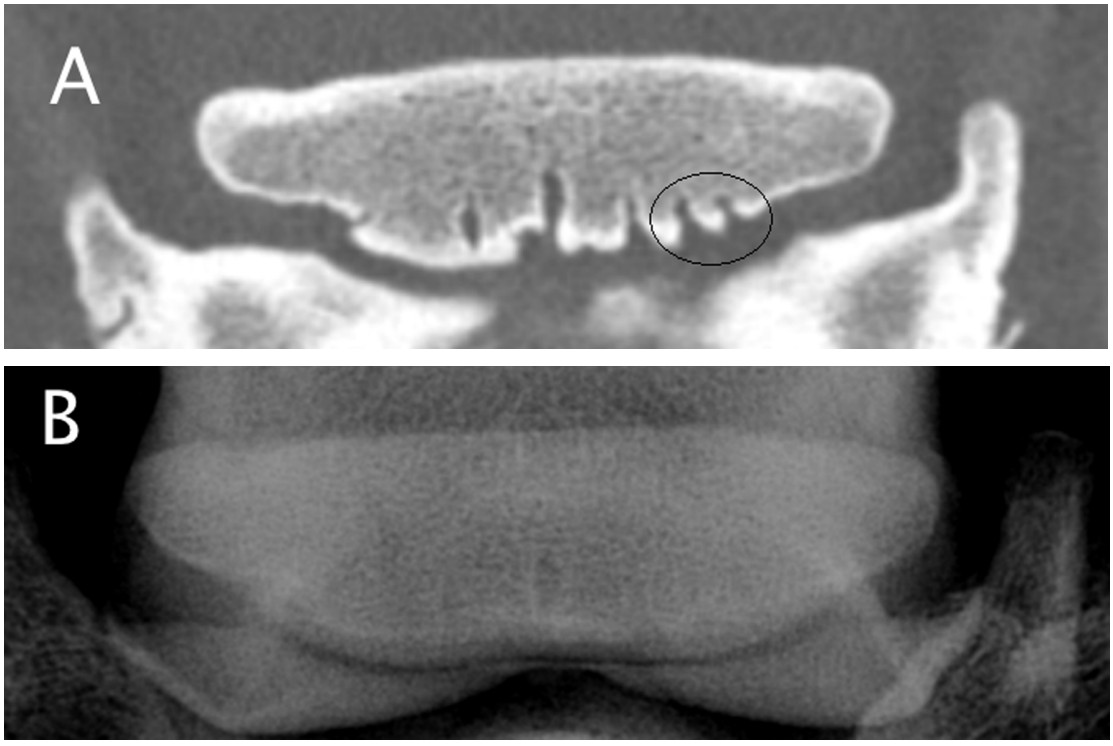

Fig. 2: Dorsally reconstructed CT image with bone window settings (A) and dorso 50° proximal-palmarodistal oblique radiograph (B) of a navicular bone. The 2 most medially located synovial invaginations on the CT image (circle) are undetectable on the radiographic image. Left = lateral.

Significantly more distal border synovial invaginations were seen on CT compared to radiography ($P < 0.001$), with an observed average difference of 1.2 (95% CI: 0.86 – 1.46). According to the 95% reference interval (95% RI: -0.99 – 3.3), a large variation of the actual differences was observed. The mean difference for the number of straight running synovial invaginations on CT versus radiography was equal to 0.94 (95% CI: 0.67 – 1.20; 95% RI: -0.91 – 2.78) and differed significantly ($P < 0.001$) from that of the dorso-/palmaroproximal running ones, which was equal to 0.36 (95% CI: 0.16 – 0.53; 95% RI: -0.86 – 1.56). The Bland Altman plots of the difference for number between both modalities for all data against their mean, is given in Fig. 3.

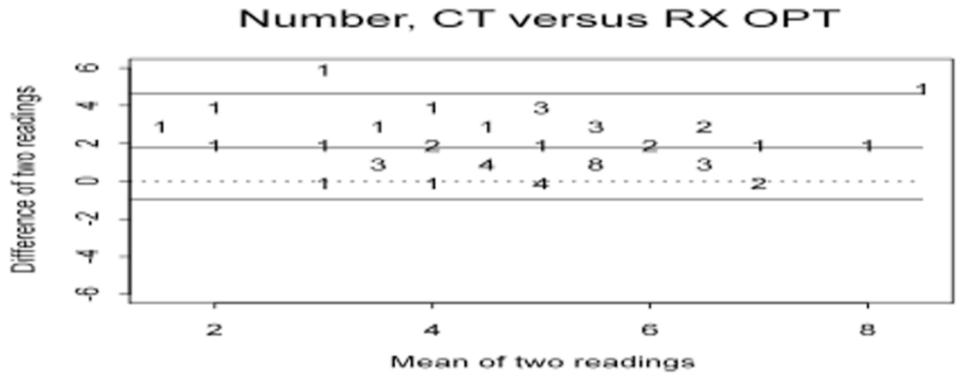

Fig. 3: Bland Altman plots: Differences of counted numbers (readings) on CT and radiographic image with hoof-specific angle (OPT) against their mean. The numerical code represents the number of navicular bones (total sum of 50) with the same difference in number against mean. Dashed line represents zero-level (no difference), upper line = mean + 2SD, middle line = mean, lower line = mean – 2SD.

The weighted- and unweighted κ-values between CT and the particular radiographic projection for number of all invaginations were low (0.37 and 0.17, respectively), representing a poor agreement between both modalities.

Depth

No statistically significant mean difference for depth between CT and the DPr-PaDiO projection was seen ($P > 0.05$). The mean difference between CT and radiography was equal to -0.0001 (95% CI: -0.02 – 0.02), meaning that there seems to be little or no bias. The 95% RI for the radiographic projection corresponds to -0.22 – 0.22, meaning that quite a large variation of actual differences between CT and radiography is present. The mean difference for the depth of the straight running distal border synovial invaginations measured on CT

versus radiography was equal to 0.01 (95% CI: -0.01 – 0.04; 95% RI: -0.23 – 0.26), and -0.02 (95% CI: -0.04 – 0.002; 95% RI: -0.19 – 0.16) for the dorso-/palmaroproximal running ones. None of the two differed significantly from zero (P > 0.05). The mean difference between the straight and dorso-/palmaroproximal running invaginations was equal to 0.03, which was also not statistically significant (P = 0.07). A Bland Altman plot of the differences for depth between both modalities for all data against their mean is given in Fig. 4. These plots show that radiography occasionally under- or overestimated the depth of the invaginations compared with CT. Moreover, the depth of the mildly penetrating invaginations tends to be routinely overestimated, whereas the depth of the deeper penetrating invaginations is mostly underestimated.

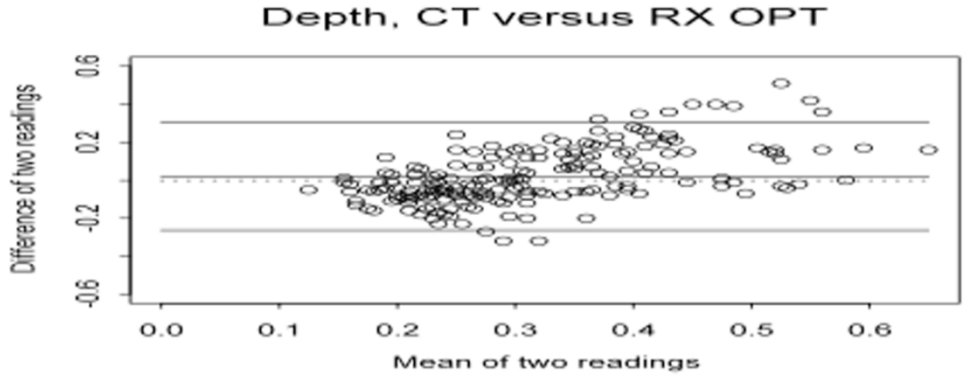

Fig. 4: Bland Altman plots: Differences of the equations of depth (readings) on CT and radiographic image with hoof-specific angle (OPT) against their mean. Each individual plot (O) represents a synovial invagination (total of 204 plots). Dashed line represents zero-level (no difference), upper line = mean + 2SD, middle line = mean, lower line = mean – 2SD.

The weighted- and unweighted κ-values between CT and the DPr-PaDiO projection for depth of all data were equal to 0.45 and 0.43 respectively, representing a moderate agreement between both modalities. The agreement between CT and the radiographic projection for depth of straight and dorso-/palmaroproximal running synovial invaginations was comparable (κ-values of 0.42 and 0.44, respectively).

Shape

In 3/8 (37.5%) feet with an equal number of distal border synovial invaginations on both the CT scans and the particular DPr-PaDiO projection respectively, the shape was comparable on both methods. The agreement between both modalities for shape2 and shape4 was good (weighted κ-value of 0.75 and 0.62, respectively).

The sensitivity, specificity (both measured for shape2) and corresponding 95% CIs of the DPr-PaDiO projection for shape, with CT as standard test, are summarized in Table 1.

Table 1: Sensitivity and specificity of the dorsoproximal-palmarodistal radiographic projection with hoof-specific angle for shape of total, straight and dorso-/palmaroproximal running invaginations with CT as standard test.

	Sensitivity (95% CI)	**Specificity (95% CI)**
Total	0.75 (0.60 – 0.87)	0.97 (0.92 – 0.99)
Straight	0.64 (0.43 – 0.82)	0.95 (0.89 – 0.99)
Dorso-/palmaroproximal	0.89 (0.67 – 0.99)	0.98 (0.91 – 1.00)

Key: CI = confidence interval

DISCUSSION

The present study was carried out to assess the variability and agreement between the morphology of distal border synovial invaginations of the navicular bone on a DPr-PaDiO radiographic projection with hoof-specific angle and CT scans. Histology is regarded as the gold standard for the diagnosis of tissue abnormalities (13). In the present study, no histological examination was performed, however, due to the possibility of reconstruction of multiplanar, high-resolution images without superimposition, CT provides detailed anatomical information of the synovial invaginations (14). Therefore, CT was assumed by the authors to be the standard test.

The mean difference of our sample data between CT and the hoof-specific radiographic projection for number was positive and differed significantly from zero, meaning that there was a statistically significant mean difference between the observations on CT and radiography. Overall, the visibility of the distal border synovial invaginations was better on CT compared to radiography. Similar conclusion was reached in previous studies (11, 14-16). In our study, the mean difference between both the modalities for number of the sample data was lower compared to the results of a previous study of the same population (1.2 versus 2) (11). In both the studies, a statistically significant mean difference between CT and radiography for number of synovial invaginations was found.

Based on the results of our study, our hypothesis can be rejected. The mean difference and corresponding 95% RI of our data between CT and the hoof-specific projection for number of the dorso-/palmaroproximal running invaginations was lower and less wide than for the straight running ones (0.36 vs. 0.94) in the present study. Both mean differences were statistically significant. Also the intervals for both groups of oriented invaginations were less wide compared to the 95% RIs for number of the invaginations of the 3 DPr-PaDiO radiographic projections described in a previous study (11). This means that the hoof-specific radiographic projection appeared better and showed a lower variance in the evaluation of the number of dorso-/palmaroproximal running distal border synovial invaginations.

The κ-values between CT and the particular radiographic projection for number of all invaginations were low, representing a poor agreement between both techniques for number. However, the weighted κ-value in the present study was higher (0.37) than in a previous study on the same horse sample (0.18) (11). However, these κ-values may not be compared since there were a different number of categories for number between both studies (7 vs. 12 categories, respectively), logically resulting in higher κ-values in the current study.

The better assessment of the distal border synovial invaginations on CT may be explained by the lack of superimposition of surrounding bone and the high sensitivity of CT for detecting bone in detail, compared to radiography. The distal border synovial invaginations that were ill-defined or undetectable on radiography were mostly small and located at the distal sloping borders of the navicular bone on the CT images. The clinical significance of these subtle CT findings remains questionable. It has been described that the presence of small synovial invaginations at the sloping borders on CT may be observed in normal navicular bones, but significant if seen on radiographs (3, 14).

Results of our study show no statistically significant mean difference for depth of the distal border synovial invaginations between CT and the hoof-specific radiographic projection. The mean differences of measurements for depth between CT and radiography were all close to zero, meaning that the hoof-specific angle may appear good for the evaluation of the depth. Nevertheless, the RIs were wide, representing a large variation of the actual differences. These findings were comparable with those described in a previous study of the same sample of horses (11). However, the radiographic projection with hoof-specific angle showed a narrower RI for the dorso-/palmaroproximal running invaginations, so lower variance of the individual observations, compared to the (standard) DPr-PaDiO radiographic projections (11). Moreover, also its κ-values were higher (weighted κ-value of 0.45 vs. 0.28 respectively), representing a moderate agreement between the hoof-angle specific projection and CT for depth of the invaginations. In comparison with the results of a previous study on our horse population (11), radiography mainly underestimated deeper penetrating invaginations as well. This may be explained by the fact that most deep invaginations on CT were ending proximally as tiny, deeply penetrating lines, which were undetectable on radiography (Fig. 5). Such a result may have clinical importance since literature describe that an increase in the depth of penetration of distal border synovial invaginations is considered a significant radiographic finding (9, 10). However, the clinical significance of these small, tiny but deeply penetrating invaginations on CT has to be examined.

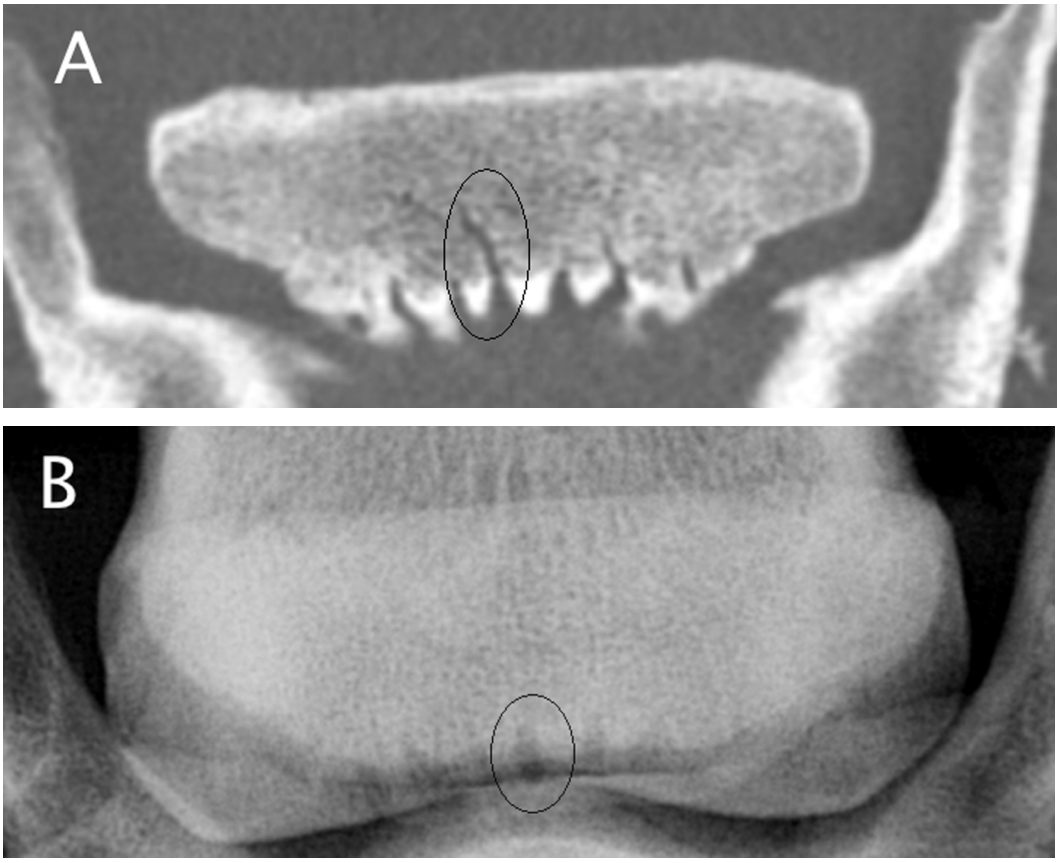

Fig. 5: Dorsally reconstructed CT image with bone window settings (A) and corresponding dorso 62° proximal-palmarodistal oblique radiograph (B) of a navicular bone, showing a deeply penetrating invagination on the CT image (circle), which is mildly penetrating on the radiographic image (circle). Left = lateral.

In the current study, the sensitivity and specificity of the DPr-PaDiO projection with hoof-specific angle for shape were high. A 97% specificity and 75% sensitivity were found, meaning that almost no false positive, but more false negative results were seen. To summarize, if an abnormally shaped synovial invagination is seen on the hoof-specific radiographic projection, there is high probability that it is effectively abnormal, but if a normal one is seen, it can be abnormal on CT (Fig. 6). A sensitivity of 89% was measured for the dorso-/palmaroproximal running distal border synovial invaginations, which was clearly higher than the sensitivity of the 3 DPr-PaDiO radiographic projections described in a previous study (11).

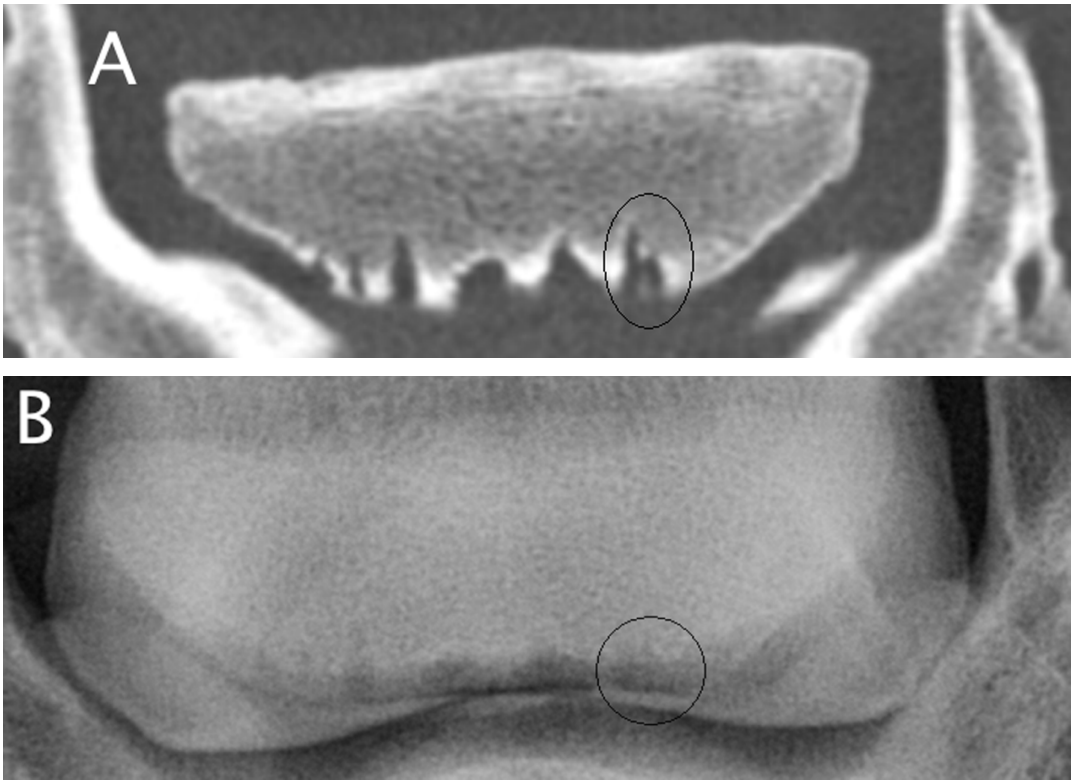

Fig. 6: Dorsally reconstructed CT image with bone window settings (A) and corresponding dorso 50° proximal-palmarodistal oblique radiograph (B) of a navicular bone, showing a branched-shaped invagination on the CT image (circle), which is conical-shaped on the radiographic image. Left = lateral.

Statistically, the κ-value was measured using a 2 x 2 table for shape2 (2 groups/categories, see above) and a 4 x 4 table for shape4 (4 categories). For the resulting 2 x 2 table, a high κ-value (0.75) was found, as for the 4 x 4 table (0.62). The depth was classified in 3 categories for the statistical analysis of the agreement (1 = mildly, 2 = moderately and 3 = deeply penetrating). In contrast, data of number were classified in 7 categories (the counted number of invaginations per bone varied from 0 to maximum 6 invaginations, equal to 7 categories), logically resulting in lower κ-values than for depth or shape (17). More specifically, κ-values of variables with different number of categories may not be compared. In theory, any value of κ much below 0.5 will indicate poor agreement. However, despite these published guidelines, no κ-value can be regarded universally as indicating some degree of agreement (17, 18). Actually, the value of κ depends on the number of categories and upon circumstances, as demonstrated in our results.

In a previous study of the same authors, a variable morphology of the distal border synovial invaginations was found between the 3 radiographic projections and CT (11). Three factors were suggested to explain these results: the variable height of the individual heels, the

different orientations of distal border synovial invaginations into the navicular bone (12) and the superimposition of the navicular bone over other structures on a DPr-PaDiO projection. In the present study, the authors hypothesized that ruling out two of the three influencing factors by measuring an optimal angle based on the height of the heels and the most common 'straight' direction of the invaginations in the navicular bone (12), a better evaluation of the majority of synovial invaginations in the individual horse would be possible. In theory, when the x-ray beam is directed perpendicular to the straight running synovial invaginations into the navicular bone, their morphology should be assessed more accurately. Unfortunately, this hypothesis can be rejected, as we found more favorable results (less variability, moderate agreement and highest sensitivity and specificity) between the specific radiographic projection and CT for the number, depth and shape of the dorso-/palmaroproximal running distal border synovial invaginations.

A potential limitation of this study could be the absence of a PaPr-PaDiO projection, which permits evaluation of the navicular bone without superimposition. However, this projection only allows evaluation of the number and width of the distal border synovial invaginations (2) and was therefore not included in our study.

We can conclude that our hypothesis can be rejected and the radiographic projection with hoof-specific angle did not assess the straight running invaginations better. Contrary, the dorso-/palmaroproximal running invaginations were assessed more accurately, however, this type of oriented invaginations were diagnosed in the minority in the navicular bones in our sample population. Overall, this radiographic projection with hoof-specific angle still showed a statistical significant mean difference with CT for number of the invaginations, as well as a a quite wide variability of the individual observations relative to their mean difference for their depth. However, this projection showed a higher sensitivity for shape of the synovial invaginations compared with the 3 DPr-PaDiO radiographic projections (11).

FOOTNOTE

[a]Mx8000, Philips Medical Systems, AE Eindhoven, The Netherlands.

[b]Osirix Image processing Software, Geneva, Switzerland.

[c]Playdoh®: Rainbow Crafts, Cincinnati, Ohio, USA.

[d]Mobilux, X-ray Equipment Verachtert, Antwerp, Belgium.

[e]Totoku monochrome LCD display, Lewisville, Texas, USA.

[f]SAS version 9.2: SAS Corporation, Cary, NC, USA.

REFERENCES

1. Colles C.M., Hickman J. The arterial supply of the navicular bone and its variations in navicular disease. Equine Vet J 1977; 9: 150-154.
2. Rose R.J., Taylor B.J., Steel J.D. Navicular disease in the horse: an analysis of seventy cases and assessment of a special radiographic view. J Eq Med Surg 1978; 2: 492-497.
3. Colles C.M. Interpreting radiographs 1: The foot. Equine Vet J 1983; 15: 297-303.
4. MacGregor C.M. Radiographic assessment of navicular bones, based on changes in the distal nutrient foramina. Equine Vet J 1986; 18: 203-206.
5. Pool R.R., Meagher D.M., Stover S.M. Pathophysiology of navicular syndrome. Vet Clinics of North Am Equine Pract 1989; 5: 109-129.
6. Kaser-Hotz B., Ueltschi G. Radiographic appearance of the navicular bone in sound horses. Vet Radiol Ultrasound 1992; 33: 9-17.
7. Wright I.M. A study of 118 cases of navicular disease: radiological features. Equine Vet J 1993; 25: 493-500.
8. Seyrek-Intas D., Tellhelm B., Reckels F.J. Interpretation and diagnostic value of some radiological findings in the navicular bone. Pferdeheilkunde 1999; 15: 406-418.
9. Robert C., Valette J.P., Denoix J.M. Correlation between routine radiographic findings and early racing career in French Trotters. Equine Vet J Suppl 2006; 36: 473-478.
10. Dik K.J. Diagnostische beeldvorming. In: De Veterinaire Keuring van het Paard. Sloet van Oldruitenborgh-Oosterbaan M.M., Barneveld A., Van Den Belt A.J. (eds). Libre BV, Leeuwarden 2007; 85-112.
11. Claerhoudt S., Bergman H.J., van der Veen H., et al. Differences in the morphology of distal border synovial invaginations of the distal sesamoid bone in the horse as evaluated with CT compared to radiography. Equine Vet J 2012; 44: 679-683.
12. Claerhoudt S., Bergman H.J., van der Veen H., et al. Computed tomographic morphology of the synovial invaginations of the distal sesamoid bone of the horse. Anat Histol Embryol 2011; 40: 55-60.

13. Murray R.C., Blunden T.S., Schramme M.C., et al. How does magnetic resonance imaging represent histologic findings in the equine digit? Vet Radiol Ultrasound 2006; 47: 17-31.
14. Groth A.M., May S.A., Weaver M.P., et al. Intra- and interobserver agreement in the interpretation of navicular bones on radiographs and computed tomography scans. Equine Vet J 2009; 41: 124-129.
15. Widmer W.R., Buckwalter K.A., Fessler J.F., et al. Use of radiography, computed tomography and magnetic resonance imaging for evaluation of navicular syndrome in the horse. Vet Radiol Ultrasound 2000; 41: 108-116.
16. Dyson S., Murray R., Blunden T., et al. Current concepts of navicular disease. Equine Vet Educ 2006; 18: 45-56.
17. Landis J.R., Koch G.G. The measurement of observer agreement for categorical data. Biometrics 1977; 33: 159-174.
18. Altman D.G. Some common problems in medical research. In: Practical statistics for medical research. Altman D.G. (ed). Chapman & Hall, London 1991; 396-439.

CHAPTER 7

Association between navicular bone shape and distal border fragmentation in Belgian Warmblood horses

Adapted from: Claerhoudt S, Pille F, Vanderperren K, Van der Vekens E, Duchateau L, Hauspie S, Saunders J.H. Association between navicular bone shape and distal border fragmentation in Belgian Warmblood horses**.** Veterinary and Comparative Orthopaedics and Traumatology 2011; 24: 132-136.

SUMMARY

The objectives of our study were to investigate whether in navicular bones from Warmbloods distal border fragmentation is associated with the shape of the proximal articular border or other radiological findings. Radiographs of the front feet of 325 normal, subadult horses presented for admission as breeding stallion were reviewed. The proximal articular border of the total of 650 navicular bones was classified as straight (n=278), convex (n=184), undulating (n=147) or concave (n=41). Distal border fragments were present in 57 navicular bones (8.8%). They were significantly more prevalent in bones with a concave (9/41; 22%) or undulating (19/147; 13%) proximal articular border compared to navicular bones with a straight (17/278; 6%) or convex shape (12/184; 7%). No other significant associations were found.

Hypothetically, since a shape-fragment association was found, and the distribution of biomechanical forces exerted on the navicular bone is assumed to be shape dependent, distal border fragments may be a result of unfavorable loading of the navicular region.

CHAPTER 7

INTRODUCTION

Navicular disease is a chronic, progressive disorder typically affecting riding horses of middle age, and causing forelimb lameness (1-3). Gross changes observed in horses with navicular disease include soft tissue injuries such as fibrillation of the dorsal surface of the DDFT, adhesions between the flexor tendon and the palmar surface of the navicular bone, abnormalities at the origin of the DSIL and the CSL, as well as distension of the DIPJ and navicular bursa (4-6). Navicular bone abnormalities, such as subchondral bone cyst formation, erosion of the flexor cortex, and the presence of one or more distal border fragments, have also been well described in horses with chronic palmar foot pain (5, 7). With the advent of magnetic resonance imaging, the soft tissue and bone injuries of the digit have been well recognised due to change in signal intensity. An association between these soft tissue lesions and injuries of the navicular bone has been documented in former studies (3-6).

Osseous fragments located adjacent to the distal border of the navicular bone are suggested to arise as avulsion fractures at the insertion of the distal sesamoidean impar ligament, dystrophic mineralization in the impar ligament or as separate ossification centers (8-11). Their significance still remains unclear, although many authors have demonstrated that distal border fragments are seen with a significantly greater prevalence in horses with clinical navicular disease (5, 7, 12), compared to clinically healthy horses (13). The presence of bony fragments is suggested to be of clinical relevance, because they may be the result of abnormal strain at the attachment of the distal sesamoid impar ligament (3, 5**,** 7, 9).

It has been suggested that the pathological changes seen in navicular disease are promoted by biomechanical overload exerted via the DDFT on the distal half of the palmar surface of the navicular bone and its surrounding tissues (12, 15-18), presumably as a result of poor foot conformation, shoeing and the horse's movement pattern (2, 3, 16-19). Also the shape of the proximal articular border is assumed to influence the distribution of the forces exerted on the bone (20, 21). The latter study reported a shape-grade association, in which a concave or undulating shape showed the highest incidence of severe radiological features, meaning that these shapes were associated with the highest risk for development of navicular disease.

The aims of this study were to determine whether distal border fragmentation is associated with: 1) the shape of the proximal articular border, and 2) other radiological abnormalities of the navicular bone. The authors hypothesized that distal border fragments are seen much more in horses with a concave or undulating proximal border shape.

MATERIALS AND METHODS

Medical records of 325 male Belgian Warmblood horses (age range: 2-4 years) admitted for evaluation as breeding stallions at the Faculty of Veterinary Medicine, Ghent University between January 2007 and April 2009, were reviewed. Radiographic examination was performed after clinical evaluation. Prior to radiography, the feet were cleaned and trimmed. Shoes, if present, were removed and the sulci of the frog were packed with modelling compound[a]. Three radiographic projections of both forefeet of all horses were made: LM, D55°Pr-PaDiO and D65°Pr-PaDiO, using a 60kV and 12.5 mAs tube[b]. The LM projection was made without a grid and the foot was placed on a wooden block with a slope of 55° with the horizontal. The D55°Pr-PaDiO and D65°Pr-PaDiO projections were performed using a grid (6:1 ratio, 103 lines/cm). The radiographic beam was kept horizontal and the foot was placed on a wooden block, so that the front of the hoof wall angled forward at 55° and 65°, respectively. Two reviewers, one board-certified radiologist (JHS) and one PhD-student (SC) assessed the radiographic images together and reached a consensus for final scoring. The radiographs of a particular horse were evaluated all in the same order: first the LM, followed by the D65°Pr-PaDiO and the D55°Pr-PaDiO projection as a last.

The shape of the proximal articular border of the navicular bone was evaluated on the D55°Pr-PaDiO projection and classified, according to the classification of Dik and van den Broek (20), as ‘concave’, ‘undulating’, ‘straight’ or ‘convex’ (Fig. 1). The distal border of the navicular bone was inspected for the presence of osseous body(ies) (‘absent’ or ‘present’) using the 3 projections. On the two DPrPaDiO projections, the distal border synovial invaginations were classified on a scale of 0-4 using the standardised radiographic classification reported by Dik (8). The elongation of the proximal extremities was evaluated as ‘smooth’, ‘mild’ or ‘severe’. On the LM projection, the presence of a defect in the flexor cortex was judged and categorized into ‘no’, ‘smooth’ or ‘sharp’ defect**;** the demarcation of the flexor cortex and medulla was classified into ‘distinct’ or ‘indistinct’.

In order to study the association between the proximal navicular border shape and distal border fragments, a logistic regression model was used, with the shape as the independent categorical variable (4 shapes: ‘straight’, ‘convex’, ‘concave’ and ‘undulating’) and presence or absence of fragments as response variable. Results were summarized using odds ratios (OR) with the ‘straight’ shape as baseline category. A significance level (P-value) of 0.05 was used. The logistic regression model was also fitted to determine whether there was an

association with proximal border shape and other navicular bone abnormalities. The association between distal border fragments and other radiological findings of the navicular bone, was evaluated by the Fisher exact test.

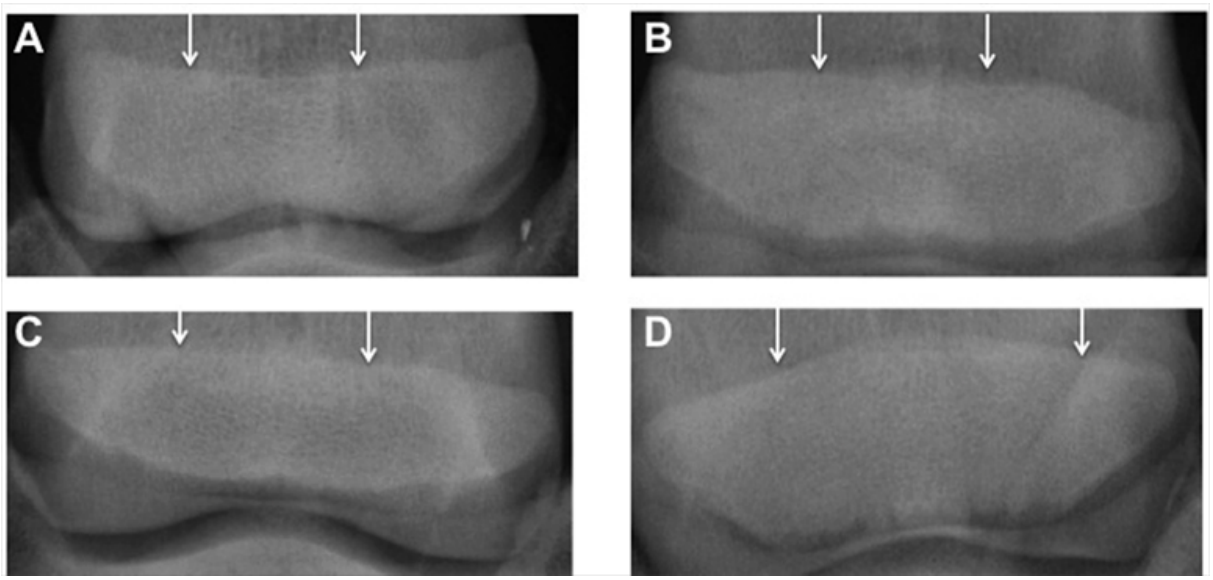

Fig. 1: Dorso 55° proximal-palmarodistal oblique radiographs showing the four different shapes of the proximal articular border of the navicular bone (arrows): A) concave, B) undulating, C) straight, D) convex.

RESULTS

The shape of the proximal articular border of the navicular bone was concave in 41/650 (6.3%), undulating in 147/650 (22.6%), straight in 278/650 (42.8%) and convex in 184/650 (28.3%) feet (Table 1).

Table 1: Prevalence (%) of proximal articular border shape associated with other navicular bone abnormalities in our study population.

	Concave (n = 41)	**Undulating (n = 147)**	**Straight (n = 278)**	**Convex (n = 184)**	**Totals (n = 650)**
Distal border fragments					
2. absent	32 (78%)	128 (87.1%)	261 (93.9%)	172 (93.5%)	**593**
3. present	9 (22%)	19 (12.9%)	17 (6.1%)	12 (6.5%)	**57**
Grade synovial invaginations					
• 0-2	37 (90.2%)	145 (98.6%)	272 (97.8%)	179 (97.3%)	**633**
• 3-4	4 (9.8%)	2 (1.4%)	6 (2.2%)	5 (2.7%)	**17**
Elongation proximal extremities					
• smooth	40 (97.6%)	140 (95.2%)	256 (92.1%)	177 (96.2%)	**613**
• mild	1 (2.4%)	7 (4.8%)	21 (7.6%)	7 (3.8%)	**36**
• severe	0 (0%)	0 (0%)	1 (0.3%)	0 (0%)	**1**
Flexor cortex defect					
• absent or smooth	41 (100%)	146 (99.3%)	278 (100%)	183 (99.5%)	**648**
• sharp	0 (0%)	1 (0.7%)	0 (0%)	1 (0.5%)	**2**
Cortex-medulla junction					
• distinct	39 (95.1%)	143 (97.3%)	273 (98.2%)	179 (97.3%)	**634**
• indistinct	2 (4.9%)	4 (2.7%)	5 (1.8%)	5 (2.7%)	**16**

Distal border fragments were found in 57/650 (8.8%) bones (Fig. 2) representing 47/325 (14.5%) horses, of which only 1 horse was unilaterally lame at the trot. Five percent of all the horses included in our study were lame, with an average lameness score of 2/5 at the trot in a straight line on a hard surface.

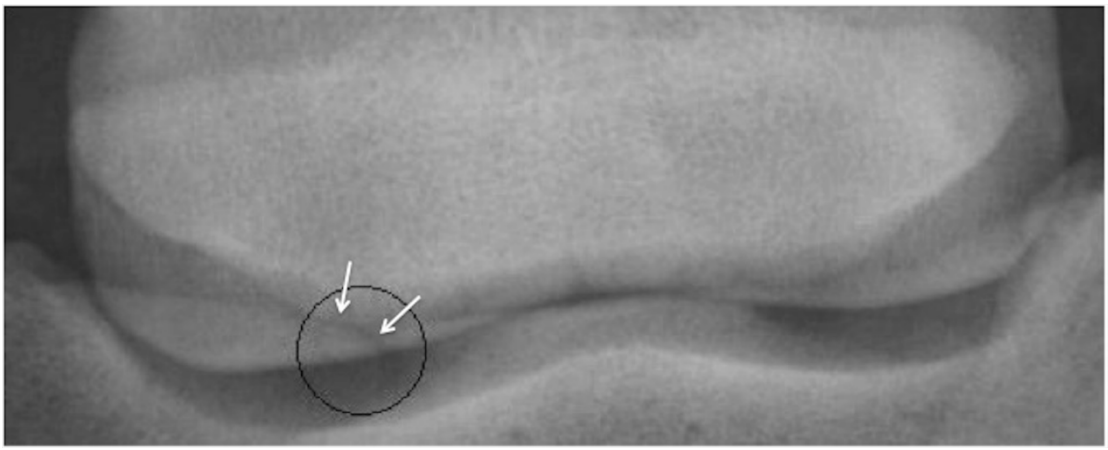

Fig. 2: Dorso 55° proximal-palmarodistal oblique radiograph of the navicular bone of the left front foot. A bone fragment (circle) at the junction between the lateral sloping and horizontal distal borders of the navicular bone is visible. Adjacent to the fragment, a defect is present in the distal border of the navicular bone (arrows). Left = lateral.

Relative to the straight navicular bone shape, fragments were significantly more prevalent in navicular bones with a concave (OR = 4.32, P = 0.0012) or undulating (OR = 2.44, P = 0.010) proximal articular border, but not in the navicular bones with a convex proximal articular border (OR = 1.07, P = 0.86). Also, fragments were significantly more prevalent in navicular bones with a concave (9/41; 22%) or undulating (19/147; 13%) proximal articular border compared to bones with a straight (17/278; 6%) or convex border (12/184; 7%). The fragments were located medially and laterally in 6/57 (10.5%) bones, medially only in 10/57 (17.5%) bones and laterally only in 41/57 (72%) bones. The osseous fragments were best visualized on the D55°Pr-PaDiO projection in 30/57 (52.6%) bones, on the D65°Pr-PaDiO projection in 14/57 (24.6%) bones and equally visible on both of the DPrPaDiO projections in 13/57 (22.8%) bones. On the D55°Pr-PaDiO views, the distal border was superimposed over the distal interphalangeal joint in 22/43 (51%) and over the distal portion of the pastern bone in 21/43 (49%) bones with distal border fragments, compared to only 3/27 (11%) and 24/27 (89%) bones respectively, on the D65°Pr-PaDiO projections. The radiographs revealed a correspondingly defect in the adjacent distal margin of the navicular bone in 57/57 (100%)

bones with distal fragments, which was best visualized on the D55°Pr-PaDiO projection in 28/57 (49.1%), on the D65°Pr-PaDiO projection in 12/57 (21.1%) and equally visible on both of the DPrPaDiO projections in 17/57 (29.8%) bones. The other results for distal border synovial invaginations, proximal extremity elongation, flexor cortex defect and cortico-medullary demarcation, are summarized in Table 1. In 517/650 (79.6%) navicular bones, no radiographic abnormality was recognized; one abnormality was found in 125/650 (19.2%) bones and two abnormalities in 8/650 (1.2%) bones. Three or more abnormalities were not found in any navicular bone in our population. From the navicular bones with fragments, 2/57 (3.5%) bones showed 'enlarged' synovial invaginations, 3/57 (5.2%) had mild elongation of their extremities, 4/57 (7%) had a smooth flexor cortex defect and in 6/57 (10.5%) affected bones, an indistinct cortico-medullary demarcation was visible.

A significant association between the shape of the proximal articular border of the navicular bone and the presence of a distal border fragment was found (P = 0.0025). The odds ratios of fragments present in the group with a concave, undulating or convex shape for presence or absence of distal border fragments, were compared to the baseline group with the straight shape. The odds ratios, as well as the corresponding P-values and confidence intervals of presence of fragments and shape, are summarized in Table 2**.** The odds of the presence of fragments in the concave and undulating group were 4.32 and 2.44 times higher respectively, than in the straight group. No significant relationship was found between the presence of a fragment at the distal border and the other radiographic abnormalities of the navicular bone (P = 0.055). A significant association between the shape of the proximal articular border and other radiographic abnormalities was also not detected (P = 0.92).

Table 2: Association of proximal navicular border shape and distal border fragments (‘straight’ shape as baseline group).

Response variable	Independent variable	Odds ratio	P-value	95%CI
Fragment	Concave	4.32*	0.0012	1.78 – 10.49
Fragment	Undulating	2.44*	0.01	1.23 – 4.81
Fragment	Convex	1.07	0.86	0.5 – 2.3

Key: * indicates the Odds ratio which differs significantly from 1.

CHAPTER 7

DISCUSSION

In our study, distal border fragments, flexor cortex defects and elongation of the proximal extremities were found with a prevalence comparable to a previous study in clinically healthy horses (13). Abnormal synovial invaginations along the distal border, that were graded 3 or 4 according to the classification of Dik (8), were less frequently diagnosed in our study (2.6%) compared to 2 other studies (11% and 17.4% respectively) (13, 14). The discrepancy in prevalences of this finding may be explained by the difficulties and differences in criteria for differentiation between 'normal' and 'abnormal/enlarged' synovial invaginations, as well as the lack of intense exercise regime and training of our young Warmblood population. Additionally, a different population (breeds and age range) was used in the studies, and the prevalence of (mildly) lame horses was not mentioned in the study of Verwilghen and co-workers (14)**.** In our study, only 5% of the horses were mildly lame at the trot, but this is not considered to be of clinical relevance, because these young horses (age range: 2-4 years) were collected from pasture and were unmanageable, so no local analgesia of the palmar digital nerves for the diagnosis of palmar foot pain was performed. A board-certified radiologist with experience in equine radiology was involved in the assessment of the radiographs in the 3 studies. An indistinct cortico-medullary demarcation was only observed in 2.4% of the bones in our study compared to 16% in a previous study (13). This difference may be explained by the use of an additional PaPr-PaDiO projection in the latter study**.** This permitted good evaluation of the cortico-medullary demarcation, specifically in horses with ossified lateral cartilages. The absence of a PaPr-PaDiO projection in our study is considered a limitation regarding evaluation of the corticomedullary junction. However, the focus of our study was to visualize distal border fragments, and this additional projection mostly not provides more information to that obtained by the DPr-PaDiO radiographic views with different angulation (55° to 65°) regarding those fragments.

In a study of middle-aged horses with clinically evident navicular disease, distal border fragments were found with a prevalence of 40% (5). This higher prevalence, compared to our results in the young stallion population (8.8%) and the prevalence in previously reported studies (5.2 % - 7%) (13, 14), may suggest that these fragments are significant findings in navicular disease horses. In the present study, the odds of finding a distal border fragment in the group with a concave or undulating proximal border shape was significantly greater than the odds of finding a fragment in the group with a straight shape. Such associations probably

have important clinical relevance, however our study was purely a radiological study. Only a few studies have examined the biomechanical forces exerted on the navicular bone, and reported that these compressive forces are much higher in horses with navicular disease, presumably as a result of poor foot conformation, shoeing and the horse's movement pattern (15-18). Previous studies have assumed that the distribution of biomechanical forces exerted on the navicular bone, is shape dependent (20, 21), however, to the authors' knowledge, no biomechanical study has yet confirmed this assumption. Hypothetically, since a shape-fragment association was found and the distribution of biomechanical forces exerted on the navicular bone is assumed to be shape dependent, distal border fragments may be a result of unfavorable loading of the navicular region. Several authors have proposed that most bony fragments located at the distal border of the navicular bone, with a correspondingly shaped defect in the adjacent navicular bone and no indication of osseous union, are most likely avulsion fractures. Their presence is suggested to be of clinical relevance, because they may be the result of abnormal strain at the attachment of the distal sesamoid impar ligament to the navicular bone (3, 5, 7, 9). To the authors' knowledge, no histological study has yet shown that distal border fragments are related to abnormal strain at the attachment of the impar ligament. However, in all of the bones with distal border fragments in our study, a correspondingly fracture bed defect was recognized in the adjacent distal margin of the navicular bone, which may strengthen the hypothesis that distal border fragments arise from an avulsion fracture.

Besides, no other association with the shape was statistically significant and also no significant association between the presence of a distal border fragment and the other radiographic abnormalities of the navicular bone was observed in our study. Furthermore, it is described that in some horses with clinically evident navicular disease, distal border fragments can occur in the absence of other pathological changes of the navicular bone (5). In our study, the majority of the navicular bones (79.6%) did not have any detectable radiographic abnormalities. However, this can be explained by the young age of our study population and quite possibly by their lack of any training.

Based on the results of our study, the D55°Pr-PaDiO projection appeared to be the best projection to visualize distal border fragments, as well as the correspondingly defect in the adjacent distal margin of the navicular bone. Because of the lower angle between the foot and the horizontal, the distal border is positioned more distally on the radiographs, frequently being superimposed over the distal interphalangeal joint. Therefore, an additional D65°Pr-PaDiO projection was made, with the distal border of the navicular bone positioned more

proximally to the distal interphalangeal joint. This D65°Pr-PaDiO radiographic projection appeared the best projection to visualize distal border fragments in a previous reported study of young male horses (14). However, the location of the distal navicular border depends on the horse's individual foot conformation.

Fragments at the distal navicular border remain diagnostically challenging using radiography. Computed tomography and MRI have shown to be much more sensitive in the detection of these fragments, however they are technically not useful in the context of purchase examination or stallion screening.

In conclusion, a statistically significant and clinical relevant association was found between a concave or undulating proximal articular border shape and the presence of a distal border fragment. Since the distribution of biomechanical forces exerted on the navicular bone are assumed to be shape dependent, distal border fragments may be a result of unfavorable loading of the navicular region. The presence of corresponding defects in the adjacent distal margin of all the navicular bones with fragments described in this study provides some support for the hypothesis that these distal border fragments are avulsion fractures. However, future histological investigation is needed, to determine the actual aetiopathogenesis of these distal border fragments.

FOOTNOTE

[a] Playdoh®: Rainbow Crafts, Cincinnati, Ohio, USA.

[b] Mobilux, X-ray Equipment Verachtert, Antwerp, Belgium.

REFERENCES

1. Hickman J. Navicular disease – what are we talking about? Equine Vet J 1989; 21: 395-398.
2. Wright I.M. A study of 118 cases of navicular disease: clinical features. Equine Vet J 1993; 25: 488-492.
3. Dyson S., Murray R., Blunden T., et al. Current concepts of navicular disease. Equine Vet Educ 2006; 18: 45-56.
4. Dyson S., Murray R. Magnetic resonance imaging evaluation of 264 horses with foot pain: The podotrochlear apparatus, deep digital flexor tendon and collateral ligaments of the distal interphalangeal joint. Equine Vet J 2007; 39: 340-343.
5. Wright I.M., Kidd L., Thorp B.H. Gross, histologic and histomorphometric features of the navicular bone and related structures in the horse. Equine Vet J 1998; 30: 220-234.
6. Blunden A., Dyson S., Murray R., et al. Histopathology in horses with chronic palmar foot pain and age-matched controls. Part 2: The deep digital flexor tendon. Equine Vet J 2006; 38: 23-27.
7. Wright I.M. A study of 118 cases of navicular disease: radiological features. Equine Vet J 1993; 25: 493-500.
8. Dik K.J. Diagnostische beeldvorming. In: De Veterinaire Keuring van het Paard. Sloet van Oldruitenborgh-Oosterbaan M.M., Barneveld A., Van Den Belt A.J. (eds). Libre BV, Leeuwarden 2007: 85-105.
9. Poulos P.W., Brown A., Brown E., et al. On navicular disease in the horse. Vet Radiol 1989; 30: 54-58.
10. Butler J.A., Colles C.M., Dyson S.J., et al. In: Clinical Radiology of the Horse. Butler J.A., Colles C.M., Dyson S.J., Kold S.E., Poulos P.W.J. (eds), 2nd ed., Blackwell Science, Oxford, UK 2000: 21-130.
11. Dyson S. Radiological interpretation of the navicular bone. Equine Vet Educ 2008; 20: 268-280.
12. Blunden A., Dyson S., Murray R., et al. Histopathology in horses with chronic palmar foot pain and age-matched controls. Part 1: Navicular bone and related structures. Equine Vet J 2006; 38: 15-22.
13. Kaser-Hotz B., Ueltschi G. Radiographic appearance of the navicular bone in sound horses. Vet Radiol Ultrasound 1992; 33: 9-17.

14. Verwilghen D., Serteyn D., Pille F., et al. Prevalence of radiographic findings in candidate sires (2001-2008). Vlaams Diergeneeskundig Tijdschrift 2009; 78: 419-428.
15. Wright I.M., Douglas J. Biomechanical considerations in the treatment of navicular disease. Vet Rec 1993; 31: 109-114.
16. Wilson A.M., McGuigan M.P., Fouracre L., et al. The force and contact stress on the navicular bone during trot locomotion in sound horses and horses with navicular disease. Equine Vet J 2001; 33: 159-165.
17. McGuigan M.P., Wilson A.M. The effect of bilateral palmar digital nerve analgesia on the compressive force experienced by the navicular bone in horses with navicular disease. Equine Vet J 2001; 33: 166-171.
18. Weaver M.P., Shaw D.J., Munaiwa G., et al. Pressure distribution between the deep digital flexor tendon and the navicular bone, and the effect of raising the heels in vitro. Vet Comp Orthop Traumatol 2009; 22: 278-282.
19. Rijkenhuizen A.B.M. Navicular disease: a review of what's new. Equine Vet J 2006; 38: 82-88.
20. Dik K.J., van den Belt A.J.M., Enzerink E., et al. The radiographic development of the distal and proximal double contours of the equine navicular bone on dorsoproximal-palmarodistal oblique (upright pedal) radiographs, from age 1 to 11 months. Equine Vet J 2001; 33: 70-74.
21. Dik K.J., van den Broek J. Role of navicular bone shape in the pathogenesis of navicular disease: a radiological study. Equine Vet J 1995; 27: 390-393.

CHAPTER 8

General discussion

In the horse, loss of performance is frequently related to locomotory pathology, of which foot pain is a common problem. For several decades, navicular disease has been considered as the most important cause of foot pain in middle-aged riding horses. This collective term includes a progressive bilateral forelimb condition involving the navicular bone and its surrounding soft tissue structures. The changes that can be observed in horses with navicular disease have been demonstrated with MRI and may involve a variety of structures, which may occur concurrently (1-4). Bony changes such as abnormal synovial invaginations and osseous fragment(s) at the distal navicular border may be related to navicular disease, however, they may also occur in non-lame horses (5-8).

This thesis identified the strengths and limitations of CT and radiography as diagnostic techniques, in assessing anatomical structures of the equine foot, particularly the distal border of the equine navicular bone. It is important to accurately characterize the distal navicular border radiographically, more specifically the distal border synovial invaginations, for diagnosis, therapy and prognosis. However, the prediction of the horse's future performance potential based on the appearance of the distal navicular border should be given with caution, since the clinical significance of abnormal invaginations (in shape, number and/or depth) and bony fragment(s) is still not known. Furthermore, different opinions exist among countries, as illustrated by the different gradation of navicular bone abnormalities in their radiographic scoring systems (9-11).

To diagnose the source of foot pain on images, a good anatomical knowledge is mandatory. The objective of the first study of this research project was merely to describe how well anatomical structures of the foot could be visualised on corresponding CT images (Chapter 3). Because CT provides excellent evaluation of the morphology of bone, the compact, subchondral, spongious bone with its trabecular pattern and distal border synovial invaginations could be clearly distinguished on the images. Computed tomography also allowed imaging of soft tissue structures of the foot when using the appropriate window width and level. This is confirmed in our study results where the general soft tissue structures of the foot could be seen using soft tissue window settings. At the level of the pastern region, the DDFT could be clearly delineated. More distally, the margins of the tendon were less sharply visible. Since the feet were disarticulated at the level of the metacarpophalangeal joint, air could enter the digital flexor tendon sheath and most likely improved the visualization and margin delineation of the DDFT and sheath cavity at that level.

Furthermore, the margins of the ligaments of the foot could also not clearly been identified on our CT images. In the literature, only a few reports compared different diagnostic imaging techniques in their degree to assess the visualization of anatomic structures in the foot. A recent study on lame horses supported our findings and reported low anatomical visualization scores for the margins of ligaments in the foot and DDFT insertion on standing low-field MRI, CT and CE-CT images (12). In that study, higher visualization scores were seen of the structures located proximal to the navicular bone with CT, while low-field MRI better visualised structures distal to the proximal border of the navicular bone. This may be explained by the use of a small region of interest (field of view) in MRI, in clinical cases mostly centered on the podotrochlear apparatus, the type of radiofrequency coil and the impaired visualisation of structures at the periphery of the magnetic field (12, 13). In comparison, MRI systems with higher field strengths show images with a higher spatial resolution and therefore higher sharpness. This is demonstrated in the study of Bolen and co-workers (14), where the DDFT and ligaments of the foot were better defined on the high-field MRI images. Also, the bone architecture, ungular cartilages, layered pattern of the hoof, synovial membrane and folds of the navicular bursa and cartilage of the DIPJ were better assessed or only visible with the high-field compared to the low-field MRI system. However, higher purchase and maintenance costs and the need for a general anaesthesia in a high-field MRI system, limit their routine use. Conversely, US is a safe, relative cheap and an easy to perform technique in routine practice. On our CT images, no clear separation could be made between the entire collateral ligaments of the DIPJ and ipsilateral ungular cartilage. With US, the proximal two-thirds of the ligaments can be seen and a better separation between the hyperechoic ligaments and hypoechoic cartilages of the foot is possible (15). However, access to the structures within the hoof capsule is generally limited and depends on the individual hoof conformation. The lack of imaging of the collateral parts of the DSIL, distal third of the collateral ligaments of the DIPJ and distal part of the DDFT is a limitation of US (16).

In theory, (small) soft tissue structures can be sharply outlined and resolved if a thin slice thickness and interslice spacing is used, to decrease partial volume and hence increase the spatial resolution and anatomic visualisation of the structures (11, 17). On the other hand, a smaller slice thickness decreases the signal to noise ratio (more image noise), resulting in less image quality. As a compromise, a larger field of view (larger voxel size) has to be used to maintain acceptable image quality. Small structures such as the DSIL are susceptible to partial volume averaging and it is required to use a small slice thickness (of 1 mm or less) to better identify this ligament, of course with appropriate adjustment of other parameter settings (4).

In our study, a slice thickness of 2 mm was used.
Puchalski and co-workers demonstrated that the soft tissue structures in the foot can be well delineated on CT by the administration of intra-arterial contrast into the medial palmar artery (18). Moreover, CE-CT increased the visualisation scores of the synovium and is useful for the diagnosis of disorders of the DDFT or the collateral ligaments of the DIPJ (12, 13). It is suggested to be an alternative to low-field MRI for the diagnosis of deep digital flexor tendinopathy (17). In general, CE-CT and low-field MRI identified soft tissue lesions more often than non-contrast (plain) CT (12). However, even with addition of contrast, high-field MRI remains the method of reference for the evaluation of the soft tissue structures of the foot.

Some limitations were contained in this descriptive study. Firstly, we did not know if the horses were lame or not. We knew that they were euthanized for reasons unrelated to the musculoskeletal system, but there was no lameness examination performed prior to death. However, to classify them as 'normal', the front limbs were inspected, palpated and radiographed prior to anatomical sectioning. The limbs that did show an external and/or radiographic abnormality were excluded from the study. However, horses with a soft tissue injury could not be excluded from our study population, since no CE-CT examination was performed on the live horses. Therefore, the term 'CT reference' is discussable since feet were used from horses with unknown lameness history. We also have to be aware that changes due to tissue decay *post-mortem* may have influenced the evaluation of the structures. However, the CT examination was performed within 24h after euthanasia and a CT image is formed using x-ray attenuation and is not based on the tissue protons in the body elements as for MRI. Therefore, alterations due to tissue decay were considered irrelevant in our study. A second limitation in our study is that only one reader has analysed the images in a single lecture. If a consensus would have been reached together with a more experienced observer, the results might have been different. For any diagnostic test that is used in practice, its accuracy (how well the test results represents the truth) and repeatability (how repeatable the test results are) have to be known. Therefore, to test the consistency of CT, an intra- and interobserver variability should have been measured for the assessment of the structures of the equine foot. A third limitation is that the structures were not graded based on visibility (no scoring system was used), which would have allow us to differentiate more strictly and in a standardized way between 0 = not visible; 1 = visible or 2 = sharply visible, and keep the variation as low as possible. Furthermore, no descriptive statistics (sensitivity and specificity)

were used, to evaluate the validity of the results on CT versus gross examination. As a fourth limitation of our study, the HU values were measured for only the DDFT, collateral ligaments of the DIPJ, CSL, ungular cartilages, hoof wall, frog and digital cushion. Contrary to the other soft tissue structures of the foot, ROIs could be drawn easily in these structures because of their size and shape, and repeatable measurements could be performed at different levels in the DDFT. However this was only performed in 3 horses. Quantitative cross-sectional area measurements of the DDFT and collateral ligaments of the DIPJ have been reported previously in 10 live horses, and the HU values on pre- and post-contrast CT images were statistically compared, to measure the degree of contrast enhancement in the tendon/ligaments (18). The comparison between the results of the latter study and ours is difficult, since the manually drawn ROIs were not exactly the same in size and at the same anatomic location in both studies. Therefore, some discrepancy between the values reported for the same structure is reasonable.

In the present study, no contrast medium was administered into the joints nor in the navicular bursa, with the result that the synovial structures, joint capsule and the (fibro)cartilage could not be delineated. Cartilage is one of the most difficult tissue to image, mainly because it is very thin. In the study of Vallance and co-workers (13), cartilage was not assessed because the diagnostic techniques used in the study (low-field MRI, CT and CE-CT) did only allow a poor visualisation of the cartilage. Indeed, the evaluation of equine articular cartilage with standing low-field MRI is a well-recognized limitation. Moreover, a statistically significant difference in the cartilage thickness of the distal phalanx has been described between weight-bearing and non-weight bearing (unloaded) conditions, with a significant increase in thickness when unloaded (19). However, for detecting focal full-thickness erosions in the articular cartilage of the DIPJ, low-field MRI imaging has been considered a sensitive technique (20). In contrast, high-field MRI has proven to better represent subchondral bone and (partial thickness) cartilage lesions, and cartilage thickness than low-field MRI (21). It is described in other joints such as the stifle that computed tomographic arthrography yields more information about the status of the articular cartilage than plain CT (22). Despite the sensitivity of CT arthrography to evaluate articular cartilage, it has a tendency to underestimate cartilage thickness due to blooming artefact. The artefact can be minimalized by reducing contrast agent concentration (dilution of the contrast medium), resulting in lower x-ray attenuation in the imaging plane of the contrast medium and in a lower attenuation gradient at the contrast medium-articular cartilage interface. Images of acceptable quality are obtained.

The mean intra- and inter-observer agreement has been assessed for the radiographic and CT evaluation of the appearance of distal border synovial invaginations of the navicular bone, and both ranged from moderate to good (κ-values of 0.48-0.80) (23, 24). To investigate the relative ability of radiography to evaluate the distal border synovial invaginations, an appropriate 'standard test' has to be used. Both CT and low-field MRI demonstrated the morphology of distal border invaginations more accurately than radiography, and MRI displayed a moderate to good agreement for the distal aspect of the navicular bone with histology (25-27). Compared to low-field MRI and radiography, CT did allow a better assessment of the navicular bone morphology, in particular of the synovial invaginations at the distal, proximal, lateral and medial sloping bone margins (24, 26, 28). Nevertheless, radiography still remains the modality of choice for purchase examination nowadays, since both cross-sectional imaging techniques (CT and MRI) are more expensive and not yet widely available in equine hospitals. Moreover, the currently used CT machines still require general anaesthesia, which is time consuming, risky and expensive for routine purchase examinations. A standing CT has been performed mainly of the equine head and provided many advantages over radiography (29). Recently, a technique has been described for standing CT of the equine foot as well (30). However, disadvantages of standing CT is that it requires a handler to be with the horse during image acquisition, so the person is exposed to radiation, the presence of motion artefacts, which are common and decrease the image quality, but also the risk for gantry damage.

To be able to evaluate how well radiography represents the distal border synovial invaginations, their morphological appearance has to be examined on the most accurate test with respect to these invaginations. The 'gold standard test' is of course histology. Unfortunately, no histological examination was performed on the navicular bones in our study. To the author's knowledge, no comparison study between CT and histology is yet published in the literature, and it would be interesting to investigate how well CT correlates with the histological findings in the equine navicular bone. Compared to conventional radiography, CT has a better contrast resolution. It images the bone morphology and alterations in higher detail (13, 26). Therefore, CT was used as the 'standard test' in our study. We used a 4-detector row spiral CT scanner, thin slice thickness of 0.6 mm, 512 x 512 pixel matrix and small pitch, resulting in images with high spatial resolution, but higher image noise. After screening the CT images of 50 navicular bones of the forefeet of 25 Warmbloods, we detected different shapes, depths and running directions (orientations) of the distal border

synovial invaginations into the bone. The most commonly observed direction was the 'straight' direction (63.4%), followed by the 'palmaroproximal' (27.1%) and 'dorsoproximal' direction (9.5%). This varied morphology seen on our images may not necessarily be assessed as a 'normal' variation, since we did not know the clinical history of our horses (lame or not, gender, training level, …), so we might have include horses with foot pain. Moreover, the distal border synovial invaginations may show a normal anatomical variation related to the gender, breed, limb, training level, age, weight… (31). Indeed, on our CT images, there were navicular bones with other abnormalities, such as a distal border fragment, but the aim of this study was only to describe the varied morphology of the invaginations, apart from the fact that the horses were lame or not, male or female, in training or not. Consequently, this study has no clinical relevance as to the varied morphology of the invaginations, it only yields descriptive information.

In the next 2 studies (Chapters 5 and 6), we used the same feet as for our CT study, to compare the morphology of the distal border invaginations seen on CT with corresponding radiographs. The shapes and depths of these invaginations, as described on the obtained CT images, were classified more as 'normal' or 'abnormal' based on the results of the literature. It would have been more interesting to correlate the different morphology (number, depth and shape) of the invaginations with the presence of other abnormalities of the navicular bone and/or DIPJ, to more strictly differentiate them as 'normal' or 'abnormal'.

We demonstrated that the variability between the 3 DPr-PaDiO radiographic projections, with angles of 45°, 55° and 65° to the horizontal, and CT was high for number and depth of the distal border synovial invaginations. A statistical significant mean difference was found between CT and radiography for the number of invaginations, and measured approximately 2 in our population of 50 horses. If we would have used a larger group of horses, this mean difference would have approached more the true value of difference between both techniques and there would be a narrower confidence interval (CI). Nevertheless, the reference interval (RI) range would stay wide independent of population size, meaning that a large variability between CT and radiography for the number of invaginations exists. For the depth of the invaginations, no statistical significant mean difference was measured between CT and radiography for the current horse population and the CI for all 3 radiographic projections were narrow. However the RI measured -0.28 – 0.32, meaning that there is a large variability of the individual observations between both techniques (difference of 0.28 cm below or 0.32 cm above zero-level, with zero-level as perfect agreement). The counted number of synovial invaginations on CT was comparable or higher in most of the cases than on corresponding

radiographs. The measured depth of the invaginations on CT and radiography was quite variable. The depth of the mildly penetrating invaginations tends to be routinely overestimated with radiography, whereas the depth of the deeper penetrating invaginations is mostly underestimated. As it has been described in the literature that the presence of >7 radiographically visible distal border invaginations and/or some deeply penetrating invaginations are suspected to be abnormal, the question arises what to do with these higher number (up to 11) and/or deep invaginations visible on CT? Of course, CT is a more sensitive imaging technique than radiography since it allows a detailed visualisation of bone without superimposition, thus the criteria used in the literature for evaluating distal border synovial invaginations on radiographs cannot be transposed to CT. Therefore, further examination of these deeper and higher number of invaginations on CT images should be performed in a comparative study with MRI or histopathology in clinically healthy and lame horses, since CT may become more common in the future.

For the shape, nearly no false positive results were seen on radiographs, which is an important finding as we do not want the horses to be inaccurately assigned as unsuitable for a future sport career. As mentioned above, radiographic detection of acute or subtle osseous changes may be limited since at least 30% change in density is required before subtle changes or lesions become visible (32). This radiographic limitation and the presence of superimposition of structures on a radiographic projection may explain the higher number of false negative results seen in our study. Our findings were comparable with those of a recent low-field MRI study (4).

During the present study, it became clear that the radiographic evaluation of distal border synovial invaginations is challenging, particularly for their depth of penetration. In fact, the radiographic measured depth of penetration of each invagination with a particular direction into the navicular bone, differs with heel height as the position of the navicular bone varies with different height of the heels (33, 34). An attempt was made to respond to this finding by measuring a hoof-angle dependent DPr-PaDiO radiographic projection, based on the individual heel height and most common ‘straight’ direction of the invaginations in the navicular bone. The morphology of distal border synovial invaginations on this radiographic projection with hoof-specific angulation was compared with their occurrence on the corresponding CT images (Chapter 6). We hypothesized that this specific radiographic projection would evaluate the straight running invaginations more accurately, however, the dorso-/palmaroproximal running invaginations were assessed more accurately. Therefore, our

hypothesis may be rejected. In comparison with the results of Chapter 5, this radiographic projection with hoof-specific angle also showed a statistical significant mean difference with CT for number of the invaginations, as well as a a quite wide variability of the individual observations relative to their mean difference for their depth. However, this projection revealed a higher sensitivity for shape compared with the 3 DPr-PaDiO radiographic projections.

The last study of this PhD thesis (Chapter 7) was performed on a large population of young Belgian Warmblood stallions. A statistical significant association of the presence of distal border fragments and a concave or undulating proximal navicular border has been found. The shape of the proximal articular border of the navicular bone has been found to be genetically determined and may be concave, undulating, straight or convex (35). A significant association between the shape and radiological changes associated with navicular disease is described in Dutch Warmblood horses, in which the concave and undulating proximal border shapes represented the poorest conformations. A shape-dependent distribution of the biomechanical forces of the DDFT exerted on the navicular bone has been suggested by Dik and co-workers (35, 36). The force of the DDFT exerted on the navicular bone is described to be a function of the force in the tendon and the curvature of the tendon around the navicular bone (37). In the early and mid-stance phase of the stride in a vertical (symmetrical) weight-bearing limb, the DIPJ is flexed and the CSL are relaxed. As the propulsion phase starts, the DIPJ extends and the tension on the CSL and DDFT increases, with increased compression on the navicular bone (38). Tension on the CSL is directed through the navicular bone to the DSIL, leading also to an increased tension on this small ligament when DIPJ extension occurs. A slight dorsoproximal displacement of the navicular bone may follow, even more lead to increased stresses on the DSIL and pressure of the tendon on the navicular bursa. An abnormal hoof conformation (typically the long toe-low heel situation), back broken foot-pastern axis or excess use are presumably contributing to navicular disease since the DDFT bears increased forces on the navicular bone in these situations (34, 38, 39). The increased strain on the sesamoidean ligaments alters the distal arterial supply to the navicular bone and/or venous outflow is restricted, resulting in an increased intraosseous pressure within the navicular and may lead to the formation of lollipop- or rounded-shaped distal border invaginations bone (38, 40-43). In a study of horses with navicular disease and sound horses, the first group experienced a positive feedback mechanism by increasing the load on their navicular bones in

early stance (toe-first landing), presumably by contraction of the DDFT in an attempt to unload their heels (37).

In our study, 10% of the navicular bones with a concave proximal border shape were characterised by rounded- to lollipop-shaped distal border synovial invaginations (scored 3-4 according to the classification of Dik) (10). A similar prevalence was found in the study of Dik and van den Broek (35). Gabriel and co-workers demonstrated that the distal border score of the synovial invaginations, described by McGregor (44), significantly varies with the limb (fore or rear), breed, exercise level, gender and age of the horse (31). Our population of horses were untrained Warmbloods coming from pasture, having varied hoof conformations, an average age of 3 years and only 5% being mildly lame at the trot, which was unspecific since no palmar digital nerve block was performed. Only the front feet of the horses were radiographed. The navicular bone of Warmbloods is described to be stronger, less porous and less prone to bone degeneration compared with Thoroughbreds (31, 45). Warmbloods were more likely to be sound in case of severe navicular bone abnormalities than Thoroughbreds of same age and training level (45).

The present study is purely a radiological study where a statistical significant association between the presence of distal border fragments and the unfavorable concave and undulating shapes of the proximal navicular border has been found. Since a shape-biomechanical load association has been suggested by others (35), but not proven with an epidemiological study, no association between the presence of distal border fragments and increased biomechanical forces exerted on the navicular bone can be made. A possible traumatic origin of the osseous bodies seen at the distal navicular border in the present study was only assumed by the authors, since all 57 bones showed a correspondingly defect in the adjacent distal border. However, the nature of the fragments can only be determined by histology. The osseous fragments embedded in the DSIL near a depression (fracture bed) in the distal border of the navicular bone without signs of osseous union, are considered to be avulsion fractures at the insertion of the DSIL to the bone and most likely a cause of pain (5, 7, 46).

The prevalence of distal border fragments in our population was 8.8%, which is higher than in 2 other studies in sound horses (7% and 1.8% respectively) (6, 8). This perhaps may be explained by the differences in population size, breeds, age, disciplines, sizes of the horses and experience of the observers used among the studies. Nevertheless, the frequency of occurence of distal border fragments is higher in horses with navicular disease (varied between 6.4 – 40%) (5-7, 46-48). The significance of bony fragments at the distal border of the navicular bone is still not well understood. The presence of distal border fragments has

been associated with lameness, but not with the severity of lameness (5, 7, 49). Yorke and co-workers did describe an increased probability of lameness with the presence of multiple fragments, but no association between fragment size and lameness grade was found (48). The clinical relevance of distal border fragments remains open to debate.

In our study, only 1/47 horses with fragments was (unilaterally) lame at the trot. Since a radiograph is a snapshot of a horse's feet, it is possible that at the time of presentation the horse is not yet lame, presumably because of its young age and lack of training. Possible future field of research would be to rescreen our population of horses at an older age, to evaluate if those with fragments develop lameness and/or other abnormal features in the navicular bone compatible with navicular disease.

In the current study, a computed radiographic system was used, providing higher quality images compared to conventional film-screen radiography, mainly due to a better contrast resolution. However, for the detection of distal border fragments, a similar low sensitivity (39.0% and 37.8% respectively), but high specificity has been described for conventional and computed radiography (99.7% and 100% respectively), using high-field MRI as a gold standard (50). Medium and large-sized fragments on MRI images were more likely identified on corresponding radiographs. A much more accurate technique to evaluate the navicular bone, particularly its distal border, is high-field MRI with a high sensitivity (92%) and specificity (93%) for the detection of distal border fragments, compared to histopathology (7). Nevertheless, a good correlation is described between the grading systems used for the evaluation of the navicular bone by MRI and radiography, resulting in a similar weighting of the navicular bones (7, 35, 50, 51).

The osseous fragments were localised with a higher prevalence at the lateral sloping margin of the distal border of the navicular bone (72% lateral versus 17.5% medial and 10.5% bilateral). A lateral location was also more frequently seen in other studies (6, 46, 48). During asymmetrical weight-bearing (extrasagittal movements such as turns, circles), a collaps of the DIPJ space is occuring at the side of compression (for example the lateral part of the joint for the limb at the inside of the circle), with a lateromotion and medial rotation of the distal phalanx and a medial rotation in the PIPJ. These movements will put tension on mainly the DDFT and DSIL and is maximal at the inside and the propulsion phase of the stride. This theory suggests a biomechanical contribution to the pathogenesis of some foot injuries such as distal border fragments of the navicular bone (15, 52).

A significant association has been described between the presence of distal border fragments and other pathological abnormalities of the distal border of the navicular bone in lame horses

(3, 49, 50). Such an association was not found in our study, most likely because of the young age and lack of training of our horses. However, distal border fragments can occur in the absence of other radiographic abnormalities.

In the literature, no information is yet available about the exact aetiopathogenesis of the osseous fragments at the distal border of the navicular bone. To elucidate the possible origin of these fragments, a combined high-field MRI and histological study should be performed on large groups of lame and non-lame horses with distal border fragments. Imaging criteria should be set up based on the characteristics of the fragments (shape, delineation/contour, size, intensity), appearance of the adjacent navicular bone and soft tissues (mainly the DDFT and DSIL) and bone activity in the medulla of the navicular bone, with histopathology as a gold standard. Biggi and co-workers already performed such a study on 1 lame horse and concluded that the fragment could be a focal osseous metaplasia or a fracture of a mature entheseophyte of the DSIL insertion, and most likely contribute to lameness (49). However, definitive differentiation will remain difficult.

A longitudinal study performed on a group of horses (for example Warmbloods) with different disciplines, which are regularly evaluated clinically and radiographed from young age (if possible from birth) until an adult age is needed, to evaluate whether distal border fragments and/or altered distal border synovial invaginations (in size, depth and number) occur, and if, at what age. Secondly, by evaluating the horses clinically and depending on their performance levels and disciplines, it would be very interesting to evaluate whether and when they develop lameness. Unfortunately, such a study is difficult to perform, because of the high cost, the large group of foals needed with unavoidable loss of horses over time and/or uncooperative owners and/or young horses.

CHAPTER 8

GENERAL CONCLUSION

In conclusion, radiography is less accurate than CT for the visualization of the synovial invaginations at the distal border of the navicular bone. In the majority of cases, radiography underestimates the number of invaginations, and does not accurately estimate the depth of the invaginations. The depth of the mildly penetrating invaginations tends to be routinely overestimated, whereas the depth of the deeper penetrating invaginations is mostly underestimated. Furthermore, radiography is only moderately sensitive for the detection of invaginations with an unfavorable shape such as 'lollipops'. This caused a too optimistic radiographic score in about one third of the cases in this study. On the other hand, the specificity of radiography for the detection of invaginations with an unfavorable shape is high.

It was found that the accuracy of the radiographic visualization of the number and depth of synovial invaginations cannot be improved by optimizing the angle of the DPr-PaDiO projection dependent the individual hoof conformation.

Finally, this PhD thesis looked at distal border fragmentation of the navicular bone. It was found that fragmentation was significantly more frequent in navicular bones with an unfavorable shape (concave or undulating proximal articular border). Furthermore, for all fragments, a correspondingly shaped defect was present in the adjacent distal border of the navicular bone. To our opinion, these findings strengthen the hypothesis that most distal border fragments are 'chip fractures', likely resulting from an unfavorable 'shape-dependent' biomechanical load exerted on the navicular bone at young age. To be clear, the clinical relevance of these fragments was not investigated in this PhD study.

REFERENCES

1. Dyson S.J., Murray R., Schramme M.C. Lameness associated with foot pain: results of magnetic resonance imaging in 199 horses (January 2001-December 2003) and response to treatment. Equine Vet J 2005; 37: 113-121.
2. Murray R.C., Schramme M.C., Dyson S.J., et al. Magnetic resonance imaging characteristics of the foot in horses with palmar foot pain and control horses. Vet Radiol Ultrasound 2006; 47: 1-16.
3. Sampson S.N., Schneider R.K., Gavin P.R., et al. Magnetic resonance imaging findings in horses with recent onset navicular syndrome but without radiographic abnormalities. Vet Radiol Ultrasound 2009; 50: 339-346.
4. Gutierrez-Nibeyro S.D., Werpy N.M., White II N.A. Standing low-field magnetic resonance imaging in horses with chronic foot pain. Australian Vet J 2012; 90: 75 – 83.
5. Wright I.M. A study of 118 cases of navicular disease: radiological features. Equine Vet J 1993; 25: 493-500.
6. Biggi M., Dyson S. Distal border fragments and shape of the navicular bone: Radiological evaluation in lame horses and horses free from lameness. Equine Vet J 2012; DOI: 10.1111/j.2042-3306.2011.00429.x.
7. Schramme M.C., Murray R.C., Blunden A.S., et al. A comparison between magnetic resonance imaging, pathology, and radiology in 34 limbs with navicular syndrome and 25 control limbs. In *Proceedings* 51th Annu of Am Ass Equine Practnrs 2005; 51: 348-358.
8. Kaser-Hotz B., Ueltschi G. Radiographic appearance of the navicular bone in sound horses. Vet Radiol Ultrasound 1992; 33: 9-17.
9. Robert C., Valette J.P., Denoix J.M. Correlation between routine radiographic findings and early racing career in French Trotters. Equine Vet J Suppl 2006; 36: 473-478.
10. Dik K.J. Diagnostische beeldvorming. In: De Veterinaire Keuring van het Paard, 3nd edn., Eds: Sloet van Oldruitenborgh-Oosterbaan M.M., Barneveld A., Van Den Belt A.J., Libre BV, Leeuwarden 2007: 85-112.
11. BTK. Leitfaden für die röntgenologische beurteilung bei der kaufuntersuchung des pferdes-überarbeitete fassung. Röntgenleitfaden, Germany 2007.
12. Vallance S.A., Bell R.J.W., Spriet M., et al. Comparisons of computed tomography, contrast-enhanced computed tomography and standing low-field magnetic resonance

imaging in horses with lameness localized to the foot: Part 1: Anatomic visualization scores. Equine Vet J 2012; 44: 51-56.

13. Vallance S.A., Bell R.J.W., Spriet M. et al. Comparisons of computed tomography, contrast-enhanced computed tomography and standing low-field magnetic resonance imaging in horses with lameness localized to the foot: Part 2: Lesion identification. Equine Vet J 2012; 44: 149-156.
14. Bolen G., Audigié F., Spriet M., et al. Qualitative comparison of 0.27T, 1.5T, and 3T magnetic resonance images of the normal equine foot. J Equine Vet Science 2010; 30: 9-19.
15. Denoix J.-M. Personal communication. ISELP, Foot & Pastern, The Netherlands, 2011.
16. Denoix J.-M., Didierlaurent D., Audigié F. Diagnosis and management of tendon and ligament injuries of the equine foot. In *Proceedings* 11th International congress of the World Equine Vet Association, Guaruj, Brazil, 2009.
17. Puchalski S.M., Galuppo L.D., Drew C.P. et al. Use of contrast-enhanced computed tomography to assess angiogenesis in deep digital flexor tendonopathy in a horse. Vet Radiol Ultrasound 2009; 50: 292-297.
18. Puchalski S.M., Galuppo L.D., Hornof W.J., et al. Intraarterial contrast-enhanced computed tomography of equine distal extremity. Vet Radiol Ultrasound 2007; 48: 21-29.
19. Evrard L., Busoni V., Bertoni L., et al. Low field MRI of the equine distal interphalangeal joint: comparison between weight-bearing and unloaded conditions. In *Proceedings* of Annu Meet Vet Diagnostic Imaging, Cascais, Portugal, 2013: 145.
20. Olive J. Distal interphalangeal articular cartilage assessment using low-field magnetic resonance imaging. Vet Radiol Ultrasound 2010; 51: 259-266.
21. Murray R.C., Mair T.S., Sherlock C.E., et al. Comparison of high-field and low-field magnetic resonance images of cadaver limbs of horses. Vet Rec 2009; 165: 281-288.
22. Crijns C.P., Gielen I., van Bree H., et al. The use of CT and CT arthrography in diagnosing equine stifle injury in a rheinlander gelding. Equine Vet J 2010; 42: 367-371.
23. Field J.R., Dobsun H., Bonnett B. Navicular syndrome: Preliminary assessment of radiographic scoring. Vet Comp Orthop Traumatol 1995; 8: 36-39.

24. Groth A.M., May S.A., Weaver M.P., et al. Intra- and interobserver agreement in the interpretation of navicular bones on radiographs and computed tomography scans. Equine Vet J 2009; 41: 124-129.
25. Whitton R.C., Buckley C., Donovan T., et al. The diagnosis of lameness associated with distal limb pathology in a horse: A comparison of radiography, computed tomography and magnetic resonance imaging. Vet J 1998; 155: 223-229.
26. Widmer W.R., Buckwalter K.A., Fessler J.F., et al. Use of radiography, computed tomography and magnetic resonance imaging for evaluation of navicular syndrome in the horse. Vet Radiol Ultrasound 2000; 41: 108-116.
27. Murray R.C., Blunden T.S,, Schramme M.C., et al. How does magnetic resonance imaging represent histologic findings in the equine digit? Vet Radiol Ultrasound 2006; 47: 17-31.
28. Tietje S. Computed tomography of the navicular bone region in the horse: a comparison with radiographic documentation. Pferdeheilkunde 1995; 11: 51-61.
29. Weller R., Dakin S., Perkins J. Computed tomography in the standing horse: technique, radiation exposures and case selection. In *Proceedings* of Annu Meet Vet Diagnostic Imaging, Cascais, Portugal, 2013: 47.
30. Desbrosse F.G., Vandeweerd J.-M.E.F., Perrin R.A.R., et al. A technique for computed tomography (CT) of the foot in the standing horse. Equine Vet Educ 2008; 20: 93-98.
31. Gabriel A., Jolly S., Detilleux J., et al. Morphometric study of equine navicular bone: variations with breeds and types of horses and influence of exercise. J Anat 1998; 193: 535-549.
32. Butler J.A., Colles C.M., Dyson S.J., et al. Foot, pastern and fetlock. In: Clinical Radiology of the Horse. Butler J.A., Colles C.M., Dyson S.J., Kold S.E., Poulos P.W.J. (eds), 2nd ed., Blackwell Science, Oxford, UK 2000: 21-130.
33. van Dixhoorn I.D.E., Meershoek L.S., Huiskes R., et al. A discription of the motion of the navicular bone during *in vitro* vertical loading of the equine forelimb. Equine Vet J 2002; 34: 594-597
34. Pearce S.G., Boure L.P., Bolger A., et al. Effect of heel elevation on forelimb conformation in horses. Aus Vet J 2004; 82: 558-562.
35. Dik K.J., van den Broek J. Role of navicular bone shape in the pathogenesis of navicular disease: a radiological study. Equine Vet J 1995; 27: 390-393.

36. Dik K.J., van den Belt A.J.M., Enzerink E., et al. The radiographic development of the distal and proximal double contours of the equine navicular bone on dorsoproximal-palmarodistal oblique (upright pedal) radiographs, from age 1 to 11 months. Equine Vet J 2001; 33: 70-74.
37. Wilson A.M., McGuigan M.P., Fouracre L., et al. The force and contact stress on the navicular bone during trot locomotion in sound horses and horses with navicular disease. Equine Vet J 2001; 33: 159-165.
38. Ratzlaff M.H., White K.K. Some biomechanical considerations of navicular disease. Equine Vet Science 1989; 9: 149-153.
39. Wright I.M., Douglas J. Biomechanical considerations in the treatment of navicular diseae. Vet Record 1993; 133: 109-114.
40. Colles C.M., Hickman J. The arterial supply of the navicular bone and its variations in navicular disease. Equine Vet J 1977; 9: 150-154.
41. Rijkenhuizen A.B.M., Németh F., Dik K.J., et al. The arterial supply of the navicular bone in adult horses with navicular disease. Equine Vet J 1989; 21: 418-424.
42. Pleasant R.S., Baker G.J., Foreman J.H., et al. Intraosseous pressure and pathological changes in horses with navicular disease. Am J Vet Res 1993; 54: 7-12.
43. Gabriel A., Jolly S., Detilleux J. et al. Radiographic study of the sound navicular bone. Part 1: What about the canals on the distal border? Ann Méd Vét 1998; 142: 345-352.
44. MacGregor C.M. Radiographic assessment of navicular bones, based on changes in the distal nutrient foramina. Equine Vet J 1986; 18: 203-206.
45. van Hoogmoed L.M., Snyder J.R., Thomas H.L., et al. Retrospective evaluation of equine prepurchase examinations performed 1991-2000. Equine Vet J 2003; 35: 375-381.
46. Wright I.M., Kidd L., Thorp B.H. Gross, histologic and histomorphometric features of the navicular bone and related structures in the horse. Equine Vet J 1998; 30: 220-234.
47. Poulos P.W., Brown A., Brown E., et al. On navicular disease in the horse. Vet Radiol 1989; 30: 54-58.
48. Yorke E.H., Judy C.E., Saveraid T.C., et al. Distal border fragments of the equine navicular bone: Association between magnetic resonance imaging characteristics and clinical lameness. Vet Radiol Ultrasound 2014; 55: 35-44.
49. Biggi M., Blunden T., Dyson S. Can distal border fragments of the navicular bone be a primary cause of lameness? Equine Vet Educ 2012; DOI: 10.1111/j.2042-3292.2012.00403.x.

50. Biggi M., Dyson S. Comparison between radiological and magnetic resonance imaging lesions in the distal border of the navicular bone with particular reference to distal border fragments and osseous cyst-like lesions. Equine Vet J 2010; 42: 707-712.
51. Jux V., Dakin S., Weller R., et al. Design and validation of a radiographic and magnetic resonance imaging grading system for navicular bone pathology. In *Proceedings* of Annu Meet Vet Diagnostic Imaging, Cascais, Portugal, 2013: 53.
52. Chateau H., Degueurce C., Denoix J.-M. Three-dimensional kinematics of the equine distal forelimb: effects of a sharp turn at the walk. Equine Vet J 2005; 37: 12-18.

SUMMARY

Lameness in the horse is frequently caused by foot pain. After a thorough clinical examination, radiography is the first imaging modality selected for the diagnosis of bony pathology in horses with foot pain. The navicular bone, also called the distal sesamoid bone, is evaluated thoroughly for radiographic abnormalities, such as bony fragment(s) at the distal border of the bone and/or abnormal synovial invaginations. The clinical relevance of these features is still a subject of controversy. According to the country where the horse is admitted for a purchase examination or as a breeding stallion for a particular studbook, these abnormalities can be considered as not relevant to moderate or even severe radiographic findings. The present PhD research is purely an imaging study where we focused on the distal border of the navicular bone.

The **first chapter** gives an overview of the anatomy of the palmar/plantar aspect of the foot (*podotrochlear* region*)* and the different diagnostic imaging modalities currently used to evaluate the equine foot. The disorders of the navicular bone are reviewed as well in this chapter.

The scientific aims of this PhD project are described in the **second chapter**.

The general aim of this research project was to describe the morphology of the distal border synovial invaginations of the navicular bone using radiography and computed tomography (CT), and to further unravel the etiopathogenesis of distal border fragments of the navicular bone.

The **third chapter** provides a detailed overview of the CT anatomy of the anatomically normal equine foot. Ten forefeet of 5 equine cadavers were used. All feet did not show any abnormality on inspection, palpation and radiographically. Computed tomography was performed on all feet with a 4-detector row spiral CT scanner. Transverse slices with a thickness of 2 mm were obtained in a proximodistal direction, and reviewed using bone and soft tissue window settings. Sagittal and dorsal reconstructions with a slice thickness of 2 mm were made. Four feet were frozen and sectioned to obtain anatomical slices in transverse, dorsal and sagittal planes. The CT images of these feet were matched with the corresponding anatomical slice.

The proximal, middle and distal phalanges, the navicular bone as well as the extensor and flexor tendons (including their distal attachments) could be clearly visualised. The collateral (sesamoidean) ligaments could be readily located, but were difficult to delineate at their

proximal attachment. The distal digital annular ligament could only be distinguished from the deep digital flexor tendon proximal to the navicular bone, and its proximal attachment could be identified, but not its distal insertion. The distal sesamoidean (impar) ligament, chondrosesamoidean, -coronal, and –compedal ligaments, 'T-ligament', axial and abaxial palmar ligaments of the proximal interphalangeal joint were seen with difficulty, and not at all slices. The lateral and medial proprius palmar digital artery and vein could be visualised occasionally on some slices. The ungular cartilages, corium and hoof wall layering were seen. The nerves, articular cartilage, fibrocartilage of the navicular bone, joint capsules and the chondroungular ligament could not be assessed.
In conclusion, CT is useful to evaluate the majority of the anatomical structures in the equine foot. The images obtained in this study can be used as a CT atlas in horses with foot pain, especially when radiography and ultrasonography are inconclusive.

In the **fourth chapter**, the morphological features of the distal border synovial invaginations of the navicular bone were described by use of CT. Fifty cadaver forefeet from 25 Warmblood horses were imaged. Computed tomography was performed on all feet with a 4-detector row spiral CT scanner. Transverse images with a slice thickness of 0.6 mm were obtained from the level of the distal aspect to the level of the proximal aspect of the navicular bone using a bone window setting. Sagittal and dorsal reconstructions with a slice thickness of 0.6 mm were made. The number, shape, depth of penetration and orientation of the synovial invaginations into the bone were evaluated.
A total of 295 distal border synovial invaginations were seen. The number of invaginations in a particular navicular bone was variable and ranged from 3 to 11. The shape was 'conical' in 118, 'linear' in 109, 'lollipop' in 38 and 'branched' in 30 invaginations. The depth of penetration of the synovial invaginations into the navicular bone was 'mild' in 195 cases, 'moderate' in 67 cases and 'deep' in 33 cases. The orientation into the bone varied from 'straight', 'dorsoproximal' and 'palmaroproximal' in 187, 28 and 80 cases, respectively.
We conclude that the CT images and knowledge gained in this study may serve for future radiographic evaluation of the distal border synovial invaginations.

In the **fifth chapter** the objective was to investigate the value of radiography in the evaluation of the morphology of the distal navicular border synovial invaginations. Computed tomography scans and 3 DPr-PaDiO radiographic projections (D45°Pr-PaDiO, D55°Pr-PaDiO and D65°Pr-PaDiO) were obtained on 50 cadaver forefeet from 25 Warmblood horses.

Computed tomography was assumed to be the standard test and performed on all feet using a 4-detector row spiral CT scanner. Transverse images with a slice thickness of 0.6 mm were obtained from the level of the distal aspect to the level of the proximal aspect of the navicular bone using a bone window setting. Sagittal and dorsal reconstructions with a slice thickness of 0.6 mm were made. On both the CT and radiographic images, the number, depth and shape of the invaginations were evaluated, and all data were statistically analyzed. For the number of invaginations, the mean differences of the sample data between CT and all 3 radiographic projections were statistically significant and approximately equal to 2, meaning that CT permits visualization of an average of 2 more invaginations compared to radiography. Also, a large individual variation against the mean difference of both modalities was seen. Comparable as for the number of invaginations, the depth of penetration showed a large variation of the individual differences against the mean difference. Radiography occasionally under- or overestimated the depth of invaginations compared with CT. Even when higher mean values applied, meaning deeper invaginations, the difference between CT and radiography seemed to increase, meaning that radiography underestimates deeper invaginations. And finally, for the shape, a sensitivity and specificity of 64% and 95% respectively, was measured for all 3 DPr-PaDiO radiographic projections, meaning that nearly no false positive results were present. To summarise, seeing an abnormal invagination on radiography, a high probability exists that this invagination is abnormal, but a normal one can in fact be abnormal.

We may conclude that radiography is appropriate for the evaluation of the shape of the synovial invaginations. However, the number and depth of these invaginations cannot be reliably evaluated on radiography. Therefore, it is important to carefully interpret the appearance of the invaginations on radiography and further (prospective) research concerning their clinical importance is required.

In **chapter six**, the objective was to compare the appearance of distal border synovial invaginations on a DPr-PaDiO radiographic projection with hoof-specific angle versus CT. Computed tomography scans and a DPr-PaDiO radiographic projection with specific slope for a particular foot, were made on 50 cadaver forefeet from 25 Warmblood horses. Computed tomography was assumed to be the standard test and performed on all feet using a 4-detector row spiral CT scanner. Transverse images with a slice thickness of 0.6 mm were obtained from the level of the distal aspect to the level of the proximal aspect of the navicular bone using a bone window setting. Sagittal and dorsal reconstructions with a slice thickness of 0.6

mm were made. On both the CT and radiographic images, the number, depth and shape of the invaginations were evaluated, and all data were statistically analyzed. Significantly more invaginations were seen on CT compared to radiography, with an observed average difference of 1.2. In none of the cases in our sample data, radiography had a higher number observed than CT. No statistically significant difference for depth between CT and the DPr-PaDiO radiographic projection was seen, but quite a large variation of the actual difference of measurements against their mean was found. The depth of the mildly penetrating invaginations tends to be routinely overestimated, whereas the depth of the deeper penetrating invaginations is mostly underestimated. The agreement between both modalities for shape was moderate to good and a high sensitivity (75%) and very high specificity (97%) for the specific radiographic projection was found.
To conclude and in comparison with the results of chapter 5, the hoof-specific radiographic projection showed a high variability with CT concerning the number and depth of the distal border synovial invaginations. However, this projection had a higher sensitivity for shape of the distal navicular border synovial invaginations.

In the **seventh chapter**, radiographs of the forefeet of 325 Belgian Warmblood stallions were reviewed. In this retrospective study, the prevalence of distal border fragments of the navicular bone and a possible correlation of these fragments with the shape of the proximal articular border and other abnormalities of the navicular bone, were investigated. Three radiographic projections (LM, D55°Pr-PaDiO and D65°Pr-PaDiO projection) of both forefeet of all horses were made. The proximal articular border was classified as 'straight' in 278, 'convex' in 184, 'undulating' in 147 and 'concave' in 41 navicular bones. Distal border fragments were present in 8.8% of the navicular bones and were significantly more prevalent in bones with a 'concave' (22%) or 'undulating' (13%) proximal articular border, compared to bones with a 'straight' (6%) or 'convex' shape (7%). No other significant associations were found.
In conclusion, we may hypothesize that the assumed association between the shape-dependent force distribution exerted on the navicular bone and the presence of a distal border fragment is likely. However, further investigation concerning their exact aetiopathogenesis and clinical impact is necessary.

The general discussion and conclusions are described in **chapter eight**.

SAMENVATTING

Voetpijn is een vaak voorkomende oorzaak van manken bij paarden. Na een grondig klinisch onderzoek, wordt als eerste keuze diagnostische modaliteit een radiografisch onderzoek aangevraagd, om de oorzaak van de voetpijn op te sporen. Hierbij wordt het straalbeen grondig geïnspecteerd op radiografische abnormaliteiten, zoals een bot fragment en/of abnormaal gevormde, diepe of toegenomen aantal synoviale invaginaties ter hoogte van de distale onderrand van het straalbeen. Het klinische belang van deze abnormaliteiten is echter nog steeds een punt van discussie. Nochtans worden ze bij hun voorkomen vaak streng beoordeeld, maar dit is afhankelijk van het land waarin het paard radiografisch wordt gekeurd. In dit doctoraatswerk, wat zuiver een beeldvormingsonderzoek is, wordt de distale rand van het straalbeen bestudeerd.

Het **eerste hoofdstuk** geeft een overzicht van de anatomie van de straalbeenregio en het straalbeen, met de nadruk op de synoviale invaginaties, en de beeldvormingsmodaliteiten die kunnen gebruikt worden in de beoordeling van de ondervoet van het paard. Alsook wordt een overzicht gegeven van de aandoeningen van het straalbeen.

In het **tweede hoofdstuk** worden de wetenschappelijke doelstellingen van dit doctoraat beschreven.
De algemene doelstelling van dit doctoraat is het nagaan of radiografie de distale synoviale invaginaties van het straalbeen accuraat weergeeft. De morfologie van de synoviale invaginaties wordt beschreven met behulp van computer tomografie (CT) en vergeleken met hun voorkomen op radiografie. Alsook wordt, in het kader van voetpijn, de pathogenese van de distale fragmenten van het straalbeen verder ontrafeld.

Het **derde hoofdstuk** beschrijft de CT-anatomie van de normale voet bij het paard. Hiervoor werden 10 anatomisch normale voorvoeten van 5 kadavers gebruikt. De CT-onderzoeken werden uitgevoerd met een 4-detector spirale CT-scanner. Dwarse CT-snedes met een dikte van 2 mm werden bekomen in een proximodistale scanrichting. De beelden werden bekeken in een bot- en weke delenvenster. Sagittale en dorsale CT-reconstructies met een dikte van 2 mm werden bijkomend gemaakt. Van 4 voeten werden anatomische coupes gemaakt in het transversale, dorsale en sagittale vlak. De CT-beelden werden vergeleken met de corresponderende anatomische coupes.

Het koot-, kroon-, hoef- en straalbeen, alsook de strek- en buigpezen (inclusief hun distale aanhechting), waren duidelijk zichtbaar op de CT-beelden. De collateraalbanden konden worden gelokaliseerd, maar waren voornamelijk ter hoogte van hun proximale aanhechting moeilijk af te lijnen van nabije weke delen structuren. Het distaal digitaal annulair ligament kon enkel proximaal van het straalbeen onderscheiden worden van de diepe buigpees, en zijn proximale aanhechting kon worden geidentificeerd, maar niet zijn distale aanhechting op het hoefbeen. Kleine ligamenten, zoals het impar ligament, chondrosesamoidean, -coronal, en –compedal ligamenten, axiale en abaxiale ligamenten van het kroongewricht, waren moeilijk en niet op alle beelden te identificeren. De laterale en mediale palmaire arterie en vene waren occasioneel te identificeren. De hoefkraakbeenderen, corium en lagen van de hoefwand waren duidelijk zichtbaar. Het gewrichtskraakbeen, fibrocartilago van het straalbeen, het gewrichtkapsel, chondro-ungulair ligament en de palmaire digitale zenuwen waren niet zichtbaar.

De conclusie van deze studie is dat CT bruikbaar is om de meeste anatomische structuren van de voet aan te duiden. Bijgevolg kunnen de beelden van deze studie gebruikt worden als een atlas voor de beoordeling van CT-beelden bij het paard verdacht van letsels in de voet, waarbij radiografie en echografie inconclusief zijn.

In het **vierde hoofdstuk** wordt de morfologie van de synoviale invaginaties ter hoogte van de distale onderrand van het straalbeen beschreven met behulp van CT. Hiervoor werden 50 voorvoeten van 25 kadavers gescand. Allen waren Warmbloedpaarden. De CT-onderzoeken werden uitgevoerd met een 4-detector spirale CT-scanner. Dwarse CT-snedes met een dikte van 0.6 mm werden bekomen vanaf het distaal tot het proximaal aspect van het straalbeen. De beeldjes werden bekeken in een botvenster. Sagittale en dorsale CT-reconstructies met een dikte van 0.6 mm werden bijkomend gemaakt. De synoviale invaginaties werden beoordeeld op hun aantal per straalbeen, hun vorm, diepte en oriëntatie van hun verloop in het bot.

Een totaal van 295 invaginaties werd geteld, en hun aantal varieerde van 3 tot 11 per straalbeen. Honderdachttien invaginaties waren ‘conisch’ van vorm, 109 ‘lineair’, 38 ‘lollipop’-vormig en 30 waren ‘vertakt’. Honderdvijvennegentig invaginaties penetreerden het straalbeen ‘mild’ diep, 67 ‘matig’ diep en 33 ‘diep’. Hun oriëntatie in het straalbeen varieerde van ‘recht’, ‘dorsoproximaal’ en ‘palmaroproximaal’ in 187, 28 en 80 gevallen, respectievelijk.

De CT-beelden en resultaten van deze studie kunnen gebruikt worden bij de radiografische beoordeling van deze distale synoviale invaginaties van het straalbeen.

Het doel van de studie in het **vijfde hoofdstuk** was om te onderzoeken of radiografie de morfologie van de synoviale invaginaties ter hoogte van de distale onderrand van het straalbeen accuraat weergeeft. Hiervoor werden 50 voorvoeten van 25 kadavers gebruikt. Allen waren Warmbloedpaarden. Van alle voeten werd een CT-onderzoek uitgevoerd met een 4-detector spirale CT-scanner en DPr-PaDi oblique radiografische projecties genomen onder 3 verschillende hoeken (45°, 55° en 65°). Computer tomografie werd beschouwd als de standaard test. Dwarse CT-snedes met een dikte van 0.6 mm werden bekomen vanaf het distaal tot het proximaal aspect van het straalbeen. Sagittale en dorsale CT-reconstructies met een dikte van 0.6 mm werden bijkomend gemaakt. De beelden werden bekeken in een botvenster. Op elk CT-beeldje en radiografische opname werd het aantal synoviale invaginaties, hun diepte en vorm geëvalueerd, en de resultaten van beide modaliteiten werden statistisch vergeleken. Het gemiddelde verschil van het aantal invaginaties tussen CT en alle 3 de radiografische opnames in de groep paarden van deze studie was statistisch significant en ongeveer gelijk aan 2. Dat wil zeggen dat op een CT-beeld gemiddeld 2 invaginaties meer worden geteld dan op een röntgenfoto van de paarden in onze steekproef. Ook op individueel niveau bestond er een grote variatie in het verschil tussen het aantal invaginaties geteld op CT en op radiografie, en een duidelijke spreiding rond het gemiddelde verschil werd gezien. Zo'n variatie op individueel niveau werd ook waargenomen voor de diepte van de invaginaties. Met radiografie werd de ene invaginatie dieper gemeten (overschat) dan op CT, terwijl de andere ondergeschat werd. Wat opviel was dat de ondiep penetrerende invaginaties meestal dieper werden gemeten vergeleken met hun diepte op CT, terwijl radiografie de dieper penetrerende invaginaties vaker onderschatte. Voor de vorm van de invaginaties werd voor alle 3 de radiografische projecties een hoge specificiteit gemeten van gemiddeld 95% en een sensitiviteit van 64%. Dit betekent dat bijna geen vals-positieve resultaten werden waargenomen op radiografie, met andere woorden, wanneer een abnormale invaginatie wordt opgemerkt op radiografie, dan is die invaginatie hoogstwaarschijnlijk werkelijk abnormaal, maar een normaal voorkomende invaginatie kan in werkelijkheid toch abnormaal zijn.

De conclusie van deze studie is dat radiografie de vorm van de synoviale invaginaties goed weergeeft, maar het aantal en de diepte van deze invaginaties vertonen veel variatie met hun voorkomen op CT. Dientengevolge, synoviale invaginaties ter hoogte van de distale

onderrand van het straalbeen moeten steeds met de nodige voorzichtigheid beoordeeld en geïnterpreteerd worden op radiografie. Verder onderzoek omtrent het klinische belang van abnormale invaginaties is vereist.

In het **zesde hoofdstuk** wordt de morfologie van de synoviale invaginaties ter hoogte van de distale onderrand van het straalbeen op een DPr-PaDi oblique radiografische projectie onder een hoef-specifieke hoek vergeleken met hun voorkomen op CT. Hiervoor werden 50 voorvoeten van 25 kadavers gebruikt. Allen waren Warmbloedpaarden. Van alle voeten werd een CT-onderzoek uitgevoerd met een 4-detector spirale CT-scanner, en een DPr-PaDi oblique radiografische projectie genomen onder een hoef-specieke hoek die werd gemeten op een LM-opname van de desbetreffende voet. Computer tomografie werd beschouwd als de standaard test. Dwarse CT-snedes met een dikte van 0.6 mm werden bekomen vanaf het distaal tot het proximaal aspect van het straalbeen. Sagittale en dorsale CT-reconstructies met een dikte van 0.6 mm werden bijkomend gemaakt. De beelden werden bekeken in een botvenster. Op elk CT-beeldje en radiografische opname werd het aantal synoviale invaginaties, hun diepte en vorm geëvalueerd, en de resultaten van beide modaliteiten werden statistisch vergeleken. Significant meer invaginaties werden gezien op CT-beelden dan op röntgenfoto's, met een gemiddeld verschil van 1.2 invaginaties. Met radiografie werd in geen enkel straalbeen van de paarden uit onze steekproef meer invaginaties geteld dan met CT. Er werd geen statistisch significant verschil waargenomen tussen CT en de radiografische projectie voor de diepte van de invaginaties. Echter was er wel een grote individuele variatie in het verschil van de gemeten dieptes op CT en op radiografie, en een duidelijke spreiding rond het gemiddelde verschil werd gezien. Ook met de specifieke radiografische opname werden dieper penetrerende invaginaties onderschat in diepte. Een matig tot goede overeenkomst tussen beide modaliteiten was aanwezig voor de vorm van de invaginaties en voor de specifieke radiografische opname werd een hoge sensitiviteit (75%) en specificiteit (97%) gemeten.

We kunnen concluderen dat wat betreft het aantal en de diepte van de invaginaties, de resultaten bevonden met de hoef-specifieke radiografische opname vertonen een duidelijke variabiliteit met deze bevonden met CT. Vergeleken met de resultaten uit hoofdstuk 5, vertoont deze specifieke radiografische opname een hogere sensitiviteit voor de vorm van de invaginaties met CT.

In het **zevende hoofdstuk** werden radiografische opnames van de voorvoeten van 325 Belgische Warmbloedhengsten beoordeeld. In deze retrospectieve studie werd de prevalentie van botfragmenten ter hoogte van de distale rand van het straalbeen en hun mogelijke correlatie met de vorm van de proximale articulaire rand van het straalbeen, alsook met andere radiografische abnormaliteiten van het straalbeen, nagegaan. Drie radiografische opnames (een LM, D55°Pr-PaDiO en D65°Pr-PaDi oblique projecties) werden genomen van alle voorvoeten. De vorm van de proximale articulaire rand op de radiografische opnames was 'recht' in 278, 'convex' in 184, 'golvend' in 147, en 'concaaf' in 41 straalbeenderen. Distale fragmenten werden in 8.8% van de straalbeenderen gediagnosticeerd en kwamen significant meer voor in straalbenen met een 'concave' (in 22%) of 'golvende' (14%) proximale articulaire rand, vergeleken met de 'rechte' (6%) of 'convexe' vorm (7%). Geen significante correlatie met de andere straalbeen abnormaliteiten werd gezien.

Gebasseerd op onze resultaten en die van vorige onderzoeken, zou een mogelijke associatie tussen het voorkomen van distale botfragmenten en de vormafhankelijke kracht inwerking op het straalbeen kunnen worden verondersteld. Doch, verder onderzoek omtrent de exacte aetiopathogenese van deze fragmenten en hun klinische belang is nodig.

De algemene discussie en conclusies van dit doctoraat worden behandeld in het **achtste hoofdstuk**.

CURRICULUM VITAE

Sarah Claerhoudt werd geboren op 19 juli 1985 te Veurne. Na het beëindigen van het secundair onderwijs in het Koninklijk Atheneum te Veurne, startte zij in 2003 met de studies Diergeneeskunde te Gent. In 2009 behaalde zij haar diploma van Dierenarts aan de Universiteit Gent met grote onderscheiding.

Haar laatstejaarsscriptie "Beschrijvende studie van fragmenten van het straalbeen en het kogelgewricht bij een BWP hengst aangeboden voor keuring" werd genomineerd voor de prijs van beste scriptie, en wekte haar interesse op in de Medische Beeldvorming. Ze startte haar wetenschappelijk onderzoek in 2009, wat werd gefinancierd door MEDEX, Loncin S.A., België. Na een succesvolle aanvraag voor een doctoraatsmandaat in 2010, vervolgde zij haar doctoraatsstudie onder leiding van professor Saunders aan de vakgroep Medische Beeldvorming van de Huisdieren en Orthopedie van de kleine Huisdieren, Universiteit Gent. Haar doctoraatsmandaat werd gefinancierd door het Bijzonder Onderzoeksfonds van de Universiteit Gent. Zij volgde tevens de Doctoraatsopleiding in de Diergeneeskundige Wetenschappen en de opleiding Laboratory Animal Science.

Sarah Claerhoudt is auteur en mede-auteur van meerdere publicaties in wetenschappelijke nationale en internationale tijdschriften en gaf presentaties op congressen.

BIBLIOGRAPHY

PUBLICATIONS IN SCIENTIFIC JOURNALS

Claerhoudt S, Pille F, Vanderperren K, Van der Vekens E, Duchateau L, Hauspie S, Saunders J.H. Association between navicular bone shape and distal border fragmentation in Belgian Warmblood horses**.** Veterinary and Comparative Orthopaedics and Traumatology 2011; 24: 132-136.

Claerhoudt S, Bergman H.J, van der Veen H, Vanderperren K, Raes E.V, Saunders J.H. Computed tomographic morphology of the synovial invaginations of the distal sesamoid bone of the horse. Anatomia, Histologia, Embryologia 2011; 40: 55-60.

Claerhoudt S, Bergman H.J, van der Veen H, Duchateau L, Raes E.V, Saunders J.H. Differences in the morphology of distal border synovial invaginations of the distal sesamoid bone in the horse as evaluated with CT compared to radiography. Equine Veterinary Journal 2012; 44: 679-683.

Claerhoudt S, Bergman H.J, van der Veen H, Duchateau L, Raes E.V, Saunders J.H. Morphology of distal border synovial invaginations of the equine distal sesamoid bone: comparison between computed tomography and a hoof-specific radiographic projection. Veterinary and Comparative Orthopaedics and Traumatology 2012; 25: 453-459.

Claerhoudt S. Distal navicular border fragments: Clinically significant or not, that is the question. Equine Veterinary Education 2013; 25: 352.

Claerhoudt S, Bergman E.H.J, Saunders J.H. Computed tomographic anatomy of the equine foot. Anatomia, Histologia, Embryologia 2013; DOI: 10.1111/ahe.12091.

Masure D, Wang T, Vlaminck J, **Claerhoudt S**, Chiers K, Van den Broeck W, Saunders J.H, Vercruysse J., Geldhof P. The Intestinal Expulsion of the Roundworm Ascaris suum is Associated with Eosinophils, Intra-Epithelial T Cells and Decreased Intestinal Transit Time. PLOS Neglected Tropical Diseases 2013; DOI: 10.1371/journal.pntd.0002588.

PRESENTATIONS

Claerhoudt S, Bergman H.J, van der Veen H, Vanderperren K, Raes E.V, Saunders J.H. Computed tomographic morphology of the synovial invaginations of the distal sesamoid bone of the horse. 28th Congress of the European Association of Veterinary Anatomists, July 28th – 31th, 2010, Paris, France. pg 322. (Oral presentation).

Claerhoudt S, Bergman H.J, van der Veen H, Duchateau L, Raes E.V, Saunders J.H. Differences in the morphology of distal border synovial invaginations of the distal sesamoid bone in the horse as evaluated with CT compared to radiography. Annual Conference of the European Association of Veterinary Diagnostic Imaging, August 30th – September 3th, 2011, London. England. pg 686. (Oral presentation).

Claerhoudt S, Bergman E.H.J, Saunders J.H. Computed tomographic anatomy of the equine foot. Annual Conference of the European Association of Veterinary Diagnostic Imaging, August 27th – 31th, 2013, Cascais, Portugal. pg 139. (Poster presentation).

DANKWOORD

In het laatste hoofdstuk van mijn doctoraatswerk wil ik heel graag de mensen bedanken die mij steeds hebben gesteund en geholpen gedurende de voorbije jaren bij het verwezenlijken van dit doctoraat.

Allereerst wil ik mijn Papa en Greta bedanken om mij de kans te hebben gegeven om de opleiding Diergeneeskunde te volgen en met glans te beëindigen, mede dankzij hun steun. Papa, heel erg bedankt om mij steeds weer op te peppen, me door dik en dun te steunen en me moed te geven als ik het weer even moeilijk had. Ik herinner me nog dat je 's avonds na het examen fysica naar Gent bent gereden met Vitessje mee, om mij een hart onder de riem te steken. Ik zag het toen even niet meer zitten, maar je motiveerde mij om mijn kopje niet te laten hangen. Ook tijdens de examens, een periode waarin ik niet altijd te genieten was, hebben jullie mij laten doen en mij gesteund. Bedankt om zo goed voor mij te hebben gezorgd en dit nog steeds te doen. Een welgemeende dankjewel!

Dit doctoraat zou natuurlijk niet tot stand zijn gekomen zonder de steun van mijn promotor, Prof. Dr. Jimmy Saunders. Als laatstejaarsstudente was ik al erg geïnteresseerd in de Medische Beeldvorming en wou ik heel graag mijn eindwerk schrijven over fragmenten ter hoogte van het straalbeen bij paarden. Dit doordat collega Yves Sheirlinck me reeds warm had gemaakt over de problematiek ter hoogte van het straalbeen. Yves, bedankt om mij dit interessante onderwerp door te spelen. Toen ik bij professor Jimmy Saunders het onderwerp voor mijn eindwerk voorstelde, was hij meteen enthousiast. Daaruit vloeide later een doctoraatsonderwerp. Jimmy, bedankt om mij de mogelijkheid te geven om op de dienst Medische Beeldvorming te doctoreren en er praktijkervaring op te doen. Je hebt mijn werk steeds kritisch verbeterd en me goed begeleid gedurende de voorbije jaren.

Daarnaast wens ik ook ons diensthoofd, Prof. Dr. Henri van Bree te bedanken voor de kans die hij me gaf om op de dienst Medische Beeldvorming te werken en ervaring op te doen.

Graag een woordje van dank voor het team dierenartsen van dierenkliniek De Lingehoeve. Vooral aan Erik en Henk heb ik veel te danken. Heel erg bedankt voor de hulp en raad bij het maken van de CT-beeldjes en het nalezen van mijn artikels. Bedankt voor de mooie figuren die ik heb gebruikt in mijn doctoraat. Erik, jouw dagen zijn vaak te kort voor al het werk dat je wilt doen/hebt, en toch maakte je tijd voor mij vrij om op mijn vragen te antwoorden en mijn artikels voor de opgegeven deadline zeer grondig en kritisch na te lezen. Je enthousiasme

werkte aanstekelijk, bedankt dat ik steeds weer op je kon rekenen! Ook de stalverantwoordelijke Dirk en hoefsmid Gert-Jan wil ik graag bedanken voor het verzamelen van de onderbenen en opkuisen van de paardenhoeven.

Tevens wil ik Prof. Dr. Frederik Pille, lid van mijn lees- en examencommissie, hartelijk bedanken voor de nuttige commentaren ter verbetering van deze thesis. Ik heb veel bijgeleerd van uw wetenschappelijke kennis en kritische bemerkingen. Bedankt dat ik steeds op je kon rekenen!

Mijn dank gaat ook uit naar de overige leden van mijn lees- en examencommissie: Prof. Dr. Bernadette van Ryssen, Dr. Els Raes, Prof. Dr. Géraldine Bolen, Prof. Dr. Annick Gabriel en Prof. Dr. Fabrice Audigié, thank you for your time and constructing comments improving this thesis.

Graag wens ik Prof. Dr. Luc Duchateau te bedanken voor de snelle statistische verwerking van mijn resultaten en de uitgebreide uitleg.

Verder wil ik al mijn collega's van de vakgroep Medische Beeldvorming en Orthopedie van de Kleine Huisdieren bedanken voor de leuke samenwerking de voorbije jaren.
Els, bedankt om zo'n lieve collega te zijn voor mij. De tijd dat we samen in de kijkruimte hebben doorgebracht, was altijd leuk en leerrijk. Naast het tellen en meten van de synoviale invaginaties en zoeken naar fragmenten, was er ook tijd voor een leuke babbel en gelach. Steeds kon ik op je hulp rekenen bij een moeilijke echografie. Het was een groot plezier om met je te mogen samenwerken, bedankt om me veel bij te leren. Veel succes met je residentie, jij zal dit kunnen!
Katrien, als laatstejaarsstudente kon ik reeds bij je terecht voor vragen betreffende 'onderzoek'. Doorheen dit doctoraat gaf je me vele tips, had je goede ideeën en stond je deur steeds open voor een leuke en vaak serieuze babbel. Bedankt om mijn artikels en dit doctoraatswerk zo grondig na te lezen en aan te passen. Veel succes met je nieuwe positie als professor, met Margot en veel geluk in de toekomst.
Stijn Hauspie, je hebt mij altijd goed geholpen en gesteund, was het niet op de kliniek, dan was het wel voor een computerraadsel met mijn Mac of om een artikel te helpen zoeken. Bedankt daarvoor! Ik wens je alvast veel plezier en succes met je huidige job en bedankt voor de leerrijke tijd samen in de kliniek.

Ook Elke wil ik graag bedanken. Altijd mocht ik je bellen om te vragen of je me even wou komen helpen op kliniek. Ik heb alvast veel van je geleerd. Geniet nu maar ten volle van je gezinnetje en veel succes in de toekomst.
Els, Katrien en Elke, merci om me te vervangen op kliniek tijdens mijn zwangerschap.
Kim, wat hebben wij een leuke tijd gehad samen. Heel erg bedankt om me steeds weer te helpen met radiografieën nemen, paarden vasthouden, en nog zoveel meer. Als studente kon ik het al goed met je vinden, wij gelijken op veel vlakken echt op mekaar. Ik hoop dat we mekaar niet uit het oog verliezen en we af en toe nog een stapje in de wereld gaan zetten samen. Ik wens je alvast heel veel plezier en een warm nestje samen met Sam in jullie woonst. Jullie huis is bijna af, een nieuw begin lacht je reeds toe. Veel succes verder!
Ook professor K. Dik en Ingrid Putcuyps wil ik graag bedanken voor de leerrijke film readings.

Olga, Caroline, Veerle, Laure and Anaïs, thanks a lot for the nice and educative time in small animal clinic.
Marnix, een dikke merci om al mijn beeldmateriaal te verwerken en mijn poster te helpen maken. Ik kon steeds weer bij je aankloppen om dat ene figuurtje te bewerken, pijltjes en cijfertjes erop te zetten, je verloor nooit je geduld door mij. Heel erg bedankt voor al je tijd!
Marnix, Casper en Marleen, bedankt om mij dikwijls op te halen en/of af te zetten aan het station bij weer eens een regenachtige dag. Casper, op jouw kon ik ook altijd rekenen voor tips en beeldjes. Heel veel succes met je doctoraat en carrière.
Michiel van de dienst Pathologie zou ik graag willen bedanken voor het maken van de anatomische coupes.

Graag wil ik de orthopedisten van de dienst Heelkunde Grote Huisdieren bedanken voor de leuke samenwerking. Kelly en Michèle, bedankt voor de leuke babbels in de kijkruimte. Jullie maakten de serie hengstenkeuringen voor mij heel wat aangenamer. Kelly, het einde van mijn doctoraat is voor ons geen afscheid, hopelijk zien we mekaar nog vaak eens terug op een zomerse barbecue of feestje. Veel geluk samen met Jan en de kinderen.

Verder wil ik mijn collega's van op het bureau, Evelien, Delphine, Yves en Kathelijn, bedanken voor de aangename momenten, ondersteunende gesprekken en goede tips die ze mij gaven. Een welgemeende dank gaat uit naar Yves voor al je hulp in het aanpassen van mijn lay-out. Zonder jou was er geen structuur in mijn doctoraat, echt bedankt voor je tijd!

DANKWOORD

Mijn vriendin Shirley wil ik graag bedanken om de Nederlandstalige hoofdstukken in dit doctoraat na te lezen en te verbeteren.
Bedankt collaga-dierenarts Marc Vandenberghe om mij op tijd en stond uit mijn bureau te halen, zodat ik de geur van de dieren en de boerenbuiten nog zou herkennen, alsook de kneepjes van het vak niet zou verleren. Ook Maya en Julie, bedankt om mij alvast een positieve feeling mee te geven in de kleine huisdieren praktijk.

Graag ook een dankuwel aan de rest van mijn familie, schoonfamilie en dichte vrienden voor hun vaste steun in de goede en minder goede periodes gedurende mijn tijd in Gent. Pepe, je hebt ons plots heel snel verlaten, ik zal je missen. Ria, ik vind het jammer dat je mijn verdediging en nog zoveel meer niet meer fysiek kan meemaken, maar heel stilletjes weet ik dat je alles volgt en nu wel heel trots op ons bent.

En tenslotte, Stijn, mijn vriend en de papa van ons kindje, heel erg bedankt voor je vaste steun en vertrouwen. Liefje, we hebben al wat watertjes doorzwommen, het is niet altijd gemakkelijk geweest, maar kijk, we zijn hier alvast doorheen en we kunnen nu uitkijken naar ons baby'tje en een mooie toekomst. Samen geraken we er! Ook mijn kleine spruit, een dikke knuffel om geduldig te wachten en me telkens weer dat extra beetje energie te geven bij een stampje of een draaiing in mijn buik. Wat zien we uit naar jouw komst!

Veel liefs,

Sarah